Automatic Detection of Diabetic Related Retina Disease in Fundus Color Images

by

Laura Juliana Uribe Valencia

Dissertation
Submitted to the Department of Electronics
In Partial Fulfillment of the Requirements for the Degree of
Doctor of Science

Doctor of Science in Electronics

at the

National Institute for Astrophysics, Optics and Electronics
January 2020
Tonantzintla, Puebla, México

Supervised by

Jorge Francisco Martínez Carballido, Ph. D.

Abstract

Diabetic retinopathy (DR) is a degenerative visual complication associated with diabetes which is rapidly increasing worldwide and currently is one of the leading causes of blindness and visual impairment in adults. Due to the rapid increase in the number of people who suffer from DR, the available number of ophthalmologists won't be enough to provide proper periodical consultation to all diabetic patients, especially in rural areas. According to current estimates by the International Agency for Prevention of Blindness (IAPB), by 2030 at least 3 million eyes must be evaluated each day (35 tests per second). Even more, given that DR is asymptomatic, when a patient perceives sight difficulties, generally is at a proliferative stage where sight damage can't be reversed. That is why is recommended to diabetic patients to have frequent eye exam; that is where automatic or semi-automatic image analysis algorithms provide a potential solution. In the present work, new methods to analyze digital fundus images of diabetic patients are proposed. Particularly, several components of an automatic screening system for diabetic retinopathy were developed using algorithms, including segmentation of anatomical structures, lesions and diagnosis.

The anatomical retinal structures: optic disc (OD) and macula were the located, exudates the lesions and Diabetic Macular Edema (DME) the diagnosis. Optic disc is relevant for several diagnosis procedures on retinal images including glaucoma and also is of high importance for bright lesion detection of Diabetic Retinopathy by extracting it and avoiding false positives. The proposed OD location approach is based on OD's characteristic high intensity and a novel method for feature's extraction that aims to represent the essential elements that define an optic disc by proposing a model for the pixel intensity variations across the optic disc. OD region location in fundus images. The proposed approach was evaluated using four known publicity available datasets: DRIVE, DIARETDB1, DIARETDB0 and e-ophtha-EX. An OD location accuracy of 99.7% is obtained for the combined 341 retinal images of the four publicly datasets.

Diabetic Macular Edema is an important complication of DR, occurs when the leakage of blood vessels causes accumulation of fluid in the macula region. In clinical practice, ophthalmologists diagnose DME based on the presence of exudates in the macular neighborhood. The macula corresponds to the central area of the retina, responsible for the most accurate and color vision due its high density of photoreceptors. The proposed macula detection algorithm initially searches for the macula region with prior information that it is the dark intensity region. A threshold is locally defined using k-means clustering. For the challenging images including those with the presence of large hemorrhages and low contrast, an alternative approach is applied based on the fact that fovea center is estimated to be at a constant distance of approximately 2.5 OD diameter of OD center and that is a region devoid of retinal blood vessels. The results are evaluated using the mean, minimum and maximum percent of overlap with the macula groundtruth. For HRF, DRIVE, Diaretdb1 and MESSIDOR publicity available datasets, the percent of [mean, minimum and maximum overlap] are [87.95%, 40%, 98%], [87.8%, 45%, 97%], [82.17%, 18%, 100%], [85.85%, 12%, 100%], respectively. Exudates are segmented using their characteristic high intensity to generate candidates and classification stage is performed by verifying that the candidates have sharp edges and a gradual variation of intensity concentrically, a characteristic observed in exudates. Finally, in the diagnosis category, we have developed an algorithm that diagnoses diabetic macular edema based on the position of the exudates previously segmented. The proposed approach was tested on MESSIDOR and Diaretdb1 datasets, obtaining a specificity of 95.65% and a sensitivity of 82.43% for MESSIDOR, and a specificity of 96.49% and sensitivity of 85.71% for Diaretdb1.

Resumen

La retinopatía diabética (RD) es una complicación visual degenerativa asociada con la diabetes, enfermedad cuya incidencia está aumentando rápidamente en el mundo y que en la actualidad es una de las principales causas de ceguera y discapacidad visual en la población adulta. Debido al rápido aumento en el número de personas que sufren de RD, en el futuro, el número disponible de oftalmólogos no será suficiente para proporcionar una consulta periódica adecuada a todos los pacientes diabéticos, especialmente en las zonas rurales. Según las estimaciones actuales de la Agencia Internacional para la Prevención de la Ceguera (IAPB), para 2030 se deberán evaluar al menos 3 millones de ojos cada día (35 pruebas por segundo). Adicionalmente, debido a que la RD es asintomática, cuando un paciente percibe dificultades visuales, generalmente se encuentra en una etapa proliferativa donde el daño visual no es reversible. Como método de prevención, se recomienda a los pacientes diabéticos que se realicen exámenes oculares frecuentes, y es allí donde los algoritmos de análisis de imágenes automáticos o semiautomáticos brindan una solución potencial. En el presente trabajo, se proponen nuevos métodos para analizar imágenes digitales de fondo de ojo. En particular, se desarrollaron varios componentes para un sistema de detección automática para la retinopatía diabética utilizando algoritmos, incluida la segmentación de estructuras anatómicas, lesiones y diagnóstico.

Las estructuras anatómicas localizadas fueron el disco óptico (DO) y la mácula, la lesión detectada los exudados y la enfermedad diagnosticada el Edema Macular Diabético (EMD). El disco óptico es relevante para una variedad de procedimientos de diagnóstico en imágenes de fondo de ojo, incluido el glaucoma; además, su segmentación es de gran importancia en la detección de lesiones brillantes en la retinopatía diabética con el fin de evitar falsos positivos. El enfoque propuesto para la ubicación del DO se basa su característica alta intensidad y en un novedoso método para la extracción de características que tiene como objetivo representar los elementos esenciales que definen un disco óptico. Se propuso un modelo para representar la variación de intensidad de los píxeles horizontalmente

pertenecientes al disco óptico. El método propuesto se evaluó utilizando cuatro conjuntos de imágenes disponibles públicamente: DRIVE, DIARETDB1, DIARETDB0 y e-ophtha-EX. Se obtuvo una precisión en la ubicación del DO del 99.7% para las 341 imágenes de fondo de ojo en conjunto.

El edema macular diabético es una complicación importante de la RD y ocurre cuando la fuga de sangre de los vasos sanguíneos provoca que se acumulen fluidos en la región de la mácula. En la práctica clínica, los oftalmólogos diagnostican el EMD en función de la presencia de exudados en la vecindad de la región de la macula. La mácula corresponde al área central de la retina y debido a su alta densidad de fotorreceptores, es responsable de la visión de alta precisión y a color. El algoritmo de detección de mácula propuesto, inicialmente busca la región de la mácula con información previa de que es la región de intensidad más baja. Un umbral local se define utilizando el agrupamiento mediante *k-means*. Para las imágenes más complicadas, incluidas aquellas con bajo contraste y con la presencia de hemorragias de gran tamaño, se utiliza un enfoque alternativo basado en el hecho de que se estima que el centro de la fóvea está ubicado a una distancia constante de aproximadamente 2.5 veces el diámetro del DO desde el centro del DO y que además es una región desprovista de vasos sanguíneos. Los resultados se evalúan utilizando el porcentaje medio, mínimo y máximo de intersección con la región de la mácula marcada por los expertos. Para los conjuntos de imágenes disponibles públicamente: HRF, DRIVE, Diaretdb1 y MESSIDOR, el porcentaje de [superposición media, mínima y máxima] es [87.95%, 40%, 98%], [87.8%, 45%, 97%], [82.17%, 18%, 100%], [85.85%, 12%, 100%], respectivamente. Los exudados se segmentaron utilizando su característica alta intensidad para generar candidatos y para la etapa de clasificación se verificó que los candidatos presentaran bordes marcados y una variación gradual de intensidad de forma concéntrica, características observadas en los exudados. Finalmente, en la categoría de diagnóstico, se desarrolló un algoritmo para el prediagnóstico del edema macular diabético teniendo en cuenta la posición de los exudados que fueron segmentados previamente. El enfoque propuesto se probó en los conjuntos de imágenes MESSIDOR y Diaretdb1, obteniendo una especificidad del 95,65% y una

sensibilidad del 82,43% para MESSIDOR, y una especificidad del 96,49% y una sensibilidad del 85,71% para Diaretdb1.

Agradecimientos

Agradezco a mis padres por brindarme las herramientas necesarias para culminar esta etapa y ser mis guías y apoyo continuo.

Agradezco a Carlos, por ser mi principal fuerza de apoyo y motivación durante todo este proceso que recorrimos juntos.

Agradezco a mis hermanos por ser ejemplos de superación personal y entrega y por sus palabras de ánimo.

Agradezco a mi director de tesis Jorge Francisco Martínez Carballido por compartir su sabiduría y enseñanzas, así como guiarme pacientemente durante el desarrollo de esta tesis.

Agradezco también al CONACYT por la beca doctoral con CVU No. 493055.

Contents

List of Figures

List of Tables

Introduction

Diabetic retinopathy (DR) is one of the most common degenerative visual complications in the diabetic population worldwide and is currently one of the leading causes of blindness. Diabetic retinopathy affects approximately 80% of people who have had diabetes for 10 years or more; 90% of these cases could be reduced if appropriate treatment and frequent eye monitoring is performed [1]. The World Health Organization has determined that 422 million people suffer from Diabetes worldwide on 2014, about 8% of annual increase and a high proportion of type 2 diabetes is undiagnosed [2].

Due to the trend in the increase in the percentage of people suffering from DR, the available number of ophthalmologists is not sufficient for the proper treatment of all patients, especially in rural areas [3]. According to current estimates [4] by the International Agency for the Prevention of Blindness (IAPB), by 2030, at least 3 million eyes will need to be evaluated every day (35 exams per second) and it is further noted that the Diabetic population will increase by 342% from those in 2014, the number of ophthalmologists will increase only by 2% on the year 2030. On the other hand, the problem is complicated by the fact that the DR does not exhibit any distinctive symptoms that the patient can perceive easily until a chronic stage of the disease is reached, which is why it is necessary to carry out frequent fundus check-ups.

The traditional evaluation process for DR detection consists of analysing the fundus images of each patient by an ophthalmologist. This method is based on comparison with the appearance of the fundus of a normal retina and the recognition of certain typical lesions, such as: microaneurysms (MAs), haemorrhages and exudates. This method is repetitive and consumes a large amount of time, in addition, the use of chemicals is necessary to dilate the eye, which demands time of the patient and produces negative side effects. These factors make the diagnosis early is made even more difficult by the lack of opportunity in time and cost for a person to carry out periodic preventive examinations.

In order to contribute to a solution to this problem, a number of computer-aided diagnostic (CAD) systems [5] have recently been developed, which aim to become an accessible and economical preliminary ophthalmologic diagnostic medium that facilitates the way in which routine preventive examinations are done indicating the need to go to the ophthalmologist in the early stages. The purpose of this tool is to facilitate and reduce the costs of timely diagnosis of DR, as well as to alleviate the workload of ophthalmologists, since qualified technicians may perform a pre-diagnosis on the basis of which they can decide whether or not the reference to the ophthalmologist of each particular case is necessary. In this way, the ophthalmologist could spend more time on patients who truly require attention rather than analysing each and every fundus image.

1.1 Background and justification

Diabetic retinopathy is the main cause of blindness among the diabetic population worldwide. Early diagnosis and treatment can prevent loss of vision. With the prominent increase in the percentage of people with diabetes, there won't be enough ophthalmologist to cover the demand of eye exams. In the Figure 1 is shown the typical diagnosis process of the diabetic retinopathy, which carries a great load of time for ophthalmologists inspecting the fundus images. It is necessary to develop systems that can monitor and locate in a reliable and efficient way the abnormalities present in the images of the fundus. Some relevant facts about the diabetic retinopathy, classified in four areas are:

1.1.1. Statistics

- By 2030, the number of people with diabetes will increase by 3.4 times of those in 2014, while growth in the number of ophthalmologists will be only 2%[1].

- Moreover, the number of diabetics worldwide is underestimated. In [2] a study established that deaths attributable to complications of diabetes in the US are not taken into account.
- On a IAPB report [3] is assured that approximately 50% of people with diabetes are currently undiagnosed.
- In Mexico City, complications caused by diabetes are the leading cause of death [4].
- Diabetic retinopathy affects approximately 80% of people who have suffered from diabetes for 10 years or more [5].
- Worldwide, DR is cause number one for blindness of people on working age [6].

1.1.2. Health area impact

- In Mexico, there are currently 3,500 registered ophthalmologists and a population of diabetics of 14 million [7], if the burden of people is divided equally by ophthalmologist, each should examine 4,000 patients and the time it would take to complete the analyzes would be 333 days per specialist.
- A low percentage of diabetics get tested. In the US, only 4 out of 10 diabetics perform their eye fundus examination per year [8].

1.1.3. Social impact

- Cost per exam.
- The duration of the examination for the patient is 2 to 3 hours with dilation of the pupil.
- Waiting time for consultation with the ophthalmologist. In the public sector, it is typically 4 to 12 weeks and 1 to 3 weeks in the private sector.

1.1.4. Economic impact

- Expenses associated with the treatment of illness (equipment, medical personnel).
- Premature pension by disability due to blindness.
- Annually the cost is estimated in 827,000 million USD

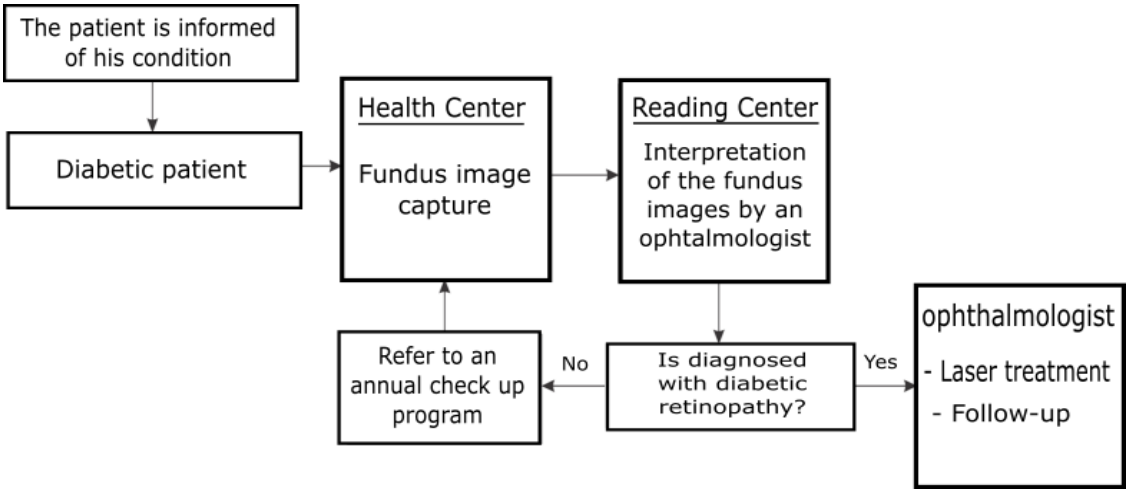

Figure 1. Typical diagnosis process for diabetic retinopathy.

1.2 Expected Contributions

- Algorithms for the pre-diagnosis of DR.
  - Facilitate widespread use in ophthalmic instruments.
  - Algorithm that meets the recommended standards necessary for the pre-diagnosis of DR sensitivity 80% and specificity 95%.
  - Unlike current methods, it is intended that the solution to be developed, be tolerant to variability in the input image (resolution, lighting, color, FoV).

- As for the classification, unlike most methods found in the literature that employ on the order of 100's of characteristics, it will be sought to reduce this number, seeking those that reflect the knowledge of the expert.

- Contribute to the early pre-diagnosis
  - Make it easier to take the exam at least twice a year.
  - No pupil dilation.
  - No need for ophthalmologist for pre-diagnosis.

1.3 Objectives

1.3.1 General objective

Design and develop a solution for the detection of two anatomical structures, one lesion associated with diabetic retinopathy and a pre-diagnosis of one retinal disease in color images of eye fundus, using multiple public image databases with different resolutions, that compete with current state of the art publications.

1.3.2 Specific objectives

1. Design and develop method(s) for the detection of one lesion associated with diabetic retinopathy, two anatomical structures of the retina and a pre-diagnosis of one retinal disease.

2. To develop a method for detecting lesions associated with diabetic retinopathy that presents a competitive performance in terms of sensitivity and specificity, according to The British Diabetic

Retinopathy Working Group these values should be at least 80% and 95% respectively [9].

3. Evaluate the results in 4 different databases of public access that include variety of pathologies, resolution and image quality to verify that the algorithm can be parameterized for different databases.

State of the art

2.1 Fundus Image Pre-processing

The fundus images are acquired by the reflection of visible light of the fundus of the retina and are captured using a fundus camera, obtaining a 2-D representation of the retinal tissues projected on the plane of the image. The medical images are typically acquired following a defined protocol, in order to ensure that the appearance of the structures is similar in any image that is acquired using the same protocol; however, the fundus images obtained from the monitoring programs are acquired in different environments using different fundus camera models which are operated by qualified technical personnel with different levels of experience, leading to a variation in the quality of the images. The above, added to a poor dynamic range of the fundus camera sensor and other characteristics of the equipment and its use, can generate images of low diagnostic quality. In this context, the notion of quality in the fundus images refers to the ability of an expert (computer-assisted ophthalmologist or diagnosis by a specialized physician) to correctly assess the patient's condition through the fundus image. In approximately 10% of the images of the retina, the artifacts present are significant enough to prevent their evaluation by an expert [10], and it is presumed that a similar ratio is inadequate for automatic analysis.

Fundus images present a large variability which can be classified in two main groups: intra-image variations and inter-image variations. Intra-image variations arise due to differences in light diffusion, the presence of abnormalities, variation in fundus reflectivity and fundus thickness. Differences between images (inter-image variability) may be caused by factors including differences in camera sensors, illumination, acquisition angle and retinal pigmentation which highly variates among patient ethnicity. The following describes some of these unwanted characteristics and that occur in the data sets.

- *Non-uniform illumination*: Despite having controlled conditions at the time of image taking, a large number of fundus images present a non-uniform illumination, which is originated due to different factors, such as: the curved surface of the retina, the pupil size (of great variability between patients), the alignment of the eye with the optical axis of the camera, and the direction and shape of the lighting source, cleanness of the lens, among others.

  Due to the fact that naturally the retina does not possess any type of internal illumination, it is necessary to illuminate it by an external light source; however, the size of the pupil whose diameter varies between 2 mm to 4 mm [11], or on dilated pupil up to 8 mm, constitutes a technical limitation; also, the characteristic concave geometry of the eye determines the intensity of the reflections of the tissues of the retina and causes that the beam of light emitted through the pupil by the source of the fundus camera, incurs unevenly on the surface of the retina, causing that part of the light intensity is lost at the edges, leading to the fact that the peripheral part of the retina appears darker than the central region as shown in Figure 2. This generates local variability of contrast and luminance, in addition, this lack of uniformity can hide structures of interest [12].

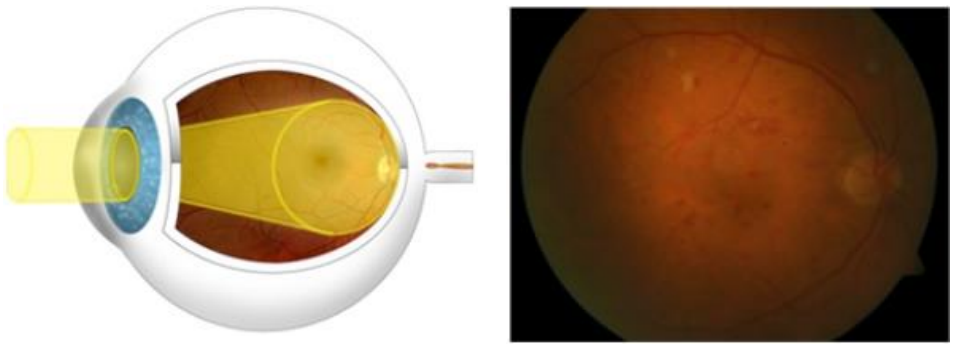

(a) (b)

Figure 2. (a) Illustration of the beam light's path from pupil to retina. (b) Fundus image showing uneven illumination problems. [13]

- *Low contrast*: In image processing, contrast is defined as the variation in color perceived in an image. Contrast enhancement techniques aim to facilitate the visual interpretation of an image by altering the visual appearance that makes an object (or its representation in an image) distinguishable from other objects and background.

  In practice, an inadequate focusing, bad positioning, poor illumination or eye movement make that the fundus images acquired present a low contrast. Additionally, the narrow thickness of the blood vessels causes the contrast between the veins and the retina tissue to be low in the obtained fundus images [14]. On the other hand, the contrast is affected by the non-uniform distribution of lighting as it causes shadows and internal reflections in the image.

- *Color variability*: The human eye is a complex optical structure sensitive to wavelengths in the range of 380 nm to 760 nm. The beam of light entering the eye is refracted when it passes from the air through the sclerotic-cornea interface. Then, it continues its journey through aqueous humor and the pupil (diaphragm controlled by the iris) where it is refracted again by the lens before passing through the vitreous humor and finally reaches the retina, where it is absorbed by the cones and rods after crossing several layers of tissue Figure 3. The sclerotic-cornea and crystalline interface are the most refractive components in the eye and together act as a compound lens to project an inverted image on the retina, the light sensitive tissue of the eye. From the retina, the electrical signals are transmitted to the visual center of the brain through the optic nerve [15].

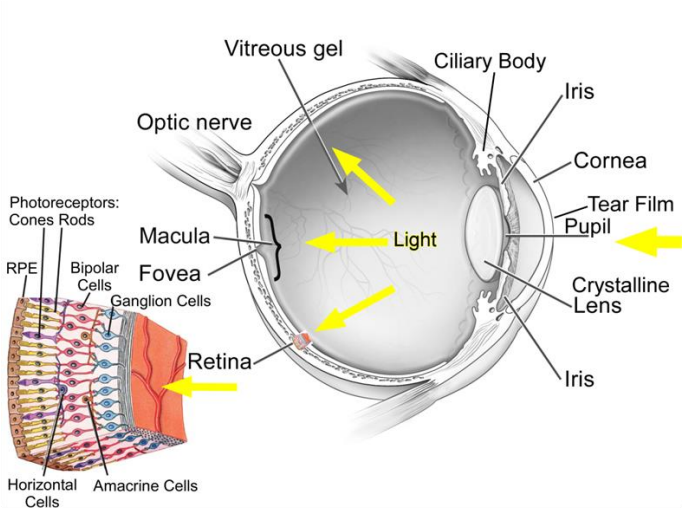

Figure 3. Illustration of the path that the incident beam of light travels since it crosses the sclerotic-cornea interface until it reaches the photoreceptors in the retina. (Modified image from National Eye Institute, National Institutes of Health).

Differences in skin pigmentation, age and iris coloration between different patients affect the color of the retina in the fundus image, hence it can't be established a standard color value for the different structures present in the fundus images as well as for possible lesions present in them, making the segmentation task a not trivial matter. Another factor is the different responses of the camera sensors for each model and brand. For example, in Figure 4 there are shown two fundus images, the one on the left corresponds to a Caucasian patient, while the one of the right to an east Asian patient, it is clearly observed that the coloration of the retina is different, given the same data set and camera.

(a) (b)

Figure 4. (a) Fundus image of a Caucasian patient. (b) Fundus image of an east Asian patient.

In patients older than 30 years it is observed that the lens becomes yellowish, and this phenomenon increases the absorption of blue light which leads to variations in the appearance of the retina. In addition, the composition of the lesions varies, giving origin to different properties of reflection, absorption and refraction. The color of the lesions could be in a range close to the retina to higher values, generating a significant contrast. Non-uniform illumination in the image also contributes to color variations [16].

Human perception has two characteristics that even the most advanced image acquisition systems haven't been able to emulate: dynamic range amplitude (DRA) and color constancy, for this reason, exists a difference between the quality of a scene that an observer sees personally and its corresponding captured image by a certain sensor that is displayed on screen or printed on paper. In practice it is very difficult to achieve the DRA of human vision using electronic equipment, mainly because the latter behave linearly, while human visual perception is essentially of nonlinear nature. On the other hand, even if high dynamic range (HDR) images of the order of 32 bits with more 10 photographic stops could be obtained, the DRA that can play a Cathode Ray Tube (CRT) or liquid crystal monitor is limited, and it is necessary to perform a tonal compression in order to be visualized completely in a medium with a shorter range [17].

In eye fundus images, the intensity of each pixel represents the amount of light reflected by the wavelengths of the Red, Green and Blue channels (RGB); however, if pictures of the same retina are taken with two different fundus cameras, the content in the Red, Green and Blue channels of the RGB color space of the lesions would be different because to changes in the illumination and the characteristic sensitivity of the camera sensor. The Photometric information should be consistent in all images that present the same injury or structure of interest; however, there are several natural sources that cause variations in photometric information, such as: changes in the device of acquisition of the image or its parameters and/or changes in the lighting source (spectral changes that depend on the type of lighting source and the surrounding illumination conditions; such as time of use , a room with windows with or without shades.

The best solution to standardize the fundus images would be to calibrate the image acquisition system; however, the fundus images are typically captured by uncalibrated systems with unknown parameters, reason whereby there is no photometric consistency between the images.

- *Over-exposure and under-exposure noise*: Figure 5 shows an example of a fundus image affected by under-exposure (a) and by over-exposure on (b). In the under-exposed image low pixels values that does not correspond to reality can be observed, this is because the incident light does not have sufficient intensity to produce a good sensor response while in the over-exposed image has high pixel values because the incident light has the necessary magnitude to produce a maximum response in the sensor. Both cases are undesirable, since both exposure deviations produce information loss on images.

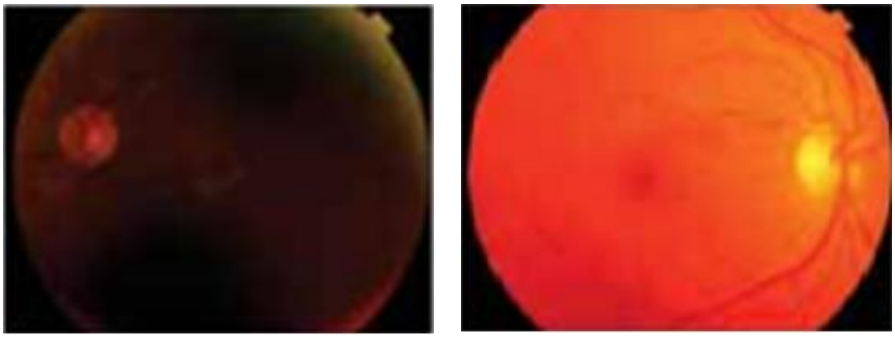

(a) (b)

Figure 5. (a) Under-exposed fundus image. (b) Over-exposed fundus image.

Once the fundus image is obtained, it can be analyzed directly without any modification on a monitor of a computer or be digitally preprocessed for later evaluation by the expert. If the original image has a lot of problems on illumination and low contrast, it makes the diagnosis difficult or it can even lead to erroneous evaluations by the ophthalmologist or grading expert. In the same way, if the original image is evaluated by computer-assisted analysis using digital image processing techniques errors can occur in segmentation of structures of interest. In general, image pre-processing aims to improve the visual quality of the image in such a way that the image resulting is of greater clinical utility and/or prepares it by highlighting certain characteristics for the subsequent segmentation stage. Typically, the preprocessing of retinal images in the literature is classified in terms of the correction for non-uniform illumination, contrast enhancement and color normalization.

Within the methods for the correction of non-uniform illumination, several general-purpose techniques have been investigated for attenuating this variation and improving the reliability of subsequent operators. Early approaches investigated space-variant filtering schemes supporting locally adaptive contrast enhancements [18]. High-pass filtering and mathematical modeling of the non-uniformity followed by subtraction of this component from the observed image [19] have also been investigated for the correction of non-uniform illumination.

Among the techniques for color normalization, are those that make use of the histogram specification [20] to ensure that all sample images match a distribution of a reference image; however, making a fundus image coincident with a reference model may lead to potentially masking specific lesion characteristics found in the original histogram. The reference model is usually obtained from an image that shows good contrast and color in accordance to the judgment of an expert. Another technique used is the color transfer [21] in which color characteristics are transferred from one image to another based on simple statistics of the image, the first step is to transform the images to a color space that minimizes the correlations between the color channels, then the means and standard deviations of the images are matched.

In the literature, there is a great variety of methods for improving contrast, aiming to increase the level of differentiation of the characteristics of the retina. These techniques are usually applied after correcting non-uniform illumination and normalizing the color of the images. Conventional methods based on the global histogram of the image such as contrast stretching and histogram equalization tend to result in loss of information in the brightest areas as well as in the dark areas of the background image, which is why adaptive enhancement of the histogram with limited contrast (CLAHE) [22] is most commonly used.

2.2 Retinal structures location

The location of the different normal ocular fundus structures such as: blood vessels, optic disc, macula and fovea, it is common within most of systems dedicated to the automatic detection of the early signs of diabetic retinopathy. In particular, the location of the optic disc, which corresponds to the visible part of the optic nerve in the eye, is an important task in systems dedicated to the detection of exudates since the optic disc shares similar characteristics of color and brightness, which can cause sections of it to be potentially erroneously

detected as exudates, negatively affecting system performance. This can be avoided if optic's disc location is known in advance. Additionally, the state of the optical disc is important in diseases such as glaucoma, diabetic optic neuropathy and other pathologies related to the optic nerve. The fovea is located in the center of the macula and is the area of the retina that is used for fine vision. Retinopathy in this area is associated with a high risk of vision loss, for this reason it is very important to locate these two areas in order to prevent complications.

- ***Optic Disc (OD) Location***

The OD is the exit point of retinal nerve fibers from the eye, and the entrance and exit point for retinal blood vessels. It is a brighter region than the rest of the ocular fundus and its shape is round when healthy. Although the OD main features and characteristics are relatively easy to describe, individual differences, diseases and other factors will influence characteristics of the optic disc, making its automatic localization a difficult task. Image quality can also affect the appearance of the OD. A retinal image may be unevenly illuminated or poorly focused, resulting in a less distinct and/or blurred OD. Optic disc location methodology involves extensive research interest [23], due to its relevance for OD diseases and as an anatomic eye's feature. The location of OD is important in retinal image analysis because it is a key reference for recognition algorithms [24], blood vessels segmentation [25], and diagnosing some diseases such as diabetes and for registering changes within the optic disc region due to diseases such as glaucoma and the development of new blood vessels [26]. The OD is also a landmark for other retinal features, such as the distance between the OD and the fovea [27], which is often used for estimating the location of the macula [28] and is also used as a reference length for measuring distances in retinal images. In addition, it is important to detect and isolate OD region because,

most of the algorithms designed to segment/detect abnormalities such as hard exudates in DR will detect lots of false positives in OD region as the color tone of the OD is like the hard exudates. Accurate identification of OD can be used to reduce the false positive rate while detecting the lesions [29]**.** The optic disc segmentation approaches, can be categorized in three groups: property-based methods, convergence of blood vessels and model-based methods; and a fourth group by combination of two or more of the first three as shown in Figure 6**.**

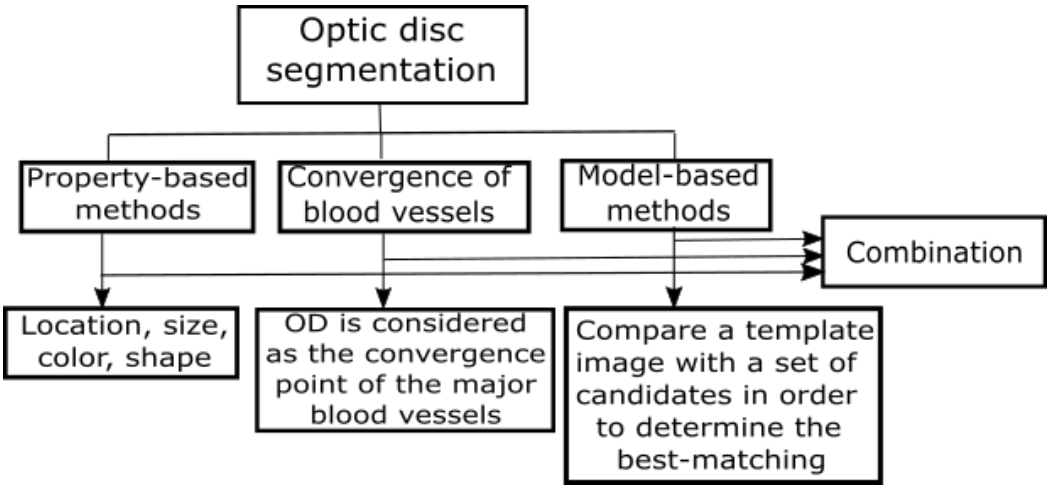

Figure 6. Optic disc segmentation approaches classification.

Property-based methods

Even though there is a significant variation in optic disc's appearance and size, it's mean diameter is clinically estimated on 1.5mm [30] (near $[1/30]^{th}$ of retina's area) and exhibits a distinctive appearance from the tissue zone that surrounds it due to the absence of pigment epithelium making OD's color paler than its surroundings. In healthy fundus images, optic disc is usually seen as a bright circular or elliptic region crossed by a tree of vessels and arteries. This category of methods is based directly on these properties of the optic disc (e.g. location, size, color and shape).

Pourreza-Shahri et al. [31] detection method is based on the fact that OD appears as a bright region in a fundus image. Radon transform (RT) is used to generate the integration of pixel intensities along different directions which leads to making Optic Nerve Head (ONH) a prominent structure in the Radon space. Only brightness information is considered in order to gain high processing speeds. This method claims to be computationally efficient without evidence, a fundus image is first partitioned into overlapping blocks or sub-images. RT is applied to each block or sub-image and the sub-images exhibiting peaks in the Radon space are then processed to locate the OD. It was reported a detection rate of 100% and 96.3% on DRIVE and STARE dataset respectively. The average computation time for the algorithm for STARE database was 2.9 s, using an Intel Core2Duo 3.33 GHz PC.

Rahebi & Hardalac [32] implemented a firefly algorithm to detect the optic disc in retinal fundus images. The firefly intelligent algorithm is an emerging intelligent algorithm that was inspired by the social behavior of fireflies. This algorithm was initially introduced at Cambridge University by Yang in 2008 [33]. The population in this algorithm includes the fireflies, each of which has a specific rate of lighting or fitness. In this method, the insects are compared two by two, and the less attractive insects can be observed to move toward the more attractive insects. Finally, one of the insects is selected as the most attractive, and this insect presents the optimum response to the problem in question. The light intensity of the pixels of the retinal image pixels is used instead of firefly lightings. The movement of these insects due to local fluctuations produces different light intensity values in the images. Because the optic disc is the brightest area in the retinal images, all the insects move toward brightest area and thus specify the location of the optic disc in the image. The results of their algorithm showed a success rate of optic disc localization of 94.38%, 100% and 95% on DIARETDB1, DRIVE and STARE dataset respectively. The average

computation time was 2.13 s for DRIVE, 2.81 s for STARE and 3.52 s for DIARETDB1 using a PC with an Intel Duo CPU, 2.00 GHz RAM.

Algorithms which relied solely on OD's properties showed to be simple, fast and reasonably robust for OD localization in normal retinal images with low variation between images. On the other hand, these algorithms may fail when there are distracters such as exudates and bright artifacts [34] in the fundus images, as well as when OD is obscured by blood vessels or in the case where OD is only partially visible.

Convergence of blood vessels

This type of method approaches location of optic disc by using the information provided by the vascular structure of the retina, since the optic nerve is the focal point of the retina's blood vessel network [35]. To locate optic disc by this method, the retinal blood vessel network is first detected.

Soares et al. [36] proposed an algorithm with a new vessel enhancement method based on a modified corner detector. A weighted version of the vessel enhancement is combined with morphological operators, to detect the four main vessels orientations $\{0^o, 45^o, 90^o, 135^o\}$. These four image functions determine an initial optic disc localization, resulting in two images vertical or horizontal orientations. Each division is averaged creating a 2D step function, and a cumulative sum of the different sizes step functions is calculated in the 2 orientations, resulting in an initial optic disc position. The final OD is determined by a vessel convergence algorithm using its two most relevant features; high vasculature convergence and high intensity values. This approach claims to be robust since it was evaluated in eight publicly-available datasets. Another relevant aspect the proposed method is that it allows a considerable illumination variance, since no illumination equalization was performed as in other methods. The authors reported a detection accuracy of 98.88%, 100%, 99.25%, 98.77%,

98.78%, 98.46%, 99% and 100% on DIARETDB1, DRIVE, MESSIDOR, STARE, E-OPHTA, DIARETDB0, ROC and HRF datasets respectively. The optic disc was localized correctly in 1752 out of the 1767 retinal images (99.15%) with an average computation time of 18.34 seconds. The method was implemented on a laptop with 2 GHz Intel Core i7 and 6 GB of RAM.

Marin et al. [37] approach consists on performing a set of iterative opening–closing morphological operations on the original fundus image intensity channel to produce a bright region-enhanced image. Taking blood vessel confluence at the OD into account, a 2-step automatic thresholding procedure is then applied to obtain a reduced region of interest, where the center and the OD pixel region are finally obtained by performing the circular Hough transform on a set of OD boundary candidates generated through the application of the Prewitt edge detector. The proposed method claims to be a suitable tool for integration into an automated prescreening system, due to its proven effectiveness and robustness, together with its simplicity. Jaccard and dice's coefficients are 0.87 and 0.92 for MESSIDOR dataset and 0.85 and 0.92 MESSIDOR-2 dataset. The average computational time was 5.425 s running on a PC with a dual- Intel Xeon CPU at 32Ghz and 32 GB of RAM capacity.

Wu et al. [38] presented a novel method to automatically localize ODs in retinal fundus images based on directional models. According to the characteristics of retina vessel networks, such as their origin at the OD and parabolic shape of the main vessels, a global directional model, named the relaxed bi-parabola directional model (R-BPDM), is first built. The main vessels are modeled by using two parabolas with a shared vertex and different parameters. A local directional model, named the disc directional model (DDM), is built to characterize the local vessel convergence in the OD as well as the shape and the brightness of the OD. Finally, the global and the local directional models are integrated to form a hybrid directional model, which can exploit the advantages of the global and local models for highly accurate OD localization. The method

proved to be effective by being evaluated on nine publicly available databases (DRIVE, STARE, ARIA, MESSIDOR, DIARETDB1, DIARETDB0, ROC, ONH and DRIONS), achieving an accuracy of 100% for each database.

Optic disc segmentation methods based on convergence of blood vessels seem to be the most efficient way to localize the optic disc in terms of accuracy and robustness; at the expense of greater time execution.

Model-based methods

The model-based methods rely in the fact that optic disc shape is approximately circular and that the pixels conforming its area are brighter than its surroundings. The method consists on comparing a template image (model) with a group of candidates in the fundus image, with the purpose of determine the candidate that exhibits the best match. The created template is applied as a running window of NxN size along the fundus image and the correlation between the template and the section of the image is calculated, the region with the highest correlation is selected as the OD region.

Dashtbozorg et al. [39] developed an automatic approach for OD segmentation using a multiresolution sliding band filter (SBF). A high-resolution SBF is applied to obtain a set of pixels associated with the maximum response of the SBF, giving a coarse estimation of the OD boundary, which is regularized using a smoothing algorithm. The algorithm segments the optic disc independently of image characteristics such as size and camera field of view and claims to be robust to variations of contrast and illumination, the presence of exudates and peripapillary atrophy caused by diabetic retinopathy, risk of macular edema, and the blurredness of images due to severe cataracts. The results on terms of overlapping score (S) are 0.88, 0.83 and 0.85 for MESSIDOR, ONH and INSPIRE-AVR datasets respectively. The algorithm was implemented using an

Intel CPU i7-2600k, 3.40 GHz, 8 GB RAM computer. The average running time was 10.6 s per image in the MESSIDOR dataset.

Wang et al. [40] used a template matching method to approximately locate the optic disc center, and the blood vessel is extracted to reset the center. This is followed by applying the Level Set Method, which incorporates edge term, distance-regularization term and shape-prior term, to segment the shape of the optic disc. Has advantages over the shape-based template matching method as it addresses the obstruction of the vessels inside the optic disc area and the intensity inhomogeneity. Authors reported a sensitivity of 93.24%, 92.58% and 94.65% on DIARETDB1, DRIVE and DIARETDB0 datasets respectively. The average computation time reported is 17.55 seconds for DRIVE, 18.25 seconds for DIARETDB1, and 18.3 seconds for DIARETDB0 on an Intel(R) Core(TM) i5-2500 CPU, clock of 3.3GHz, and 8G RAM memory PC.

Mary et al. [41] used an active contour model (ACM). An OD segmentation scheme is designed to infer how the performance of the well-known gradient vector flow (GVF) model compares with nine popular/recent ACM algorithms by supplying them with the initial OD contour derived from the circular Hough transform. This article gives a systematic performance comparison of a judicious choice of ten widely recommended ACM techniques, which are employed to segment the OD from 169 annotated retinal fundus images of various categories. The outcome of the study suggests that the GVF-based Xu-ACM initialized with the contour produced by the CHT outclasses the rest of the state-of-the-art variants of ACM. The result in terms of Hausdorff distance value is 33.49 ± 18.21 for RIM-ONE dataset.

Molina-Casado et al. [42] approach consists in a pre-processing stage including intensity normalization using a contrast stretching method and resizing of the original retinal image. Next, the detection of the set of OD candidates is done using correlation with template matching (TM). The template consists of a set of three squared shape objects with width of four times the OD radius size.

Finally, using inter-structure relational knowledge (i.e., distance relations with another retinal structures as macula and veins), false candidates are eliminated. The success rates reported were: 99.33% for MESSIDOR, 96.63% for Diaretdb1, 100% for DRIONS and 100% for ONHSD.

The approaches based on vessels-convergence and template matching proved to achieve better sensitivity rates than that achieved by the property-based methods, since the number of false responses were greatly reduced in the presence of other similar abnormal artifacts. But, on the other hand, such approaches obviously take more processing time than property-based methods [23].

Combination of methods

This group correspond to those OD segmentation methods that don't rely only on the OD's properties, convergence of vessels or matching a template. Instead they combine two or more of the above methods exposed.

Harangi & Hajdu [43] stated that there´s no reason to assume that any single algorithm would be optimal for the detection of various anatomical parts of the retina. It is difficult to determine which the best approach is, because good results were reported for healthy retinas but weaker ones for more challenging datasets containing diseased retinas with variable appearance of ODs in term of intensity, color, contour definition and so on. To overcome this, they studied and adapted some of the state-of-the-art OD detectors and finally organized them into an ensemble framework in order to combine their strengths and maximize the accuracy of the localization of the OD. Authors reported a sensitivity of 98.88%, 100%, 98.33% and 98.46% on DIARETDB1, DRIVE, MESSIDOR and DIARETDB0 datasets respectively.

Ren et al. [44] based the identification of OD location candidate regions on high-intensity feature and vessels convergence property. Secondly, a line operator filter for circular brightness feature detection is designed to locate the OD

accurately on candidates. Thirdly, an initialized contour is obtained by iterative thresholding and ellipse fitting based on the detected OD position. Finally, a region-based active contour model in a variationally level set formulation and ellipse fitting are employed to estimate the OD boundary. The reported sensitivity on MESSIDOR database was 98.67%.

Qureshi et al. [28] proposed an efficient combination of algorithms for the automated localization of the optic disc and macula in retinal fundus images. An ensemble of algorithms based on different principles can be more accurate than any of its individual members if the individual algorithms are doing better than random guessing. They suggested an approach to automatically combine different optic disc and macula detectors, to benefit from their strengths while overcoming their weaknesses. Authors reported a detection percentage of 97.79, 100 and 97.64 on DIARETDB1, DRIVE and DIARETDB0 respectively.

Basit & Fraz [45] method for automatic detection of the optic disc locus and optic disc boundary extraction is proposed based on morphological operations, regional properties, and marker-controlled watershed transform. The claimed advantages over other methods are: it works well on a vast variety of illuminations present in retinal images, it only extracts the main blood vessels centerline from the image and the combination of extracted vessels centerline and local maxima make the proposed method more tolerant to error for the optic disc location. The reported sensitivity on DIARTEDB1, DRIVE and CHASE_DB1 databases was 73.47%, 89.21% and 48.34% respectively.

Xiong & Li [46] approach has three main steps: region-of-interest detection, candidate pixel detection, and confidence score calculation. The features of vessel direction, intensity, OD edges, and size of bright regions were extracted and employed in the proposed OD locating approach. Authors claim that compared with the methods using vessel edge information only, the improvement on candidate pixel detection and the confidence value achieves promising results in the following situations: the images with dark OD due to uneven illumination

and low contrast; the retinal images with incomplete OD; the images with bright exudates, whose size and intensity are similar to OD. The results on terms of success rate of OD localization are 97.8%, 100%, 95.8% and 99.2% on DIARETDB1, DRIVE, STARE and DIARETDB0 databases respectively.

Haloi et al. [47] used a saliency map based method to detect the optic disc followed by an unsupervised probabilistic Latent Semantic Analysis for detection validation. The validation concept is based on distinct vessels structures in the optic disc. By using the clinical information of standard location of the fovea with respect to the optic disc, the macula region is estimated. Authors claim that this method gives 100% accuracy in optic disc detection in different challenging images with pathological symptoms. Reported detection accuracies are 100%, 100%, 98.8% on DIARETDB1, MESSIDOR and STARE datasets respectively.

Díaz-Pernil et al. [48] proposed a method where image edges are extracted using a new operator, called A Graphical P segmentation (AGP-color segmentation), which is a variation of the Sobel operator. The resulting image is binarized with Hamadani's technique and, finally, a new algorithm called Hough circle cloud is applied for the detection of the OD. The proposed algorithm considers the complete RGB color space for image processing and does not need any parameter to be fixed. Reported sensitivities for DIARETDB1 and DRIVE datasets are 91.8% and 89.9% respectively. The mean consumed time per image is 7.6 and 16.3 s for DRIVE and DIARETDB1, respectively. The algorithm was implemented on a computer with a CPU AMD Athlon II ×4 645 and 4 GB DDR3 to 1600 MHz of main memory.

Fan et al. [49] method employed supervised learning to train an OD edge detector by using structured learning. The edge detector is applied to the three channels of RGB and an optimal set of edge features is calculated automatically using the random forest classifier for each channel. Next, thresholding is performed on the edge map, obtaining a binary image of the OD. Finally, circle Hough transform is applied to approximate the boundary of OD by a circle. The

authors reported an overlap area of 0.86, dice coefficient of 0.91, accuracy of 0.97, and a true positive and false positive fraction of 0.91 and 0.01 for the MESSIDOR, DRIONS and ONHSD public datasets overall. The average computational time obtained for OD segmentation is 1.7494 s. The algorithm was implemented using a PC with an Intel (R) Core (TM) i-5 4210 M CPU at 2.60 GHZ and 4 GB of RAM.

Discussion

The optic disc segmentation algorithms were classified into four groups: property-based methods, convergence of blood vessels methods, model-based methods and combination of methods. However, direct comparison is difficult because different groups of researchers tend to use different metrics, image databases and number of images to train the classifier to measure the performance of their algorithms. Consequently, it is difficult to do a meaningful comparison among them. Despite using the same evaluation measures, different implementations of the metrics may influence the final results [50]. As a remark, it is important to differentiate between OD segmentation, OD localization and OD detection. OD detection output will be the position, or a bounding box of the OD if it exists in the image, while OD's localization goal is to delimitate the OD's region more accurately and OD segmentation is the process of assigning a label to every pixel in fundus image that belongs to the OD.

From the reviewed literature, the methods based on the properties of the optic disc (shape, brightness, size, etc.) achieved good results in fundus images where absent or slightly abnormalities were present, but these methods usually failed to detect the optic disc in pathological images where abnormalities, such as large clusters of exudates were present, confusing them with the optic disc due to their similar properties. Therefore, diverse OD segmentation approaches that not only rely on the properties of the optic disc were followed by researchers.

Among these approaches, a recurrent one is: convergence of blood vessels methods, which exploits information provided by the vascular tree of the retina, since the optic disc is considered as the convergence point of the major blood vessels. This group of methods achieve better sensitivity rates than those achieved by the property-based methods, since the number of false responses were greatly reduced in the presence of large clusters of exudates and bright artifacts. But, as a drawback, these approaches take more processing time than the property-based methods. Table 1 shows the summary of the reviewed OD location approaches. The methods marked in bold correspond to the best performing, taking into account the OD success rate and the number of datasets considered.

Author	**Dataset**	**Method type**	**#Images**	**OD success rate**
Pourreza-Shahri et al. [31]	DRIVE STARE	Property based	40 81	100 (78/81) 96.3
Rahebi et al. [32]	DIARETDB1 DRIVE STARE	Property-based	89 40 81	(84/89) 94.38 100 (88/89) 98.88
Soares et al. [36]	DIARETDB1 DIARETDB0 DRIVE e-ophtha-EX	**Convergence of blood vessels**	**89** **130** **40** **82**	**(88/89) 98.88** **(128/130) 98.46** **100** **(81/82) 98.78**
Wu et al. [38]	DIARETDB1 DIARETDB0 DRIVE STARE	**Convergence of blood vessels**	**89** **130** **40** **81**	**100** **100** **100** **100**

Wang et al. [40]	DIARETDB1 DIARETDB0 DRIVE	Model based	89 130 40	(88/89) 98.88 (126/130) 96.92 100
Molina-Casado et al. [42]	DIARETDB1 DRIONS OHNSD	Model based	89 110 99	(86/89) 96.63 100 (87/87) 100
Harangi et al. [43]	DIARETDB1 DIARETDB0 DRIVE	Combination of methods	89 130 40	(88/89) 98.88 (128/130) 98.46 100
Qureshi et al. [28]	DIARETDB1 DIARETDB0 DRIVE	Combination of methods	89 130 40	(87/89) 97.79 (127/130) 97.64 100
Basit & Fraz [45]	DIARETDB1 DRIVE	Combination of methods	89 40	(88/89) 98.88 100
Xiong & Li [46]	DIARETDB1 DIARETDB0 DRIVE STARE	Combination of methods	89 130 40 81	(87/89) 97.75 (129/130) 99.23 100 (77/81) 95.8
Haloi et al. [47]	DIARETDB1 STARE MESSIDOR	Combination of methods	89 81 1200	100 (80/81) 98.8 100
Díaz-Pernil et al. [48]	DIARETDB1 DRIVE	Combination of methods	89 40	(81/89) 91.8 (36/40) 89.9

Table 1. OD detection success rates (expressed in %) from the reviewed state of the art approaches for OD location.

2.3 Diabetic Macular Edema (DME)

Diabetic Macular Edema is an important complication of diabetic retinopathy and one of the worldwide leading causes of partial or total vision loss [51]. Diabetes Mellitus is the primary cause of DME and DR and is characterized by the appearance of pathologies and retinal vessel damage. In diabetes mellitus, the blood glucose level raises due to disturbance in insulin dynamics. The high blood glucose concentration affects the blood vessels along with the nerve cells inside the kidneys, brain, heart, and eyes. Worldwide, 93 and 21 million people are affected by DR and DME respectively, and their prevalence are of 6.96% and 10.2%, respectively [52].

All patients who have been diagnosed with diabetes, either type 1 or type 2, are at risk of developing DR and DME. DR is a progressive disease of the retina that involves pathological changes of the blood vessels, and consequently results in the presence of one or more abnormal features recognizable by a trained observer. The common abnormal features seen on fundus images (Figure 7) include microaneurysms, hemorrhages, hard exudates and cotton wool spots.

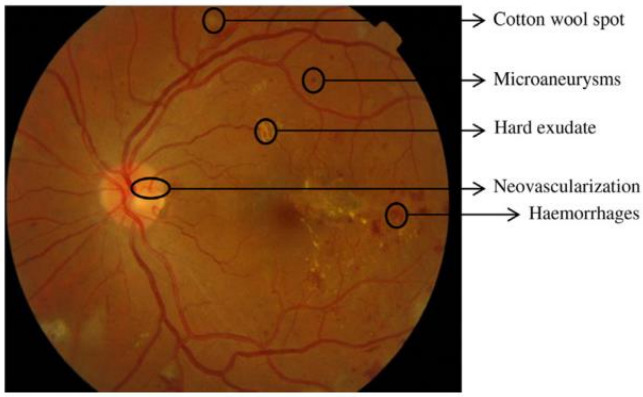

Figure 7. Common abnormal features seen on fundus images from DIARETDB1.

The progression of DR can be divided into several stages. First, as the blood glucose level increases, the permeability of the capillaries increases and there is a loss of elasticity of the endothelial capillary wall. This is the stage of mild non-proliferative diabetic retinopathy (NPDR). The appearance of microaneurysms is an early clinical sign of DR, which can be clinically seen as deep red spots varying from 15 µm to 60 µm in diameter. Microaneurysms are basically the saccular outpouchings of the capillary wall, most likely due to the loss of retinal capillary pericytes and thickening of basement membrane. There is a continuous turnover of microaneurysms over time, and the rupture of microaneurysms can give rise to the formation of intraretinal hemorrhages, which are seen as small pin point (dot) red spots. Hemorrhages are sometimes indistinguishable from microaneurysms and they can be classified together as 'intraretinal red lesions'.

With disease progression, there is an increase of intraretinal accumulation of fluid caused by the breakdown of endothelial tight junctions in microaneurysms or retinal capillaries in DR. This marked the retinopathy progression to moderate and severe NPDR in which vascular permeability and the capillary walls develop a thicker basement membrane, which is referred to as retinal thickening. The accumulated fluid in the retinal nerve fiber layer is termed "hard exudate" which appears clinically as well defined, yellowish white intraretinal deposits in fundus images. Exudates could be mistaken with cotton wool spots, which appear as puffy, yellow white spots in fundus images. They often look like exudates but are smaller and less defined. The formation of cotton wool spots is caused by a halt in axoplasmic flow in the nerve fiber layers. If the accumulation of fluid occurs in the macular region, then it is highly probable that Diabetic Macular Edema will develop. The macula corresponds to the central area of the retina, responsible for the most accurate, sharp and color vision due to its high density of photoreceptors and its size is approximately the radius

of one diameter of the OD. The fovea located at the center of macular region is accountable for visualizing fine details of a scene.

In clinical practice, ophthalmologists diagnose DME based on the presence of exudates in the macular neighborhood. DME is classified into Non-Clinically Significant Macular Edema (NCSME) and Clinically Significant Macular Edema (CSME) [53]. The presence of clinically significant DME is an important indication for the initiation of laser treatment. A description on the characteristics of DME severity is shown in Table 2. The patients with CSME will be affected with moderate vision loss, if untreated within 3 years [53].

Classification of DME	**Clinical findings**	**Location**
NCSME	Retinal thickening	Lesion present >1 and > One-disc diameter (1 DD) from the center of the fovea.
CSME	HE Haemorrhages with or without microaneurysms (HMA) Retinal thickening Blot Haemorrhages (HA) HE HMA	Lesion present <= 1 DD from the center of the fovea.

Table 2. Classification of DME severity

In Figure 8, the relevant regions that define the severity of DME are illustrated. Automated detection of the macular region, exudates and their respective locations are the crucial steps in the development of an automated diagnostic system for DME.

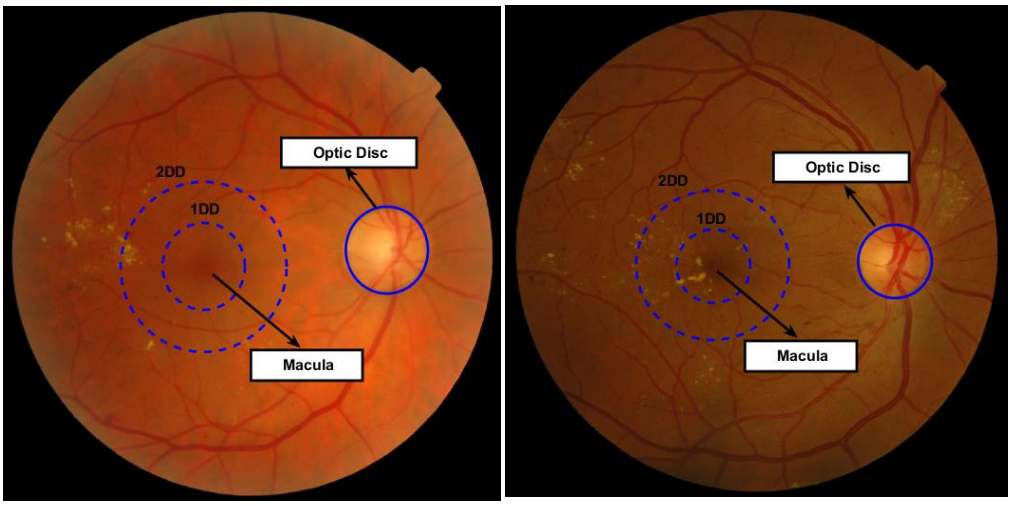

Figure 8. Typical fundus images of (from MESSIDOR dataset): (a) NCSME, and (b) CSME.

2.4 DME diagnosis using color fundus images

Early detection of the signs of DME can greatly reduce the chances of progression of vision loss with timely treatment. Hence, the research efforts for developing automatic methods that can aid in the early diagnosis of this disease. Since DME occurs when exudates reach the macula area, automated and reliable detection of macula and hard exudates are essential tasks of computer aided diagnostic systems for DME. There are several imaging techniques used for the clinical examination of DME, including: fundus ophthalmoscopy, fluorescein angiography (FA), biomicroscopy, color fundus imaging, optical coherence tomography (OCT), and retinal thickness analyzer (RTA) [53].

However, considering that fundus photography is economic and easily available [54], it is the most suitable technique for large scale image analysis and monitoring of DME. In the literature, there are several reported methods for the detection of macula, exudates and edema using color fundus images, next section includes a brief description of them.

2.4.1 Macula and fovea detection

In color fundus images, macula is identified as a darker object located on the temporal side of the optic nerve head. Since the macula contains the highest concentration of photoreceptors is responsible for visual acuity. Any damage in macula region or presence of abnormalities like exudates, cotton wool spots and red lesions could lead to loss of central vision. The progressive damage in the macula or presence of hard exudates near to macular region is an eye disease recognized as Clinically Significant Macular Edema (CSME).

Macula characteristics: The macula is a round area in the central region of the retina, which measures about 3 to 4 mm in diameter [55] and is responsible for central and high-resolution vision. In the fundus color images, macula can be observed as a darker/red-brown color oval-shaped object located on the temporal region of retina. An important characteristic of the macula region is that is devoid of vessels. Located at the center of the macula, there is a small depression that appears as a round dark area of approximately 1 mm of diameter, called fovea. Anatomically, the center of the fovea is located at the range of 2 to 2.5 optic disc (OD) diameters on average from the OD center [55]. The fovea radius is between one third and one fourth of the macula radius, and the macula radius is approximately equal to one OD diameter.

However, macula detection is not an easy task, as the whole macula area is not generally distinguishable in retinal color images. The contrast in the macular region is often low and it can be obscured by the presence of lesions, including large clusters of hard exudates and/or hemorrhages. On the other hand, the color and intensity of the macula varies greatly across individuals due to variations in the levels of pigment associated to factors such as ethnicity, diet, age and disease conditions. Algorithms for macula detection often fail when there is presence of large hemorrhages, as macula exhibits similar intensity/texture of red lesions.

From the literature review, macula localization methods can be categorized in three main groups: visual-based methods, positional constraints-based methods and hybrid methods.

Visual-based methods

In this category, there are included the approaches that attempt to find the macula using exclusively the visual properties of the fovea, i.e. intensity, size, shape and texture.

Akram et al. [56] approach consists of the detection of macula using a detailed set of features and Gaussian mixtures model-based (GMM) classifier. First, contrast enhancement on green channel is applied to improve the contrast of dark regions. Next, the binary map for possible macular region is created from above contrast enhanced image by applying a low adaptive threshold value. Blood vessels are extracted using the method reported on [57] and subtracted, so that, only the dark candidate objects remain. Next step is to extract for each candidate region a number of features. Finally, classification is done by using GMM. The author reported an accuracy of 97.2% for MESSIDOR dataset and 98.22% for HEIMED dataset.

Geetha et al. [58] proposed method avoids knowledge of other retinal structures and attempts data mining techniques to segment macula. Unsupervised clustering algorithm is used for this purpose. A heuristic based clustering in which initial centers are selected based on measures defining statistical distribution of data is incorporated in the proposed methodology. The approach comprises three stages: image pre-processing, data mining and image postprocessing. The pre-processing stage includes image cropping, green channel extraction, contrast enhancement using CLAHE and application of mathematical closing. Next, the pre-processed image is subjected to heuristic based clustering yielding a binary map. The binary image is post-processed

to eliminate unwanted components. Finally, the component which possessed the minimum intensity is determined as macula and its center constitutes the fovea. The authors reported accuracies following the 1R criterion of 100%, 100%, 96.92%, 97.75% 98.81%, 90% and 99.33% for HRF, DRIVE, DIARETDB0, DIARETDB1, HEI-MED, STARE and MESSIDOR, respectively.

Positional constraints-based methods

Positional constraint-based methods to locate the macula rely on obtaining an estimation of the fovea center location making use of its known anatomical features regarding its position on the retinal surface i.e. approximate distance from OD and the absence of vessels.

Kao et al. [59] proposed method, comprises four stages. In the first step, the fundus image is processed to find the region-of-interest excluding the dark areas around the fundus image. In the second step, the optic disc center is localized using a template matching method. In the third step, the disc–fovea axis (a line connecting the optic disc center and the fovea) is determined, based on the vessel-free region. Finally, the fovea center is located around the center of the disc–fovea axis by matching the fovea template around the center of the axis. Adaptive Gaussian templates were used to localize the centers of the optic disc and fovea for the images with different resolutions. The authors reported accuracy values of 93.1%, 92.1% and 97.8% for the DIARETDB0, DIARETDB1 and MESSIDOR databases, respectively.

Deka et al. [60] approach for macula detection consists in investigating the structure of blood vessels (BV) in the macular region. Macula localization process consists of pre-processing using CLAHE and detection of blood

vessels. For detection of BV 5th order Discrete Wavelet Transform (DWT) decomposition and morphological opening operation is applied. Next, using property of BV structure where the macula neighborhood is lack of BV whereas, maximum number BV present in the neighborhood of OD, a ROI that contains the macula is selected. Finally, the BV are removed from the ROI using morphological closing operation, the image is inverted and region growing is applied to segment out the macula region. The authors reported an accuracy 100%, 97.75%, 95.5%, 100%, and 96% for DRIVE, MESSIDOR, DIARETDB1, HRF, STARE datasets, respectively.

Hybrid methods

In this category are the methods that combine visual and positional constraint-based methods with the aim of exploiting the benefits of both techniques.

Aquino et al. [55] method comprises first, on an acceptable fovea center estimation by using a priori known anatomical features with respect to the optic disc and the vascular tree. For this purpose, the line delimiting the superior and inferior vessels defined as raphe is located using the method reported on [61], [62] and the fovea center is assumed to reside at a fixed distance along this line at 2.5 OD diameters from the OD center. Second, a morphological processing is employed to improve the obtained fovea center estimation when the fovea is detectable in the image; otherwise, it is declared indistinguishable and the first result is retained. The methodology was tested on the MESSIDOR and DIARETDB1 databases using of a distance criterion between the obtained and the real fovea center. Fovea center in the brackets between the categories Excellent and Fair (fovea centers primarily accepted as valid in the

literature) made up for 98.24% and 94.38% of the cases in the MESSIDOR and DIARETDB1, respectively.

Author	Dataset	Method type	#Images	Accuracy
Akram et al. [56]	MESSIDOR	Visual based	1200	97.2
	HEIMED		169	98.22
Geetha et al. [58]	DIARETDB1	**Visual based**	**89**	**97.75**
	DRIVE		**40**	**100**
	STARE		**81**	**90**
	DIARETDB0		**130**	**96.92**
	MESSIDOR		**1200**	**99.33**
	HEIMED		**169**	**98.81**
	HRF		**45**	**100**
Kao et al. [59]	DIARETDB0	Positional con-	130	93.1
	DIARETDB1	straints based	89	92.1
	MESSIDOR		1200	97.8
Deka et al. [60]	DRIVE	**Positional**	**40**	**100**
	MESSIDOR	**constraints**	**1200**	**97.75**
	DIARETDB1	**based**	**89**	**95.5**
	HRF		**45**	**100**
	STARE		**81**	**96**
Aquino et al. [55]	MESSIDOR	Hybrid	1200	98.24
	DIARETDB1		89	94.38

Table 3. Macula detection success rates (expressed in %) from the reviewed state of the art approaches for macula location.

Table 3 shows the summary of the reviewed macula location approaches. The methods marked in bold correspond to the best performing, taking into account the accuracy rate and the number of datasets considered.

2.4.2. Exudate segmentation

Exudates are constituted by the yellow deposits that leak from the blood vessels onto the posterior pole of the fundus image, these lesions are developed in diabetic patients when diabetes has remained uncontrolled a long time. Exudate detection acts as a marker in diagnosing DME.

Exudates characteristics: Exudates are yellow-white lesions with relatively distinctive borders. The exudates consist of lipids and proteins that flow from the damaged blood vessels of the retina. They appear as bright patterns and their contrast is high compared to the background. From a visual inspection, the exudates appear indistinctly yellowish with different sizes, shapes and locations, as shown in Figure 9. They are usually seen in bands, groups or in large circular structures.

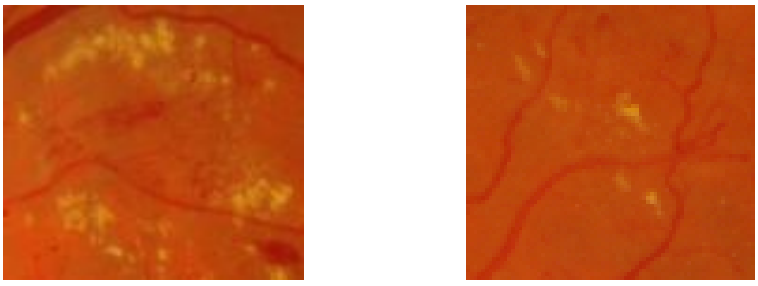

(a) (b)

Figure 9. (a) Circular cluster of hard exudates. (b) Flame-shaped hard exudates.

The segmentation methods for exudates, can be categorized in five groups: thresholding-based; morphology-based; region growing-based; supervised; and hybrid.

Thresholding based methods

Thresholding approaches employ local and global gray-level analysis to segment retinal exudates. Exudates have higher gray level compared to the nearby retinal background in the green component. Due to significant gray level change (shadows and poor illumination) in the whole image. It is quite difficult to find a global threshold that distinguishes the exudates from the background. Therefore, a local threshold is calculated for sub-windows of the fundus image, per its local histogram.

Garaibeh et al. [63] assumed that the color mode for image is bimodal where the number of pixels belongs to the background is much higher than the pixels that belong to exudates. A benefit from this feature is that the mean of the whole image is closer to the mean of the pixel that belongs to background. Then, subtracting, the mean of the whole image from the image will produce an image that mainly contains exudates. Then, they removed the noise using median filter. After that, a thresholding technique was applied to separate exudate pixels from others. A sensitivity of 92.1% was reported on DIARETDB0 dataset.

Reza et al. [64] proposed method made use of: preprocessing algorithms to make the bright object features more distinguishable from the background, markers to modify the gradient image that control over-segmentation and watershed segmentation to trace the boundary from the marker modified gradient. The advantages of the proposed method are: there is no need to select different threshold value for different test images those of which are varying with different brightness and contrast conditions (the method proposed in this study only

relies on H-minima, which requires a fixed threshold) and it automatically segments all bright lesions in a color fundus image with the possibility to distinguish between hard exudates and cotton wool spots. A sensitivity and specificity of 94.90% and 100% were reported for STARE and DRIVE dataset jointly.

Mathematical morphology-based methods

In the mathematical morphology-based methods, morphological operators are applied to identify structures with specific shapes (such as vessels). These structures are then removed, and exudates can be extracted.

Harangi et al. [65] proposed a method for exudate detection which combines the mainstream approaches within a single framework. Taking advantage of several image enhancement methods for recognizing the precise boundaries of candidates extracted by a morphology-based candidate extractor. The final exudate contour is found by a combination of contour candidates. Finally, a region-wise classifier is applied to decide whether the candidates should be considered as exudates or not. Sensitivity and specificity of 0.92 and 0.68 were reported for DIARETDB1 and sensitivity of 0.87 and specificity of 0.86 for HEI-MED dataset.

Esmaeili et al. [66] method is composed of three main stages and does not require user initialization and is robust to the changes in the appearance of retinal fundus images. Bright candidate lesions in the image are extracted by employing Digital CUrvelet Transform DCUT and modification of curvelet coefficients of enhanced retinal image. Since both optic disk (OD) and bright lesions are bright features in fundus images, in this work a new curvelet-based method is presented for OD detection and discrimination of bright lesions from rest of image in low-contrast color fundus images. A sensitivity of 98.4% and a specificity of 90.1% were reported on DIARETDB1 dataset.

Akram et al. [67] approach consists in generating a feature set for each region depending upon their shape, gray level, color and statistical based properties. The true MA regions are selected and classified using a hybrid classifier which is a weighted combination of multivariate m-Mediods, GMM and SVM. The main contribution of this work is that it improves the accuracies of all three stages using accurate vascular segmentation, sound feature set and hybrid classifier for accurate detection of MAs. The proposed method introduces the elimination of blood vessel pixels prior to MAs detection and enhances the feature space before applying the classifier. A sensitivity and specificity of 98.64% and 99.69% were reported for DIARETDB1 and DIARETDB0 datasets jointly.

Region growing based methods

For region growing based methods, spatial gray-level contiguity features are employed for retinal exudate segmentation. This segmentation approach examines neighboring pixels of initial seed points and determines whether the neighbor pixels should be added to the region.

Pereira et al. [68] applied a new approach for segmenting exudates based on Ant Colony Optimization (ACO). ACO is a branch of a larger field referred to as swarm intelligence and it is inspired by observation of the collective foraging behavior of real ant colonies. Using artificial ant colonies, the problem solutions are constructed within a stochastic iterative process by adding solution components to partial solutions. Each ant constructs a part of the solution using artificial pheromone, which reflects the ant's accumulated experience and heuristic information depending on the problem. A sensitivity of 0.80 and a specificity of 0.99 were reported on HEI-MED dataset.

Supervised methods

Supervised methods are literature's most frequent works. A feature vector is constructed for each pixel or pixel cluster, to be classified with a machine learning approach into exudates or non-exudates. The features are based on the color (typically gray level in green channel), brightness, size, shape, edge strength, texture, and contextual information of pixel clusters. Among the most frequent machine learning approaches are: neural networks [69], support vector machines (SVMs) [70], [71], [72], and the Naïve Bayes classifier [73].

Bhargavi et al. [70] used a combination of existing techniques in order to achieve better sensitivity, specificity and accuracy. The bilateral filtering is applied as a preprocessing step, contrast enhancement is done to increase the contrast between foreground with exudates and background elements like optic disk and vessels. To characterize the segmented lesions, texture features are used. Finally, they use a support vector machine classifier to distinguish the lesions and non-lesions images. 20 features are used for SVM classifier. A sensitivity and specificity of 100% and 94.6% were reported for DIARETDB1 and MESSIDOR datasets jointly.

Akram et al. [73] proposed a method for detection and classification of exudates in colored retinal images. The novel technique uses filter banks to extract the candidate regions for possible exudates. It eliminates the spurious exudate regions by removing the optic disc region. Then it applies a Bayesian classifier as a combination of Gaussian functions to detect exudate and non-exudate regions. Sensitivities of 99.5%, 97.72%, 93.7% and specificities of 98.35%, 96.15%, 98.38% were reported on DIARETDB1, STARE and DIARETDB0 datasets respectively.

Hybrid methods

This group correspond to segmentation methods that don't rely only on the lesions' properties (color, shape, size), matching a template or applying supervised learning only. Instead they combine two or more of the above methods.

Liu et al. [74] presented a location-to-segmentation strategy for exudate segmentation, with three stages: anatomic structures removal stage, exudate location stage and exudate segmentation stage. To describe the local texture structures of the exudate regions, the histogram of CLBP (Cluster Local Binary Patterns) is used, in which both the local difference sign and magnitude between the exudate pixel and neighboring background pixels are considered. An exudate region segmentation method from the located patches is proposed. Because the patches include both exudate regions and background regions and there exists high contrast between them, size is exploited prior and regional contrast prior about the exudate regions for segmentation. A sensitivity of 83% and a specificity of 75% were reported on DIARETDB1 dataset and a sensitivity of 76% on E-ophtha dataset.

Imani et al. [64] proposed a method for exudate detection based on Morphological Component Analysis (MCA) algorithm. This algorithm offers a signal separation method which utilizes sparsity property to separate the sources. The MCA was utilized to separate vessels from lesions in the retinal images for a separate analysis. By cleaning the retinal images, exudate lesions are easily segmented using dynamic thresholding and mathematical morphology. Sensitivities of 89.01%, 80.32% and specificities of 99.93%, 99.83% were reported on DIARETDB1, and E-ophtha datasets respectively.

Author	Dataset	Method type	#Images	Sensitivity/ Specificity
Garaibeh et al. [63]	DIARETDB0	Thresholding based	130	92.1 / -
Reza et al. [64]	STARE DRIVE	Thresholding based	81 40	94.9 / 100 jointly
Harangi et al. [65]	DIARETDB1 HEIMED	Mathematical morphology-based	89 169	92 / 68 87 / 86
Esmaeili et al. [66]	DIARETDB1	Mathematical morphology-based	89	98.4 / 90.1
Akram et al. [67]	DIARETDB1 DIARETDB0	Mathematical morphology-based	89 130	98.64 / 99.69 jointly
Pereira et al. [68]	HEIMED	Region grow-ing based	169	80 / 99
Bhargavi et al. [70]	DIARETDB1 MESSIDOR	Supervised	89 1200	100 / 94.6 jointly
Akram et al. [73]	DIARETDB1 STARE DIARETDB0	**Supervised**	**89** **81** **130**	**99.5 / 98.35** **97.72 / 96.15** **93.7 / 98.38**
Liu et al. [74]	DIARETDB1 e-ophtha-EX	Hybrid	89 82	83 / 75 76 / -

Imani et al. [64]	DIARETDB1	Hybrid	89	89.01 / 99.93
	e-ophtha-EX		82	80.32 / 99.83

Table 4. Exudate segmentation reported sensitivity / specificity (expressed in %) from the reviewed state of the art approaches for exudate segmentation.

Table 4 shows the summary of the reviewed exudate segmentation approaches. The method marked in bold correspond to the best performing, taking into account the sensitivity and specificity rates and the number of datasets considered.

2.4.3. Computer-Aided Diagnosis of DME using color fundus images and exudates location

Generally, computer-aided systems for the diagnosis of DME include three stages: pre-processing, macula detection and exudates segmentation. Pre-processing is done in order to enhance the image contrast and remove blood vessels. Morphological, texture and image-based features are extracted for macula and exudates classification. DME grading is performed either by identifying location of exudates from macula or using classification algorithms. The most recent methods for DME grading found in the literature are described below.

Acharya et al. [75] proposed method is based on Radon transform (RT), discrete wavelet transform (DWT) and discrete cosine transform (DCT). Pre-processing with CLAHE of the fundus image is followed by RT. Next, top-hat transformation is used to enhance the gradient of dark and bright pixels in the fundus image. The DWT and discrete cosine transform (DCT) are used to decompose

the sinogram image into various frequency coefficients. These coefficients are converted into 1D vector by arranging the coefficients in zig-zag manner. This 1D signal is subjected to locality sensitive discriminant analysis (LSDA). Finally, four supervised classifiers: decision tree (Dt), K-nearest neighbor (K-nn), Probabilistic neural network (Pnn) and Support Vector Machine (SVM) are used to classify the three classes normal, NCSME and CSME using significant features. The authors reported an accuracy of 97.01%, 88% and 94.16% for normal, NCSME and CSME cases, respectively.

Medhi et al. [76] proposed approach is implemented in two stages. The first stage involves preprocessing where illumination correction is applied to the input image and resizing to 768x576 resolution; next, the optic disc is masked to avoid false detection during bright lesion identification. The second stage comprises DME detection and its analysis. Here, the retinal lesions including microaneurysms, hemorrhages and exudates are identified by applying mathematical morphology processing to the green and hue plane color images. The macula and the fovea locations are determined using intensity property of processed red plane image. Different circular regions are thereafter marked in the neighborhood of the macula. The presence of lesions in these regions is identified to confirm positive maculopathy. Later, the information is used for evaluating its severity. The authors reported and average accuracy of 98.86% and an average specificity of 98.05% for DRIVE, Diaretdb1, MESSIDOR and HRF publicly available datasets altogether.

Marin et al. [77] proposed methodology consists in applying digital image processing algorithms to the retinal image in order to obtain a set of candidate regions to be Exudate (Ex), which are validated by means of feature extraction and supervised classification techniques. First, the fundus image is pre-processed for background homogenization, green channel pixels are corrected according to intensity and contrast values that are representative of the

background in its neighborhood, these values are estimated by mean and local standard deviation. Next, and adaptive noise-removal filtering is applied. The filter works with a small-sized neighborhood and a noise variance, set to the statistical mode of the local variance values. For candidate generation of exudates, adaptative global thresholding is applied. Optic disc is extracted using the methodology described in [37] to avoid false positives. Finally, a supervised classification process using a regularized local regression is applied to detect those regions considered as actual exudates. The features include, color and edge strength-based features and features based on responses from Gaussian and Difference of Gaussian (DoG) filter bank. The author reported a sensitivity of 90% and a specificity of 69.39% for MESSIDOR dataset.

Akram et al [56] proposed approach consists of a novel method for accurate detection of macula using a detailed feature set and Gaussian mixtures model-based classifier. The method consists of three phases: exudate detection, macula detection and grading of DME. In first phase, the all possible regions which may be considered as exudates are extracted and represented with a number of features. Morphological closing is applied to the fundus image to remove the effect of blood vessels and dark lesions. Next, an adaptive contrast enhancement technique [78] is applied, followed by the convolution with a filter bank based on Gabor kernel. Following, a binary map containing candidate exudate regions by applying adaptive threshold value using Otsu algorithm and then the OD is detected using averaging and Hough transform given in [79]. The features extracted for each candidate exudate region are: area, compactness, mean green channel intensity, mean hue, mean gradient magnitude, entropy, energy and third moment. Exudates are classified using a hybrid classifier combining GMM and SVM. In second phase, macula detection is performed by generating a detailed set of features and Gaussian mixtures model-based (GMM) classifier. In last phase, macular coordinates and location of exudates are used to grade the input image in one of the two stages of edema: Non CSME and CSME. The

classifiers are modelled at lesion level using randomly selected 70% of data as training and remaining 30% data as testing. The experiments are repeated 10 times and their average results are given. The authors reported an average value of 97.3%, 95.9% and 96.8% for sensitivity, specificity and accuracy for both datasets MESSIDOR and HEI-MED altogether.

Table 5 shows the summary of the reviewed DME diagnosis approaches. The method marked in bold correspond to the best performing, taking into account the sensitivity and specificity rates and the number of datasets considered.

Author	Dataset	#Images	Performance measure
Acharya et al. [75]	MESSIDOR	300	Acc=94.16%
Medhi et al. [76]	MESSIDOR	**694**	**SN=98.86%, SP=98.05%**
	DIARETDB1	**38**	**Jointly**
	DRIVE	**40**	
	HRF	**45**	
Akram et al. [56]	MESSIDOR	1200	SN=97.3%, SP=95.9%
	HEIMED	169	Jointly
Marin et al. [77]	MESSIDOR	1058	SN=90%, SP=69.4%

Table 5. DME reported performance measurement from the reviewed state of the art approaches for DME diagnosis.

Materials

3.1 Datasets and Groundtruth

Groundtruth consists in annotations performed by clinically qualified persons (specialized or specializing medical doctors, or other trained professionals for specific tasks), denoted as "experts". To be a reliable source of annotations from multiple experts should be included. In general, the image annotations are essential for training supervised algorithms, as well as for their evaluation and comparison. Such information is typically collected by manually annotating a set of images. Figure 10 shows an example of one of the images of DIARETDB1 dataset with their respective Groundtruth, which in this case corresponds to the exudates present in the whole image.

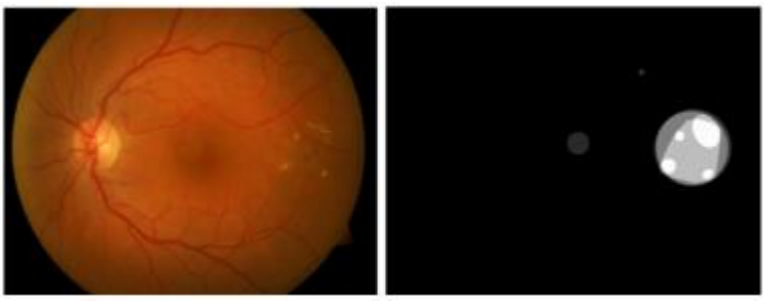

Figure 10. Original image (Left) and its respective GT (Right).

In the Table 6 the datasets found in the review are listed, including its name, number of images, resolution and groundtruth included.

Dataset name	**Dataset size**	**Image size (pixels)**	**Groundtruth**
DIARETDB1	89 images	1500x1152	Microaneurysms, Hemorrhages and exudates.

DRIVE	40 images	565x584	Vessels.
MESSIDOR	1200 images	1440x960, 2240x1488, 2304x1536	Retinopathy grading, exudates and optic disc
STARE	81 images	700x605	Vessels and optic disc
DIARETDB0	130 images	1500x1152	Microaneurysms, Hemorrhages and exudates
ONHSD	99 images	760x570	Optic disc
ROC	100 images	768x576	Microaneurysms
E-OPHTHA-EX	82 images	1440x960	Exudates
CHASE_DB1	28 images	999x960	Vessels
HRF	45 images	3504x2336	Optic disc and vessels
MESSIDOR-2	1748 images	1449x960	Optic disc
INSPIRE-AVR	40 images	2392x2048	Vessels
RIM-ONE	159 images	2144x1424	Optic disc
DRIONS	110 images	600x400	Optic disc
HEI-MED	169 images	2196×1958	Exudates
ARIA	143 images	768x576	Vessels, optic disc and fovea

Table 6. Datasets for DR segmentation.

3.2. Comparison difficulties

In the Figure 11 the comparison difficulties found among the methods reviewed are summarized.

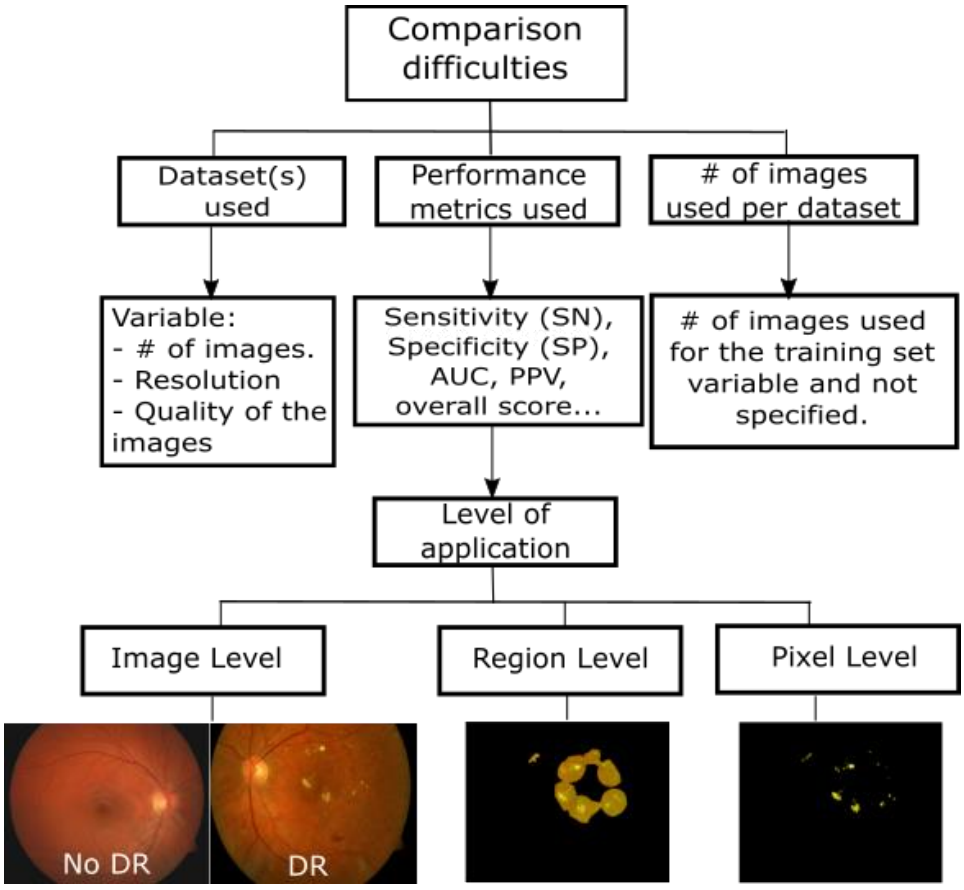

Figure 11. Comparison difficulties among methods.

3.3. Performance Measures

Diverse evaluation strategies are adopted depending on the type of algorithm under review. A diagnostic system with a binary output (healthy/ill) based on an image is typically evaluated against a Groundtruth using the Sensitivity (SN) and the Specificity (SP). Sensitivity is also referred to as true positive rate or recognition rate. It can be used to assess the percentage of positive cases that are correctly classified. Specificity is the true negative rate; that is, the proportion of negative cases that are correctly identified. The higher the sensitivity and specificity values, the better the diagnosis. Another figure of merit used for

the quantitative evaluation of the segmentation algorithms is done by calculating the Precision, Accuracy, Positive Predictive Value and F-score. These parameters are computed as:

$$Sensitivity\ (SN) = \frac{TP}{TP + FN}$$

$$Specificity\ (SP) = \frac{TN}{TN + FP}$$

$$Accuracy\ (Acc) = \frac{TP + TN}{TP + TN + FP + FN}$$

$$Precision\ (PE) = \frac{TP}{TP + TN}$$

$$Positive\ Predictive\ Value\ (PPV) = \frac{TP}{TP + FP}$$

Considering both the sensitivity and PPV, the mean F −score is computed by:

$$F - score = \frac{2 * SN * PPV}{SN + PPV}$$

Where:

TP (True positive): Correctly identified, namely, ill patient diagnosed as ill.
FN (False negative): Incorrectly rejected, namely, ill patient diagnosed as healthy.
TN (True negative): Correctly rejected, namely, healthy patient diagnosed as healthy.
FP (False positive): Incorrectly identified, namely, healthy patient diagnosed as ill.

In Table 7 these concepts are summarized, with an example of the possible outcomes of a diagnostic test for N number of subjects.

		True clinical status according to GT		Total
		Abnormal	**Normal**	
Result of the diagnostic test	**Abnormal**	True positives (TP)	False positives (FP)	**Abnormal= TP + FP**
	Normal	False negatives (FN)	True negatives (TN)	**Normal= TN + FN**
	Total	Abnormal cases = TP + FN	Normal cases= FP + TN	**TP+FN+FP+TN=N**

Table 7. example of the possible outcomes of a diagnostic test for N number of subjects.

Sensitivity in essence, measures how good an analysis is in finding any anomaly, if it exists, represents the actual proportion of positives that are correctly identified. *Specificity* is a measure against false positives, showing how reliable an analysis is, representing the proportion of negatives that are correctly identified. Since sensitivity is a more significant measure than specificity, most researchers propose highly sensitive schemes for the detection of DR [80].

Nevertheless, the majority of researches found in the literature use some of the figures of merit previously exposed, still is difficult to directly compare them. That is because, sensitivity and specificity can be applied at different levels:

Image level: sensitivity refers to the rate of images correctly identified as abnormal and specificity refers to the rate of images incorrectly Identified as abnormal.

Lesion level: Where TP is the area (in pixels) that truly identified lesions, FN is the area of lesion marked by the algorithm as normal, FP is an area marked falsely as lesion, and TN is the area truly identified as normal.

Pixel level: Used mostly for accuracy analysis. True positive (TP) is the number of lesion pixels correctly detected, false positive (FP) a number of no-lesion pixels which are detected wrongly as lesion pixels, false negative (FN) number of lesion pixels that were not detected and true negative (TN) a number of no-lesion pixels which were correctly identified as non-exudate pixels.

The calculation of sensitivity and specificity based on pixel classification is an impartment for comparison between different algorithms. For physicians, it is better to classify images as normal or abnormal. Abnormal image is an image that contains exudates and/or microaneurysms. Abnormal cases may need medical attention and follow up.

Receiver Operating Characteristic (ROC)

Originally, the ROC curves analysis was developed to evaluate the precision in the classification between signal and noise in the theory of signal detection, but recently this method has been adopted in several areas of research. In computer vision the ROC analysis is widely used, for example for the comparative evaluation of facial recognition algorithms [81] and in the methods of visual object categorization [82], but also the ROC analysis is recognized and used in the field of medical research [83], since it turns out that the ROC analysis is in agreement with the way medical decisions are made.

The ROC curve plots the fraction of sensitivity versus false positive rate (1-specificity). When the curve is closer to the top left corner, algorithm performance would be better. The Area Under the ROC Curve (AUC) is used as a measurement of this behavior Figure 13**.** To create the ROC curve, typically a thresholding parameter is varied. An example of a ROC curve is shown in Figure 12**.**

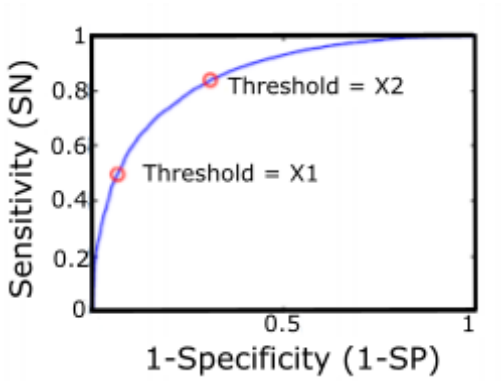

Figure 12. Receiver operating characteristic curve (ROC).[13]

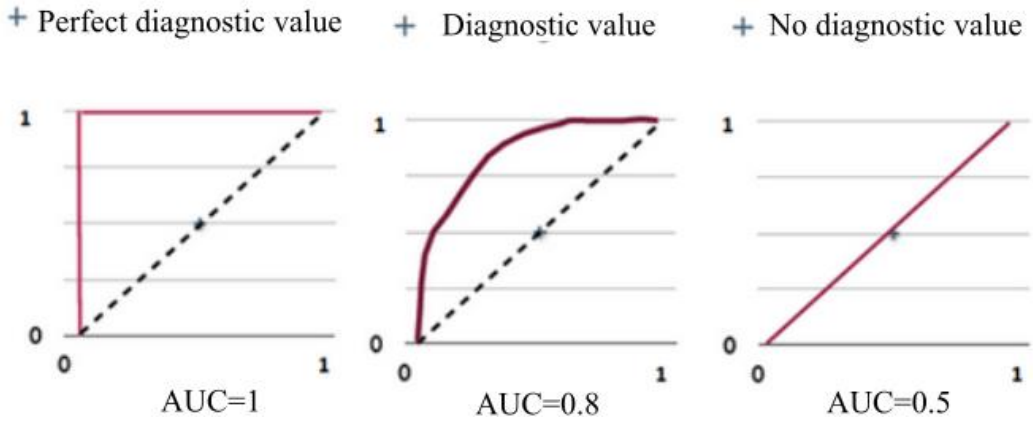

Figure 13. AUC values for different ROC curves.

A ROC curve demonstrates several things [84]:

1. It shows the tradeoff between sensitivity and specificity (any increase in sensitivity will be accompanied by a decrease in specificity).

2. The closer the curve follows the left-hand border and then the top border of the ROC space, the more accurate the test.
3. The closer the curve comes to the 45-degree diagonal of the ROC space, the less accurate the test.
4. The area under the curve is a measure of test accuracy.

Free-Response ROC Curve (FROC)

Region based analysis can be summarized using Free Response Operating Characteristic (FROC) curves. This is similar to ROC analysis, except that the false positive rate on the x-axis is replaced by the number of false positives per image. In this case a definition of a detected region is needed and a typical approach expects a 50% overlap between the annotated and detected regions to indicate a true positive.

Error function (Err2) (for Optic Disc only)

$$Err2 = \frac{1}{TP} \sum_{(x_{res}, y_{res}) \in ODR} d((x_{res}, y_{res}), (x_{man}, y_{man}))$$

Where $d((x_{res}, y_{res}), (x_{man}, y_{man}))$ is the Euclidean distance of the detected OD center (x_{res}, y_{res}) and the manually given OD one (x_{man}, y_{man}).

Oratio (for Optic Disc only)

$$Oratio = \frac{TP}{TP + FP + FN}$$

Jaccard coefficient (JC) (for Optic Disc only)

$JC(S_{exp}, S_{Real})$ is defined as the ratio between the intersection and union of the automatically obtained OD segmentation (S_{exp}) and the one considered as ground truth (S_{Real}):

$$JC(S_{exp}, S_{Real}) = \frac{\#\ (S_{exp}\ \cap\ S_{Real})}{\#\ (S_{exp}\ \cup\ S_{Real})}$$

Dice coefficient (DC)

$DC(S_{exp}, S_{Real})$ is defined as the size of the intersection of S_{exp} and S_{Real} divided by their average size:

$$DC(S_{exp}, S_{Real}) = \frac{2 * \#\ (S_{exp}\ \cap\ S_{Real})}{(\#\ (S_{exp}) + \#\ (S_{Real}))}$$

Overlapping score (S)

The overlapping score measures the common area between the OD region obtained using the automatic method (A) and the region delimited by experts (E), being defined by:

$$S = \frac{Area\ (A\ \cap\ E)}{Area\ (A\ \cup\ E)}$$

Methods

4.1 Optic disc Location

The location of the different normal ocular fundus structures such as: blood vessels, optic disc, macula and fovea, is a common task within most of the automated detection systems for the detection of the early signs of retinopathy diabetic and diabetic macular edema.

In particular, the location of the optic disc, which corresponds to the visible part of the optic nerve in the eye, is an important task in systems dedicated to the detection of exudates since the optic disc shares similar characteristics of color and brightness, which can cause sections of it to be potentially erroneous detected as exudates and therefore negatively affecting the system performance. This can be avoided if OD correct location is known in advance. Additionally, the state of the optical disc is important in diseases such as glaucoma, diabetic optic neuropathy and other pathologies related to the optic nerve.

In the fundus image, the optic disc is characterized as a circular bright region where the temporal and nasal veins emerge towards the eye, however, in retinal images containing exudates, the brightest circular region could not correspond always to the optic disc. For this reason, the methods that rely solely on finding the brightest circular region or the bright region with the highest variation, only present good performance in images of healthy retinas, but fail to correctly locate the optic disc in images containing exudates.

This chapter describes the proposed method for the optic disc location, including a previous performance analysis of some thresholding techniques for OD location in color fundus images, considering different image conditions and the effect of applying a previous preprocessing technique on the segmentation performance. The proposed OD location approach is based on OD's characteristic high intensity and a novel method for feature's extraction which aims to

represent the essential elements that define an optic disc by proposing a model for the pixel intensity variations across the optic disc (column wise).

Optic Disc properties

The optic disc or papilla is the most prominent feature of the fundus image, it corresponds to the region of the retina where the retinal cell fibers leave the eye to the brain forming the optic nerve. This area lacks sensitivity to light stimuli since it has neither cones nor rods, therefore it is known as point blind.

Although there is a significant variation in the appearance and size of the optic disc, it is clinically estimated that it has an average diameter of 1.5 mm [30] (about 1/30 of the retina area) and has a distinct appearance to the area of retinal tissue that surrounds it, since the absence of the pigmentary epithelium makes the color of the optical disc more pale than its surroundings. In the fundus images corresponding to healthy retinas, the optic disc is usually seen as a bright region of circular or elliptical shape traversed by veins and arteries.

Inside the papilla, there is a physiological excavation where there are no nerve fibers called cup. The ratio between the diameter of the cup and the diameter of the optical disc is less than 0.3 in healthy people. Retinal vessels emerge from the center of the optic disc. The central artery and vein of the retina are divided into two short branches, called superior and lower which in turn again divides in four branches, called superior nasal and temporal vein/artery and a lower nasal and temporal vein/artery. The arteries are thinner and present a less intense red than the veins. The diameter of a central vein when crossing the margins of the optical disc is approximately 0.125 mm (1/40 of the retina diameter) and is used as a measure of comparison in some retinal lesions [85].

The contour of the optic disc typically presents a variable contrast where usually the temporal zone is brighter than the nasal area, which can be observed

smaller. One aspect that is unique to each optical disc is the pattern which form the blood vessels when they cross the contour Figure 14.

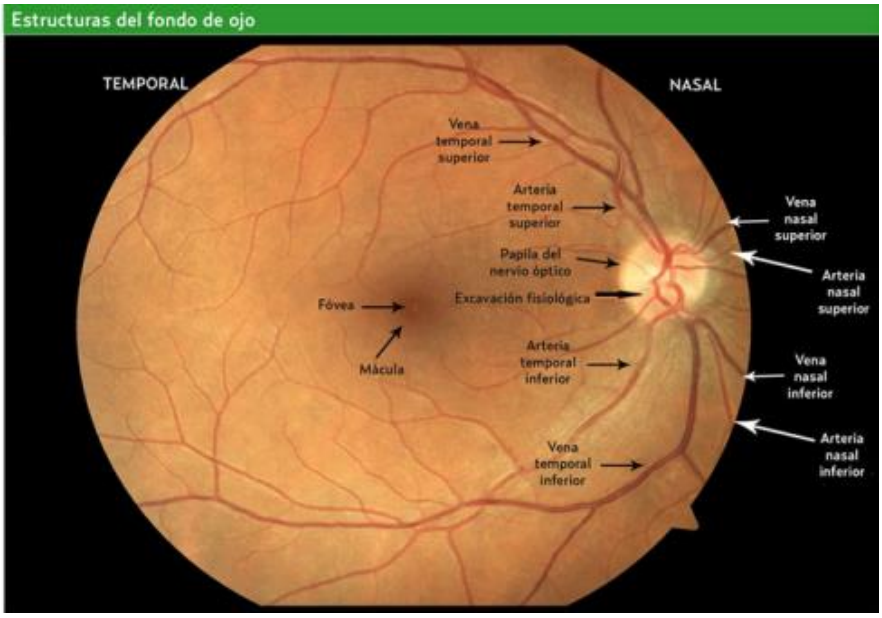

Figure 14. Normal fundus structures [85]

There are several factors that difficult the correct location of the optic disc, for example, in some of the images the edges of the optic disc are not clearly visible, in addition, some parts of the optic disc can be obscured due to the blood vessels that pass through it. Moreover, when there is presence of lesions such as exudates or severe lighting problems; the pixels that have the highest intensity values in the image do not always correspond to the optic disc, affecting the reliability of the OD location methods based solely on the intensity information.

Another problem present in the fundus images is the non-uniform illumination, and is attributed mainly to technical errors on the fundus photography protocol and/or due to the spherical shape of the eye, that affects the even distribution of the light beam of the external light source, as a result, the appearance of the edges of the optic disc are less distinguishable and/or blurred.

There may also be bright regions around the edge of the optic disc due to a disease called peripapillary atrophy Figure 15. It is important to consider these variations in appearance, size and location during the development of the methodologies for automatic detection of the optic disc. Figure 16 shows some examples of background images of the eye where different anomalies are observed in the appearance of the optic disc.

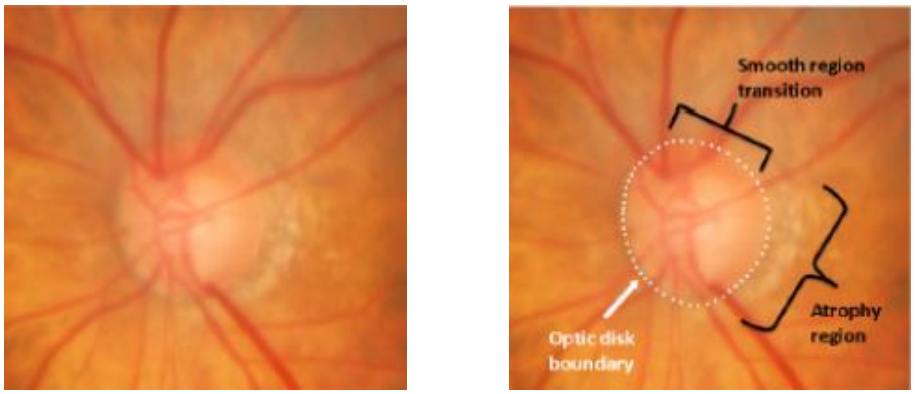

(a) (b)

Figure 15. a) Original fundus image b) Optic disc edge appears not defined and variation in hue can be observed due to peripapillary atrophy. [86]

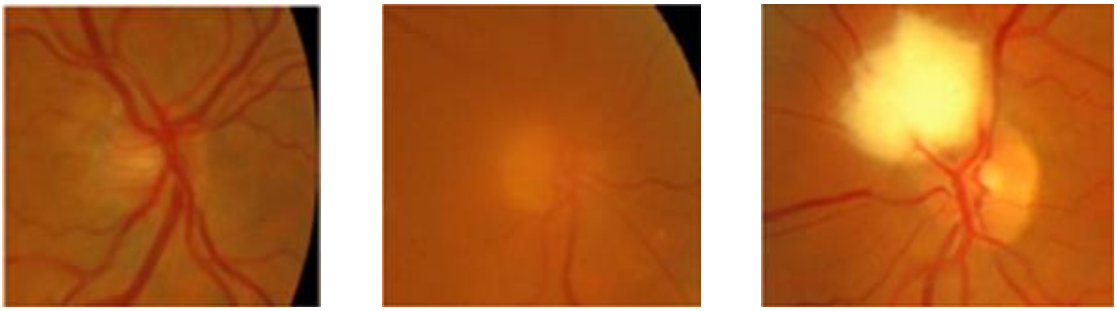

(a) (b) (c)

Figure 16. Abnormalities in the appearance of the optic disc. a) Non-uniform brightness b) Blurred appearance due to cataracts c) Myelinated optic nerve fibers connected at the edge of the optic disc. [81]

In synthesis, the shape, color and size of the optic disc can have great variation, especially in the presence of the typical lesions of diabetic retinopathy; therefore, location methods based solely on these properties present results that are not robust and unreliable. In the proposed location methodology, it is taken into account that the optic disc, besides being a bright circular/elliptical region, is the area of the retina where the main veins converge, characteristic that is invariable in the fundus images.

4.2 Analysis of thresholding techniques for OD location in color fundus images

As part of the research work, a review was published on a paper in 13th International Conference on Electrical Engineering, Computing Science and Automatic Control (CCE), Mexico, City, 2016, Mexico named “Thresholding Methods Review for the Location of the Optic Disc in Retinal Fundus Color Images” [87]. In this paper, thresholding methods are evaluated to locate the optic disc in color fundus image; different image conditions were considered i.e. quality and contrast and the effect of applying a previous preprocessing technique in order to evaluate the segmentation performance.

In the Figure 17, a common optic disc location scheme is shown, highlighting in red the segmentation and region of interest extraction, which was the scope of this analysis. The segmentation techniques analyzed were: the triangle method [88], mean peak method [89] and maximum entropy thresholding method [90]. These techniques were selected from a list found in [91], where 40 thresholding techniques are studied. The selection of these three methods was made on best results basis, found for optic disc segmentation on a group of DIARETDBv1 fundus images. CLAHE was selected for pre-processing, as is commonly used for improving the contrast of fundus images in the literature.

As green plane in the fundus image provides best contrast, it is used to extract the Region of Interest (ROI). To compare the performance of the three methods, we extracted the optic disc of the 89 retinal images in DIARETDBv1 dataset, these images constitute the Groundtruth.

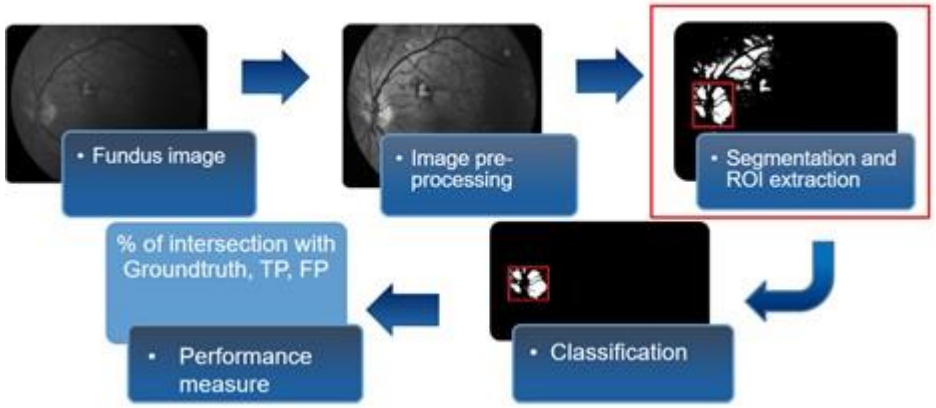

Figure 17. OD location scheme

The proposed analysis includes three main stages: first, the 89 images from DIARETDBv1 dataset were divided into 3 groups according with its quality and contrast, this is done to analyze how the condition of the image affects each thresholding method output. The second stage includes an analysis of the effect of applying a previous preprocessing technique. For this purpose, each thresholding method is applied to 2 versions of the image: first one is the original green channel of the image and the second one is the original green channel processed with CLAHE. The final stage consists of the thresholding performance comparison, and it is done by calculating the average intersection of the segmented area with the corresponding pixels of the Groundtruth. Figure 18 summarizes the proposed methodology.

The eye images are normally photographed in non-uniform lighting environments. Before we apply any image processing techniques for feature analysis, these images usually are pre-processed. CLAHE enhances the contrast of the

grayscale image by transforming the values. It operates on small regions in the image, called tiles, rather than the entire image. Each tile's contrast is enhanced, so that the histogram of the output region approximately matches the histogram specified by the 'distribution' parameter. The result of applying this technique over a fundus image is shown in the Figure 19**.**

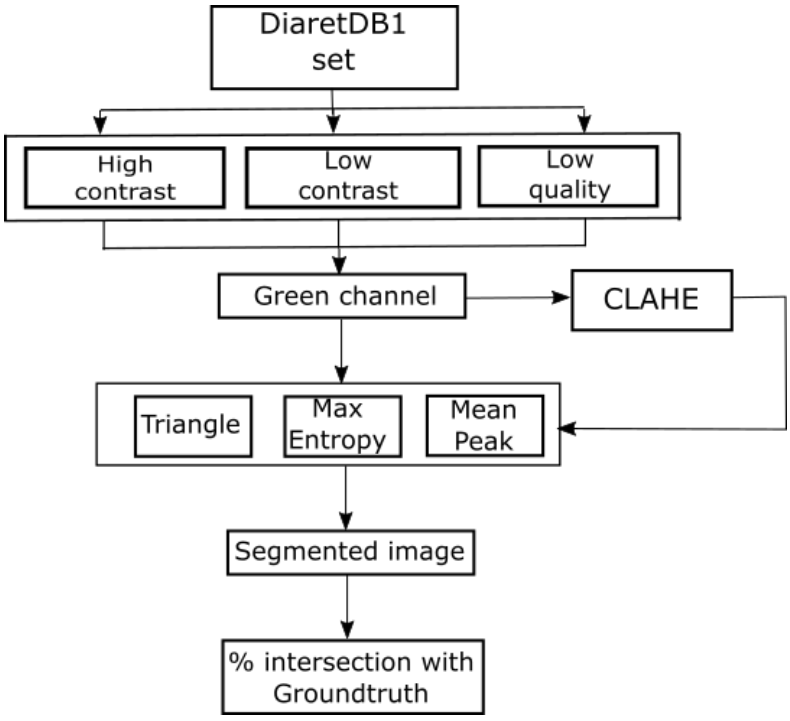

Figure 18. Methodology for OD location.

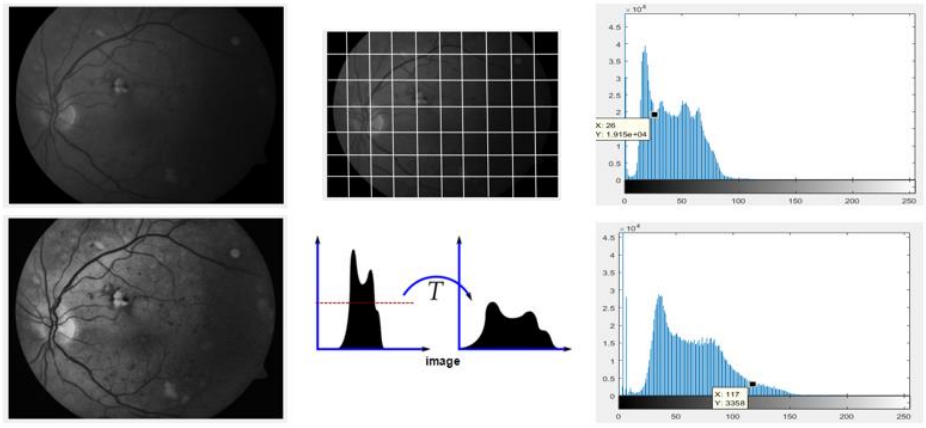

Figure 19. Pre-processing techniques: CLAHE.

Triangle thresholding technique is particularly effective when the object pixels produce a weak peak in the histogram. The result of applying this segmentation method over a fundus image is shown in the Figure 20.

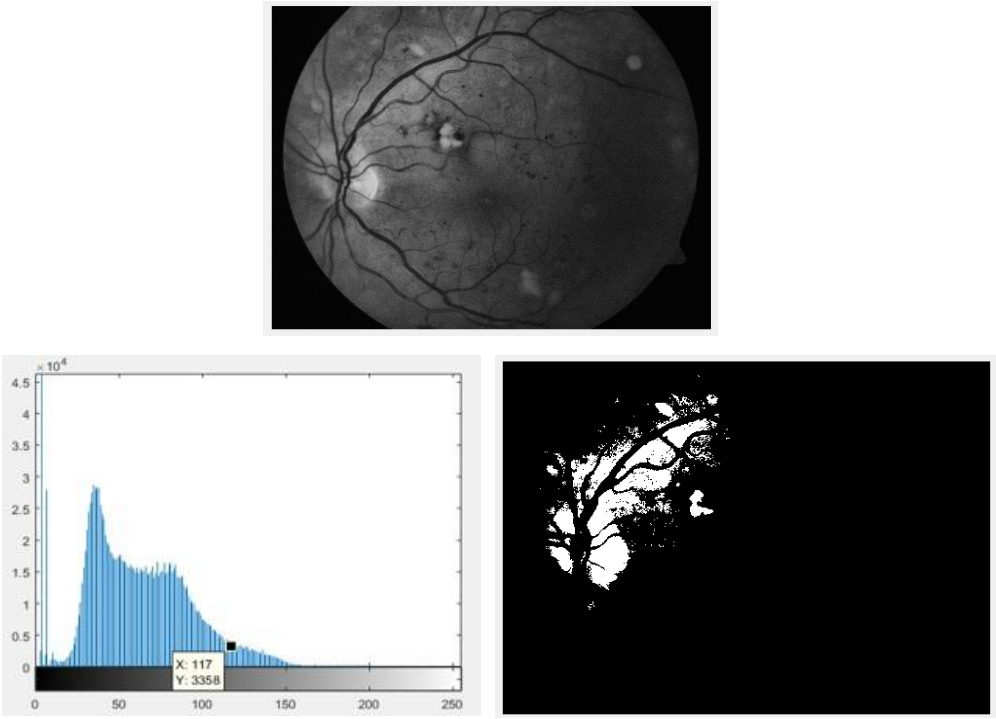

Figure 20. Segmentation methods: Triangle.

Mean Peak thresholding method is based on the form and shape properties of image histograms. The result of applying this segmentation method over a fundus image is shown in Figure 21**.**

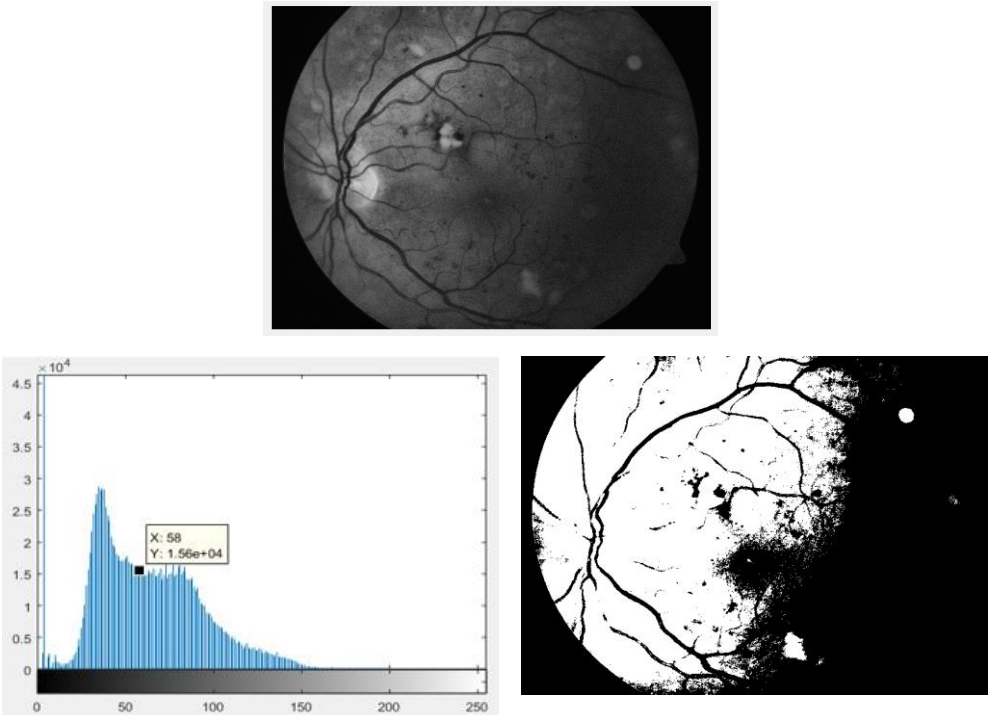

Figure 21. Segmentation methods: Mean Peak.

Maximum entropy thresholding method uses the entropy of the distribution of gray levels in the picture. The result of applying this segmentation method over a fundus image is shown in the Figure 22.

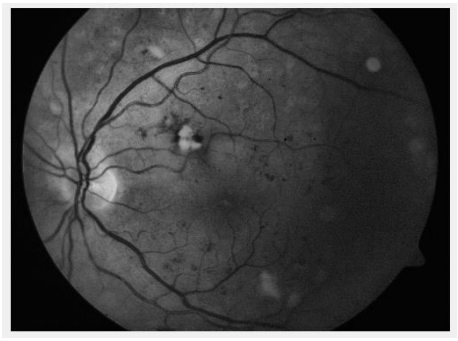

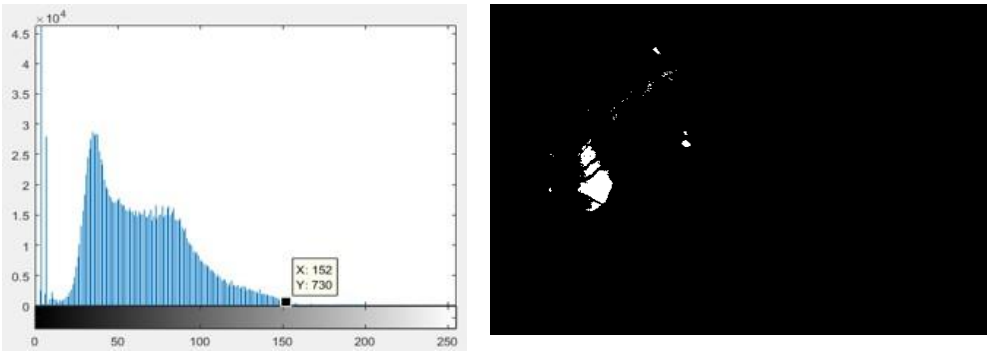

Figure 22. Segmentation methods: Maximum Entropy.

From the results obtained, in terms of OD location, CLAHE preprocessing shows a great improvement for all thresholding methods; passing from 25, 3, and 1 of 89 non-detecting ODs for Mean Peak, Maximum Entropy, and Triangle to 1, 0, and 0 respectively. From all results Triangle thresholding method performs consistently better than Maximum Entropy and Mean Peak. However, there is room to research for better methods in low-contrast and low-quality images for thresholding that improves a quality segmentation of optic discs in fundus images. On the other hand, the OD accuracy could be improved, discriminating candidate regions considering properties of the optic disc (e.g. its circular shape, presence of vessels, size, etc.). The proposed optic disc location method was developed taking into account these considerations, later in a section will describe the optic disc location approach proposed in detail.

4.3 Optic Disc Location methodology

The results of this work were published in the Biomedical Signal Processing and Control Journal with title: "Automated Optic Disc Location from fundus images: Using local multi-level thresholding, best channel selection, and an Intensity Profile Model" [92].

Most methods for the location of the optical disc fail when pathological lesions such as exudates [93] [82] occur, while others present a high computational cost [41][38]. In this chapter a new method is described for the location of the optic disc. The proposed methodology combines OD's characteristic high intensity with the unalterable fact that the optic disc is crossed for the arc formed by the main arcade of blood vessels, with this information, a profile pixel intensity variation for the OD is modelled. The methodology comprises four main stages: OD pixel region candidate generation, promising OD regions detection, promising candidate features extraction, and classification. The proposed method consists in a top-down approach, namely, a group of high intensity local regions with coarse level features are defined first and next finer features on extended regions with minimum requirements on size and intensity distribution are extracted. The flowchart illustrating the different tasks for each of the four main stages is shown in Figure 23, and will be detailed in the following subsections.

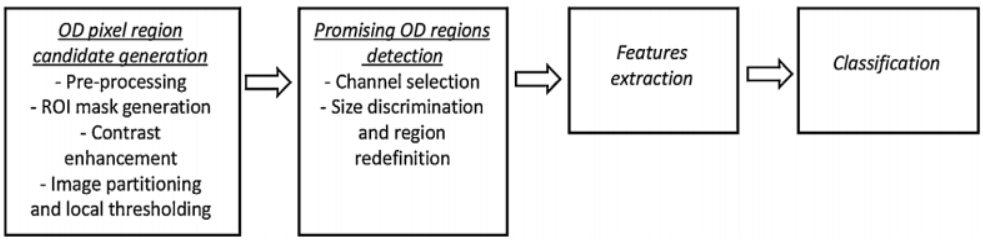

Figure 23. Overview of Optic disc location methodology.

- **OD pixel region candidate generation**

The main aim of this stage is to extract all the regions that present local high intensity values, in this way is ensured that all OD promising regions are considered for the subsequent processing stages. The tasks involved in this stage, include: (1) preprocessing, (2) region-of-interest mask generation, (3) contrast enhancement and (4)

image partitioning and local thresholding. Table 8. describes the steps of the algorithm to generate the OD pixel candidate.

As stated before, fundus images quality varies greatly due to many external and internal factors i.e. fundus camera settings, illumination conditions, spherical geometry of the eye. To mitigate these undesired effects preprocessing is applied to the fundus image. To improve softness of the image, a median filter of size 3 × 3 is applied. The filter of the median is selected because it allows to eliminate artifacts and unwanted structures in the image without significantly affecting the edges.

Algorithm 1: Candidates generation	
	input : Original image of dataset (Diaretdb0, Diaretdb1, e-ophtha)
	output : Image containing potential OD regions (ImgC)
1	Preprocess image for noise reduction
2	Mask out left and right dark region of the image
3	Redefine initial and final column excluding masked region
4	Determine OD's Diameter estimate
5	Enhance contrast of the green channel
6	Use one horizontal and three vertical bands for most probable OD location
7	**Begin**
8	**for** each vertical band
9	Use 3 threshold bands from maximum to mode pix value
10	Generate a RGB (ImgC) for the three bands
11	Red is high threshold band
12	Green is medium threshold band
13	Blue is low threshold band
14	**end**
15	**End**

Table 8. Algorithm to generate the OD pixel candidate.

Median filter operates replacing the value of a pixel f(x,y) with the median of all of the pixels in the neighborhood of that pixel as shown in Equation 1.

$$f_{med}\,(x,y) = median\,\{f(s,t)\}, sz\,\epsilon\, I\ odd\ and\ greater\ than\ 1,$$
$$s = \left\{ x - \frac{sz-1}{2}\ to\ x + \frac{sz-1}{2} \right\} and\ s \neq x,$$
$$t = \left\{ y - \frac{sz-1}{2}\ to\ y + \frac{sz-1}{2} \right\} and\ t \neq y$$

Equation 1. Median filter

The ROI rectangle refers to the resulting fundus image where the surrounding dark zones are excluded. These dark areas are removed to save computing time and to reduce noise. The semi-circular foreground region is referred as ROI. The mask image is a binary image where the ROI pixels are set to one and the background pixels to zero. On Figure 25, the stages for ROI rectangle extraction using the image on Figure 24, are shown. ROI rectangle for the original image is generated as follows:

(1) The pixels with intensity value below 10 on channels red and green are set to zero for the purpose to smooth the non-retina zone. (2) A range filter with a 15x15 window is applied. Range filter is used to enhance the borders of the image, as the highest values correspond to the regions with the highest local variation, the result is shown in Figure 25(a). The range filter is defined by Equation 2. (3) The 20 percent highest intensity pixels values are segmented Figure 25(b). (4) A sum of pixels by column is done, and the rightmost and leftmost peak values with value higher than one fifth of the image height are selected as ROI first 'c_0' and last 'c_1' column coordinates. Rows range are reduced to the 70 percent central band, given that no OD will be at top or bottom 15 percent. As given in Equation 3.

$$Range\big(A(x,y)\big) = \max[A(x+i, y\ +j)] - \min[A(x+i, y\ + j)],\ \ where\ i,j\ \epsilon\ \left(-\tfrac{sz-1}{2}\ to\ \tfrac{sz-1}{2}\right),\ sz\,\epsilon\, I\ odd\ and\ greater\ than\ 1$$

Equation 2. Range filter.

$$ROI_{height} = [0.15 * height\ to\ 0.85 * height,\ c_0\ to\ c_1],$$
$$ROI_{width} = c_0 - c_1 + 1$$

Equation 3. ROI width and height definition.

OD diameter approximate value, is defined as $Diam = \left\lfloor \frac{ROI_{width}}{6} \right\rfloor$.

Figure 24. Original fundus image.

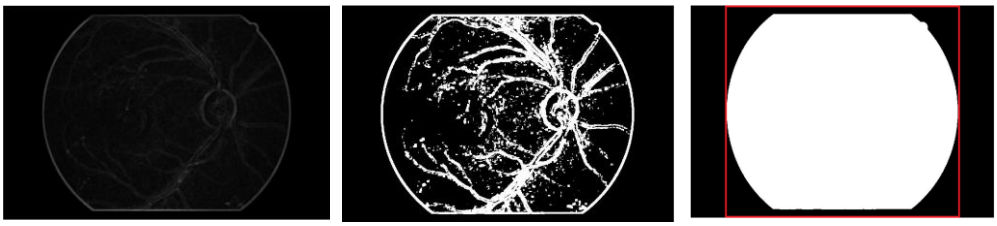

(a) (b) (c)

Figure 25. (a) Result of applying a range filter with a 15x15 window. (b) Result of applying a threshold of the highest 20 percent of image (a). (c) Region-of-interest (ROI) rectangle (red).

From the previous analysis, CLAHE showed promising results for improving the contrast and the OD thresholding results. Other conventional methods based on the global histogram of the image such as contrast stretching and histogram equalization, tend to result in loss of information in the brightest areas as well as in the dark areas of

the background image. CLAHE operates in small regions of the image, improving the contrast by local equalization of the histogram, whereby small regions of interest are highlighted throughout the image. To enhance contrast of the fundus image, CLAHE is applied to the green channel of the ROI rectangle.

As mentioned earlier, non-uniform illumination induces undesired local intensity variations, hence the application of a global high intensity threshold value to locate the OD region is not reliable. To extract more meaningful information from the fundus image, a partition into windows or sub-images for the extraction of local OD candidate regions is applied. The image division is done accordingly to the previously estimated OD diameter: one horizontal band and three vertical bands are defined based on OD's diameter. For each of the three bands, a threshold based on the maximum and the mode intensity value is calculated. Using the green channel, the sub-divisions and local threshold values are defined as:

$$\text{Horizontal band: } \boldsymbol{winR} = [1.25 * Diam \ to \ imageHeight - 1.75 * Diam]$$

$$\text{Vertical bands: } \boldsymbol{winC} = \{ [c_0 \ to \ 1.75 * Diam], (1.75 * Diam \ to \ 3.75 * Diam], \ (3.75 * Diam \ to \ c_1 \ ]\}$$

$$\boldsymbol{delta} = \frac{window \max value - window \ mode \ value}{4.75}$$

$$\boldsymbol{threshold} = window \max value - delta$$

For each of the three defined sub-regions, the pixels with intensity values higher than their local *threshold*, are considered as possible OD regions, and together conform the image containing the OD candidates (Img_{ODcand}). On Figure 26, an illustration of fundus image partitioning along with the result of applying their local thresholding is shown.

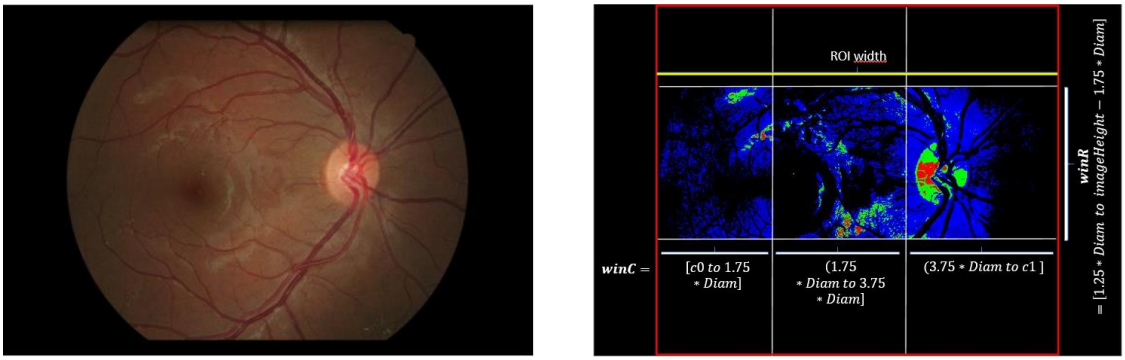

(a) (b)

Figure 26. (a) Original fundus image (b) Image partitioning and local thresholding. Img_{ODcand} is the set of all red sub-regions.

- **Promising OD regions detection**

Once all the relevant local high intensity regions are extracted, more detailed features select most promising ones. The approach consists in going from a group of regions with coarse level features to finer features on extended regions with minimum requirements on size and intensity distribution. The steps to select regions with better characteristics to contain an OD, include the channel selection, which is done by selecting the one with better contrast between red and green channels. For contrast evaluation, the image is partitioned, a median filter of size 7 × 7 is applied to both channels and an index based on the difference between the maximum intensity and the mode value of each subregion is calculated by Equation 4.

$$ic = \frac{maximum\ intensity\ value - mode\ value}{mode\ value}$$

Equation 4. Index for contrast evaluation

As high contrast images show a wide distribution of gray levels in their histograms, and as mode intensity value is an approximation of the background intensity value (retinal tissue), the higher *ic* index indicates the channel which has a major level of differentiations between the background and the bright structures of the retina, including the OD. The channel with better contrast between green and red is selected for posterior processing.

As the images from the datasets present different resolutions, all the size constraints are defined with respect to the *Diam* value, in this way the proposed methodology is independent from image resolution. For the size discrimination of the region candidates from $Img_{ODcand,}$ a minimum of (1/20)**Diam* and a maximum of *Diam* for height and width is established. Then, to analyze the local distribution of each remaining region candidate, is necessary to center around the pixels with higher intensity and extend the size to match with the actual OD size. The center is calculated using the '*WeightedCentroid*' concept, which considers pixel intensities in the image region as weights in the centroid calculation, intensities used are defined by the yellowish proportion of pixels in the region. Then, the region is extended around the centroid coordinates by half of Diam. Next, a threshold value is calculated for each candidate:

$$diff = (maximum\ value - mode\ value)$$

$$delta = \begin{cases} \frac{diff}{4.75}, & if\ diff > 30 \\ 6\ , & if\ diff \leq 30 \end{cases}$$

$$Threshold_e = maximum\ value - 3 * delta$$

$Threshold_e$ aims to segment a high intensity section of the histogram, as generally optic disc cup shows higher intensity than OD. The resulting regions again are filtered by size: minimum and width and height of Diam/10 and Diam/8, respectively.

Remaining regions are extended by *Diam*/9 on each side and height by *Diam*/2 at the top and bottom. A profile consisting of the maximum intensity values per column is calculated for the remaining extended regions, mean value of this profile is defined as *avgChx*. Figure 27 (a) gives a candidate region and (b) shows its profile of the maximum intensity values per column. Promising OD regions are selected if prominences above *avgChx* have width higher than *Diam/10*.

(a)

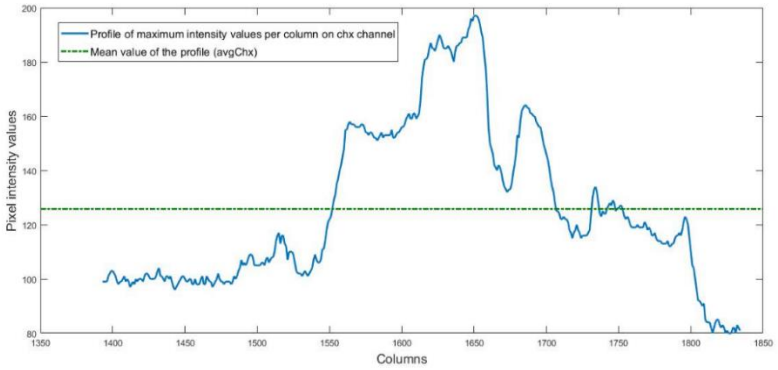

(b)

Figure 27. a) OD candidate region (b) Profile of the maximum intensity values per column on chx channel for image (a).

- **Feature's extraction**

  The purpose of this stage is to calculate a set of features for all the regions labeled as promising OD regions. Feature's extraction step is applied for cases where there is more than one candidate OD region on a fundus image as detailed in Figure 28.

  The proposed method for feature's extraction aims to represent the essential elements that define an optic disc by modelling the pixel intensity variations across the optic disc (column-wise). On an ideal fundus image quality and illumination conditions, OD's column-wise intensity change behavior could be seen as an stable left-background zone (LB), followed by the border of the first bright OD section

(LL), where the intensity difference will be positive growing, next change in intensity difference will be expected when the vein is reached (V), where it is expected that the intensity difference will negatively grow until the limit of the second bright OD section is reached (RL), at which point again the intensity difference will be positive growing until the OD border is reached where the intensity difference will negatively grow until the right-background zone (RB) is reached where the intensity difference will be stable again.

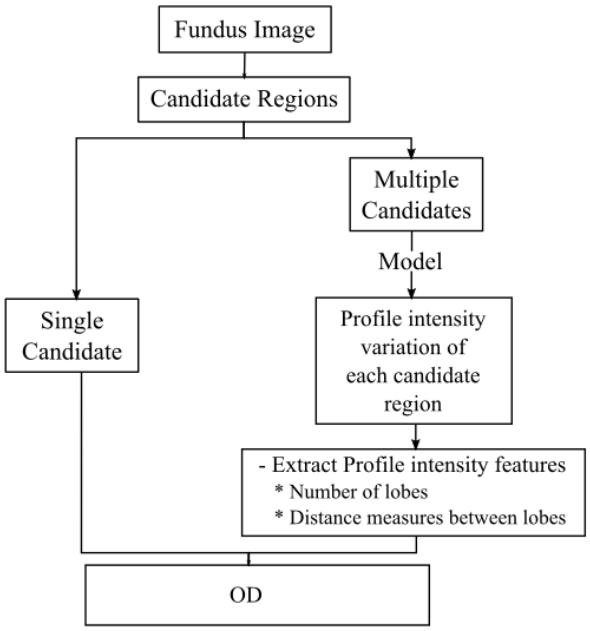

Figure 28. Overview of the proposed steps for feature's extraction.

Modelling this column wise pixel intensity variation of an optic disc as depicted in Figure 29 where we highlight the five change sections previously described as LB-LL-V-RL-RB. These five sections and their distances will be the set of features to distinguish between the OD and the other candidate regions.

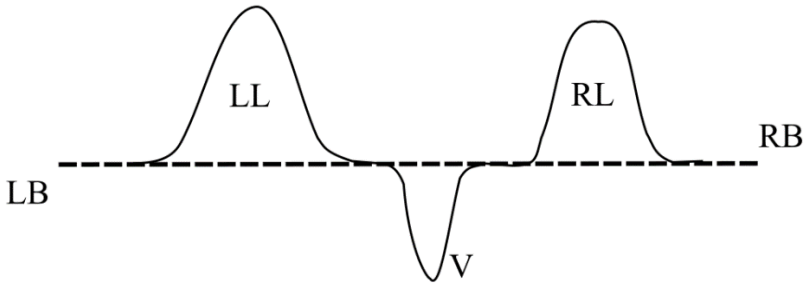

Figure 29. Profile pixel intensity variation column wise model of an ideal OD.

Where: Left-Background (*LB*), Left-Lobe (*LL*), Vasculature (*V*), Right Lobe (*RL*) and Right Background is (*RB*).

The steps used to model the column-wise pixel intensity variation profile Figure 29 are: (1) Pre-processing candidate regions. (2) Redefining possible OD pixel region. (3) Candidate image regions segmentation using Superpixels. (4) Calculate column-wise pixel intensity variation profile.

In order to highlight the veins, a minimum filter with window size of 7 is applied to the green channel of each candidate region, then to improve region contrast, a scale factor (*sf*) is applied. *sf* is calculated as:

$$sf = \frac{255}{Maximum\ pixel\ value\ on\ the\ candidate\ region}$$

In general, we observed that candidate OD regions often contain large zones of background and undesired artifacts due to low quality and the non-uniform illumination. Knowing that borders can be seen as high intensity changes in contiguous pixel positions and aiming to redefine a region whose column limits correspond to the OD borders, we calculated for each pre-processed candidate region, the profile of maximum pixel intensity values per column (Figure 30. blue) and its difference per columns

(Figure 30. red). The highest difference values define what is expected to be the OD borders (positive for left-border) and negative for veins and right-border positions (Figure 30. yellow). The new limits for the columns of the candidate regions are defined by the leftmost and rightmost positions of up to seven highest absolute differences considered as relevant (Figure 31).

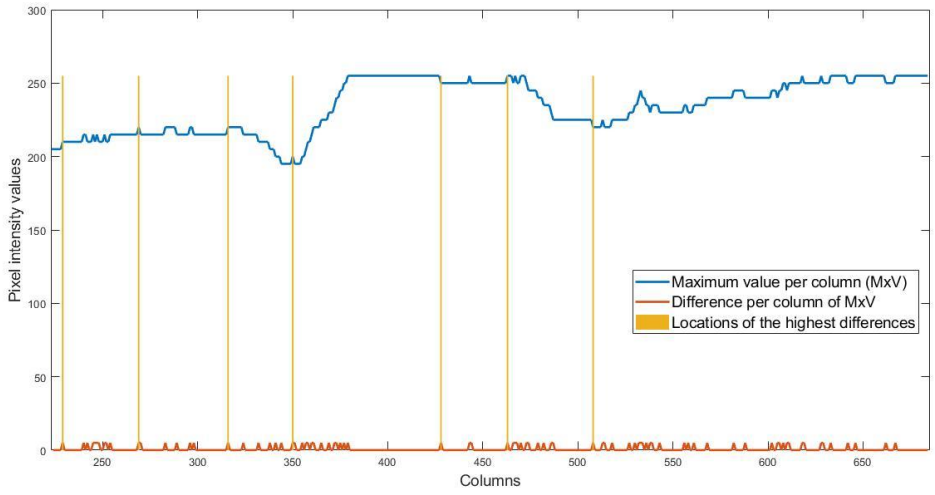

Figure 30. Maximum pixel intensity values per column (blue), intensity difference per column (red), column locations of the highest difference values (yellow).

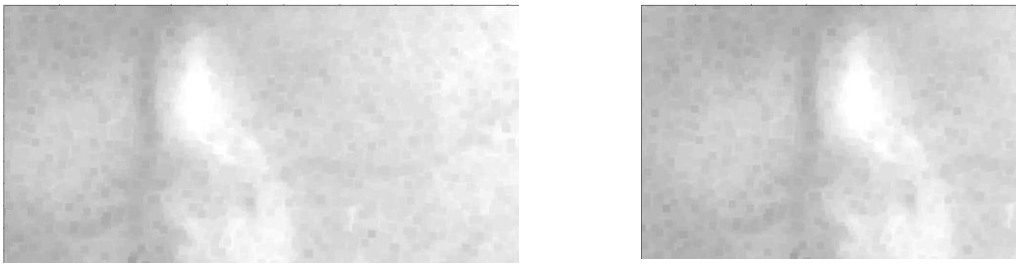

(a) (b)

Figure 31. (a) Pre-processed candidate image region. (b) Pre-processed candidate image region with redefined column limits.

The concept of superpixel was first introduced by Xiaofeng Ren and Jitendra Malik in 2003 [97]. Superpixels segmentation aims to group connected pixels with similar gray levels to create visually meaningful pixel regions while heavily reducing the amount of data for subsequent processing steps. The clustering method selected for the superpixel segmentation was the simple linear iterative clustering (SLIC) algorithm [98] and the number of superpixels for each candidate image region is set to 15. Figure 32 (a) shows the result of applying the superpixel segmentation to a candidate region. The image in Figure 32 (b) correspond to set each pixel intensity value of a superpixel region to the value of the mode of the region, this new color representation of the superpixel regions has the intent of reduce intensity variability.

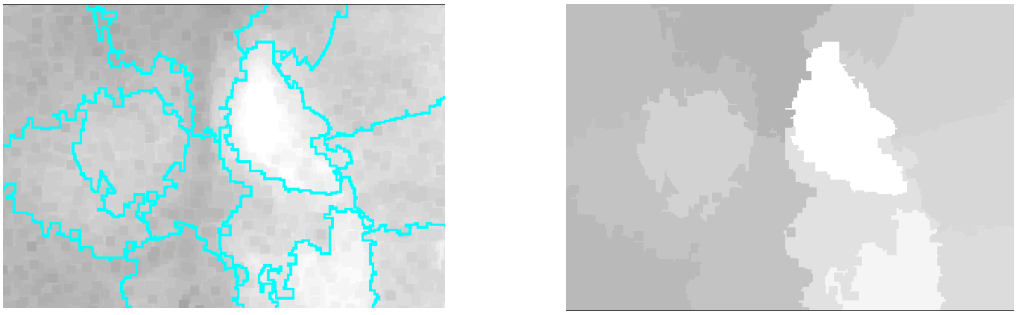

(a) (b)

Figure 32. (a) Superpixel segmentation of the candidate image region. (b) Each superpixel region value is set to its mode value (Imgspxls).

To represent the column wise pixel intensity variation, first, the maximum intensity value per column is calculated as depicted in Figure 33 (b). Next step is calculating the difference per column of the maximum intensity values as shown in Figure 33 (c) and finally, to soften details, a moving mean filter with a size of the expected vein diameter (*OD radio/10*) is applied to the differences profile Figure 33 (d). This final profile (*Diff_Profile*), will be the profile which will be compared with the profile pixel

intensity variation column wise model of an ideal OD (Figure 29) for optic disc candidate region classification.

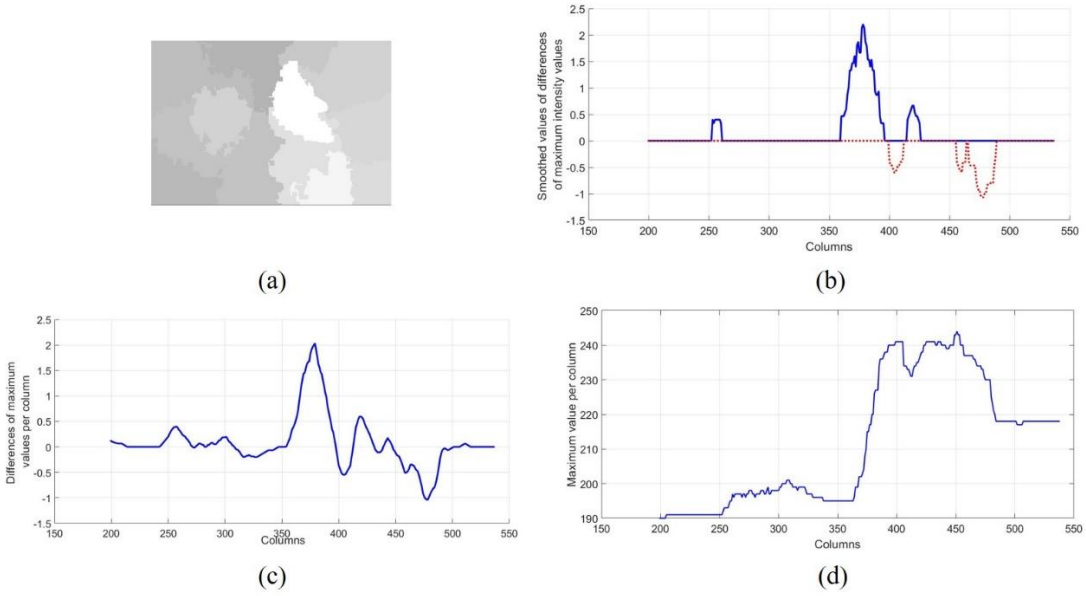

Figure 33. (a) Imgspxls. (b) Maximum intensity value per column of Imgspxls. (c) Difference per column of the maximum intensity values (d) Diff_Profile, result of applying a moving mean filter with a size of the expected vein diameter (OD radio/10) to (c).

- **Feature's set and classification**

The pattern on *Diff_Profile* that defines an Optic disc region is the presence of a Left Lobe (LL), a Right Lobe (RL) and Vasculature (V) between them, the distances from LL to V and V to RL must correspond to approximately (2/3) OD diameter and (1/3) OD diameter in any order. A sample of this behavior in a true OD region candidate is depicted in Figure 34 (c).

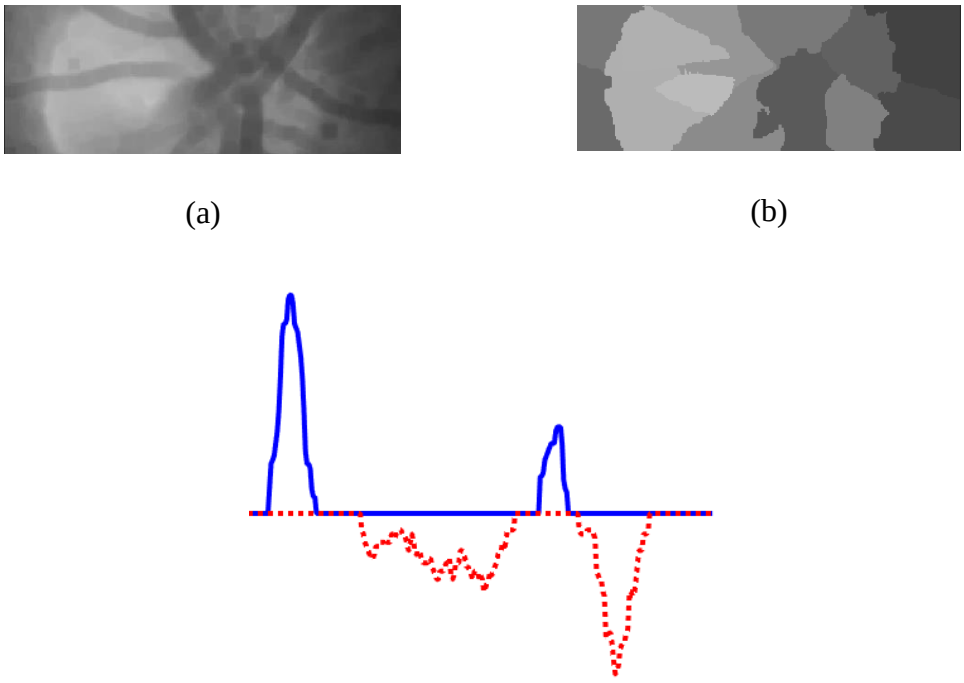

Figure 34. (a) OD region candidate. (b) *Imgspxls* representation for OD region candidate. (c) *Diff_Profile*, showing the pattern LB-LL-V-RL-RB.

The proposed approach proved to be simple and reliable; especially for challenging images, including images with poor illumination, pathological changes, with dark OD due to uneven illumination and low contrast, with partial OD section and images with bright exudates whose size and intensity are similar to OD. The robustness of the proposed technique is guaranteed by evaluating the method in four publicly-available datasets: DIARETDB1[20], DIARETDB0 [21], e-ophtha-EX [22], and DRIVE [23] obtaining a disc detection success rate of 100%, 100%, 98.78% and 100% respectively. Distinctly, since anatomical features calculated are relative to image's original resolution, the results of the proposed approach were achieved without any transformations to the sizes of the input images, making our detection algorithm scalable in terms of image resolution. Unlike most approaches, since no training was required for the

classification stage, no additional datasets are needed for this task and the results are calculated using all images of the datasets.

4.4 Detection of the fovea, macula and exudates for the pre-diagnosis of Diabetic Macular Edema (DME)

Diabetic Macular Edema (DME), an important complication of DR, occurs when the leakage of blood vessels causes accumulation of fluid in the macula region. In clinical practice, ophthalmologists diagnose DME based on the presence of exudates in the macular neighborhood. The macula corresponds to the central area of the retina, responsible for the most accurate and color vision due its high density of photoreceptors. Since the pigmented epithelial cells in the macula are taller and contain more pigment compared to cells elsewhere in the retina, the fovea region appears to be the darkest region of the retina. This region is also devoid of retinal blood vessels. The fovea is the shallow depression located at the center of the macular region. Fovea has an oval shape and a diameter equal to 1.5mm being nearly equal to the diameter of the optic disc. In addition, OD location can be used for fovea center estimation since both structures are separated approximately at a constant distance of 2.5 OD diameter. The severity of DME is evaluated by the presence of exudates in a determined region around fovea. It is called Clinically Significant Macular Edema (CSME), if exudates presence is confirmed in the circle of 1 OD diameter around fovea and Non-Clinically Significant Macular Edema, when there is presence of exudates outside the region defined around 1 OD diameter around fovea. Hence, automatic detection of fovea is essential in the development of computer-aided diagnosis (CAD) system for DR and DME.

The challenges for the accurate localization of the fovea includes the presence of hemorrhages which could be similar in shape, size and intensity. Moreover, the localization

task can be difficult due to the low quality of some fundus images, including underexposure, overexposure and uneven illumination resulting in low contrast images.

The proposed approach is a novel and robust technique for automatic fovea detection. The algorithm initially searches for the fovea region with prior information that it is the darkest intensity region. A threshold is locally defined using k-means clustering. For the challenging images including those with the presence of large hemorrhages and low contrast, an alternative approach is applied based on the fact that fovea center is estimated to be at a constant distance of approximately 2.5 OD diameter of OD center and that is a region devoid of retinal blood vessels. The accuracy of the technique will be tested on four publicly accessible retinal datasets: Diaretdb1, MESSIDOR, DRIVE and HRF. Figure 35. shows the overview of the proposed methodology for macula region location.

- **Methodology**

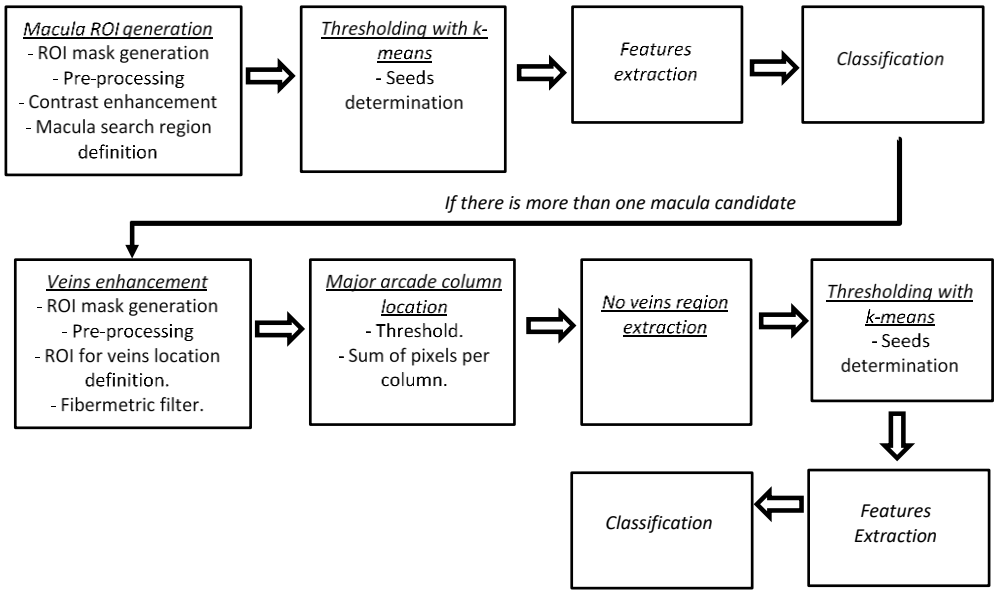

Figure 35. Overview of the proposed methodology for macula region location.

- **Macula ROI location**

The purpose of this stage is to determine the region of interest corresponding to macula. First, applying the same procedure as for optic disc location, the dark zones surrounding fundus image are excluded from further processing, and the approximation of the diameter *Diam* is calculated.

In general, macula is located in the central region of the fundus images. Then, to reduce the macula search region, image height is redefined by Equation 5 and image width as Equation 6.

$$winR = ([r0\ (1.25 * Diam)\ (r1 - (1.25 * Diam))])$$

Equation 5. Image height definition

$$winC = ([c0\ (c0 + 1.25 * Diam)\ \big(c0 + (4.5 * Diam)\big)\ c1])$$

Equation 6. Image width definition

Pre-processing includes applying a minimum filter with size of 5x5, to enhance the darker structures of the fundus image. CLAHE is used for contrast improvement and a moving mean filter of size 5x5 for noise reduction. Figure 37. illustrates the macula ROI generation steps.

Figure 36. Original fundus image.

(a) (b) (c)

Figure 37. (a) ROI excluding dark regions per column. (b) Result of applying the pre-processing stages and CLAHE on image (a). (c) Macula search region definition.

- **Thresholding with k-means**

k-means clustering [94] is used to perform image segmentation. The algorithm seeks to group the pixels with similar intensity values denominated as clusters. The points within a cluster should be similar to each other, hereby the goal is to minimize the distance between the points within a cluster. K-means clustering technique seeks to minimize the distance of the points in a cluster with respect to their centroid. K-means is a centroid-based algorithm, or a distance-based algorithm, where the distances are calculated to assign a point to a cluster. In K-means, each cluster is associated with a centroid and the main objective is to minimize the sum of distances between the points and their respective cluster centroid.

The starting centroid values selection play a crucial role in the correct segmentation of the desired structures. The starting centroid intensity values are selected as the relevant local minimum and maximum values from the histogram of the macula ROI defined earlier. For cluster pixels-centroid distance measurement *cityblock* Equation 7 is selected.

$$d(x,c) = \sum_{j=1}^{p} |x_j - c_j|$$

Equation 7. Cityblock distance measurement.

Sum of absolute differences. Where, *x* is an observation (that is, a row of x) and *c* is a centroid (a row vector). Each centroid is the component-wise median of the points in that cluster. In Figure 38, the result of the thresholding with k-means stage is shown in the case when the image has good contrast and there is no presence of red lesions of similar size.

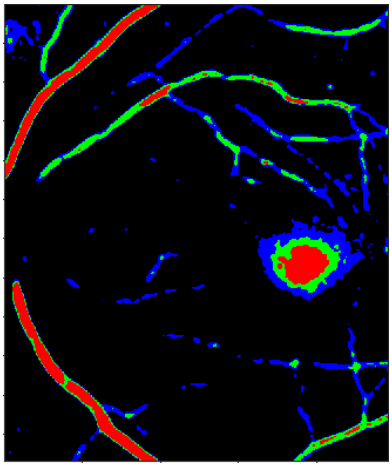

Figure 38. Result of applying k-means thresholding to Fig.36(c)

- **Features extraction and classification:**

The clusters selected for further processing are the ones defined by the three lowest intensity centroids, as they are expected to correspond to the lowest intensity structures: macula, blood vessels and red lesions. As the fovea is a small pit located near the center of the macula, a concentric low intensity distribution is observed on the macula region; going from fovea with the lowest intensity passing for the macula zone with slighter

higher intensity and finally ending when background is reached. This pattern is considered, along with the eccentricity and the expected area are considered as the features for macula classification. If only one candidate region fulfills these features, there is no need for further processing as there is only one macula candidate showing a concentric pattern for the three lowest levels. On the contrary further processing is done including blood vessels enhancement. Figure 39. shows a case where there is more than one macula's center candidate due to the image has presence of red lesions of similar size and the contrast is low.

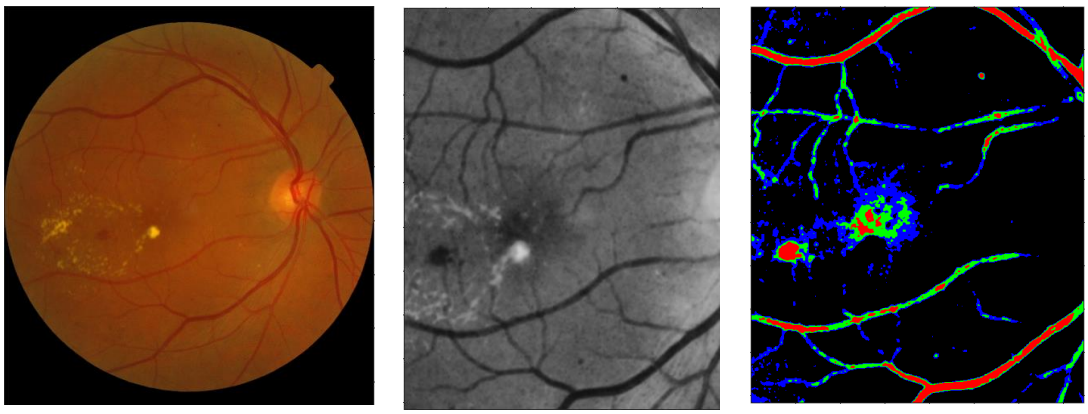

(a) (b) (c)

Figure 39. (a) ROI excluding dark regions per column. (b) Macula search region definition. (c) Result of applying k-means thresholding to (b)

- **Blood vessels enhancement**

As, stated earlier, the following stages only are necessary for the cases where macula two or more regions fulfill the features proposed. For this cases, which include the challenging images with the presence of large hemorrhages and/or low contrast, the approach is based on the fact that fovea center is estimated to be at a constant distance of approximately 2.5 OD diameter from OD center main arcade of vessels and that is a region devoid of retinal blood vessels.

The pre-processing and ROI mask stages are the same from the macula ROI generation stage, as from ROI for veins location definition, width is defined by *winR* and height by *winC*:

$$winR = ([1 + \ (r * 0.15) \ r - (r * 0.85)])$$

Equation 8. Image height definition

$$winC = ([c0 + 0.5 * Diam \ \ \big(c1 - (0.5 * Diam)\big) \ ])$$

Equation 9. Image width definition

Then, next step consists in finding the main arcade vessels, for this purpose vessel enhancement is applied. Vessels are enhanced using the *fibermetric* filter [95], this filter was specifically designed by the authors for blood vessel enhancement on magnetic resonance angiography images (MRA) and digital subtraction angiography images (DSA).

This technique seeks for tubular regions using the local second order ellipsoid. The result of applying this filtering with a window size of *Diam/9* to the image of Figure 40 (a) is shown in Figure 40 (b).

- **Major arcade column location and no vessels region extraction**

Once, vessels are enhanced, next step consists in applying thresholding to extract the major arcade of vessels. The *fibermetric* filter response is higher in the dark objects whose size approximates to the window size, for this reason the threshold is set to the 25% highest intensity pixels, the result of applying this threshold is shown in Figure 40 (c). Next, a vector consisting of the sum column of pixels with width *Diam/9* is calculated, the major arcade location is found as the maximum peak value location

from this vector. Macula probable column region is now defined using the fact that is at a constant distance of approximately 2.5 OD diameter from OD center (vertical region enclosed in red on Figure 40 (c)), then to define the probable macula row region the fact that macula region is devoid from blood vessels is used. A row-wise sum is done, and the local minimums positions with most separation between them are chosen as the limits of the probable macula row region (horizontal region enclosed in blue on Figure 40 (c)).

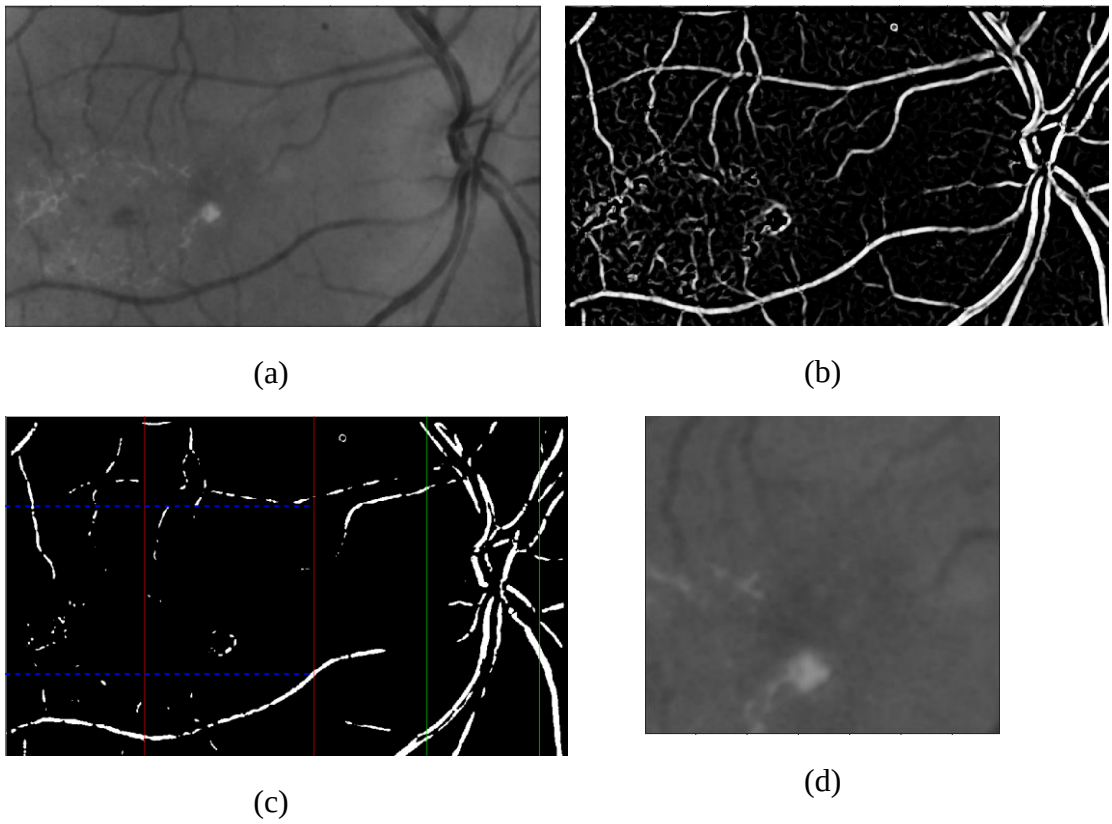

Figure 40. (a) Macula search region definition. (b) Result of applying fibermetric filter to image (a). (c) Result of applying a thresholding for the highest intensity values on image (b). Region enclosed by the green vertical lines correspond to the zone of highest sum of veins (OD), region enclosed by red lines correspond to the probable macula region around 2.5 OD diameter from OD center and the horizontal region enclosed by the blue lines correspond to the horizontal region with lowest density of veins. (d) Extraction of the probable macula region.

- **Thresholding with k-means**

Again, to segment the macula, thresholding with k-mean clustering is applied. Macula search region now is defined as the region of 1 OD diameter around the center of the probable macula region image. In this case, the starting centroid intensity values, are calculated considering the lowest intensity values of the macula search region. Starting centroid values, are defined by *centroids_c*:

$$centroids\_c = minimum\ intensity\ value + n * delta\_c$$

Equation 10. Centroids centers definition

$$delta\_c = mode\ intensity\ value - \frac{minimum\ intensity\ value}{6}$$

where the values for *n* go from 1 to 6. Figure 41 shows the result of thresholding with k-means the macula search region.

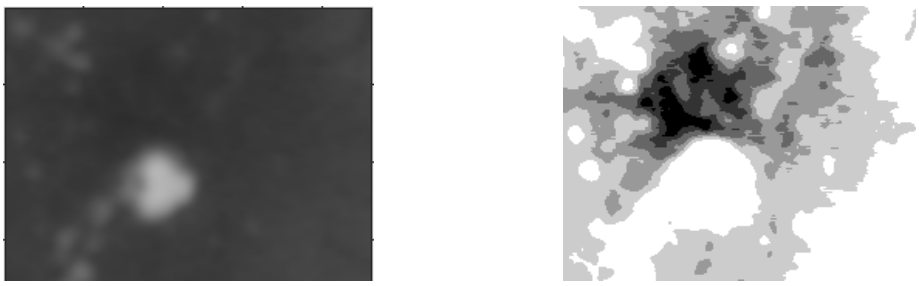

(a) (b)

Figure 41. (a) Region of 1 OD diameter around the center of image on ***¡Error! No se encuentra el origen de la referencia.*** *(d) (b) Result of applying k-means thresholding on image (a).*

- **Features extraction and classification**

Again, the clusters selected for further processing are the ones defined by the three lowest intensity centroids and the features defined are the previous ones defined: concentricity low intensity pattern, eccentricity and the expected area are considered as the features for macula center classification. On Figure 42, is shown the macula classification based on the analysis of concentric patterns of the three lowest levels of the thresholded with k-means image. In case that none region fulfils the features, macula center is selected as the center of the macula search region.

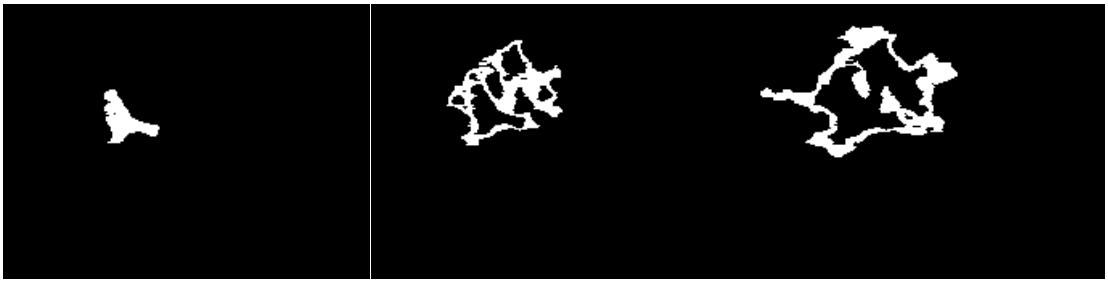

(a) (b) (c)

Figure 42. Analysis of concentric patterns of the three lowest levels of image on Figure 41.(b) (a) First level of k-means (b) Second level of k-means (c) Third level of k-means.

- **Exudates segmentation**

Once the macula center is established from the previous stage, the relevant region for DME evaluation is defined as the circular region with diameter of 1 DD for Clinically Significant Macular Edema (CSME). The purpose of the exudate's segmentation stage is to establish if there is presence of exudate in this region. Exudates segmentation is performed following three main stages: exudates candidate generation, features extraction and classification.

- **Exudates region candidate generation**

The purpose of this stage is to generate all the bright regions that potentially could be classified as exudates. First, the circular region with diameter of 1 DD around the macula center calculated is extracted for further processing. Preprocessing with median filtering with size 3x3 is applied to the green and red channel to reduce noise. Next, a channel which we named GR is calculated dividing the green channel by the red channel. GR channel creation aims to represent the yellow tonalities found in the image, as it is known that exudates present this color characteristic in fundus images. As the perception of contrast varies according with the range of grays levels present in the image, when the majority of the pixels are concentrated on the low intensity gray values, the brighter regions are less distinguishable. For this reason, in the cases where the yellow tonalities found are of low value, a sharpening filter [96] is applied in order to accentuate the borders. The index *pM* is proposed to evaluate if the majority of the yellow tonalities found are of low value. *pM* is calculated as the division of the mode of the green channel by the mode of the green channel. Sharpening filter is applied only if *pM* value is lower than 0.4.

From the observation of the patterns of exudates lesions, we determined that exudates intensity variation present a gradual shift in concentric form, going from high intensity values at its center to lower values as background is reached. Aiming to represent this pattern, a contour map of the image is calculated. The contour map [97] is represented by isolines, a series of curves along where the function has a constant value, so that the curve joins points of equal value. More generally, a contour line for a function of two variables is a curve connecting points where the function has the same or similar value. The number of contours for the contour map representation is set to five, as the top three are expected to represent the brighter structures, the lower the dark objects, including the vessels and the second contour aims to represent the background.

Once the contour map with the five regions is extracted, the higher three contours are used to evaluate the concentric pattern characteristic, the regions formed by contours that are contained into each other are selected as exudate candidates. The exudate candidate generation algorithm is shown in Table 9. On Figure 43 is shown the result of the described stages for exudate region candidate extraction.

Algorithm 2: Exudate candidates region generation

input : Original image from dataset (MESSIDOR, Diaretdb1)
output : Image containing potential exudates (ImgE)

```
1  Extract the ROI centered in the macula search region (1DD around)
2  Preprocess image for noise reduction
3  Calculate GR channel as: green channel/red channel
4  Calculate pM as: Mode green channel/Mode red channel
5  If pM<0.4
6  Apply a sharpening filter to GR channel
7  end
8  Extract contours from GR channel with five levels
9  Determine the contour regions that are contained into each other
10 Begin
11 for the three highest intensity contours
12     Determine the contour regions that are contained into each other
13       Generate an RGB (ImgE)
14          Red contains the pixels of the highest intensity contour
15          Green contains the pixels of the second highest intensity contour
16          Blue contains the pixels of the third highest intensity contour
17  end
18 End
```

Table 9. Algorithm to generate the exudates region candidates.

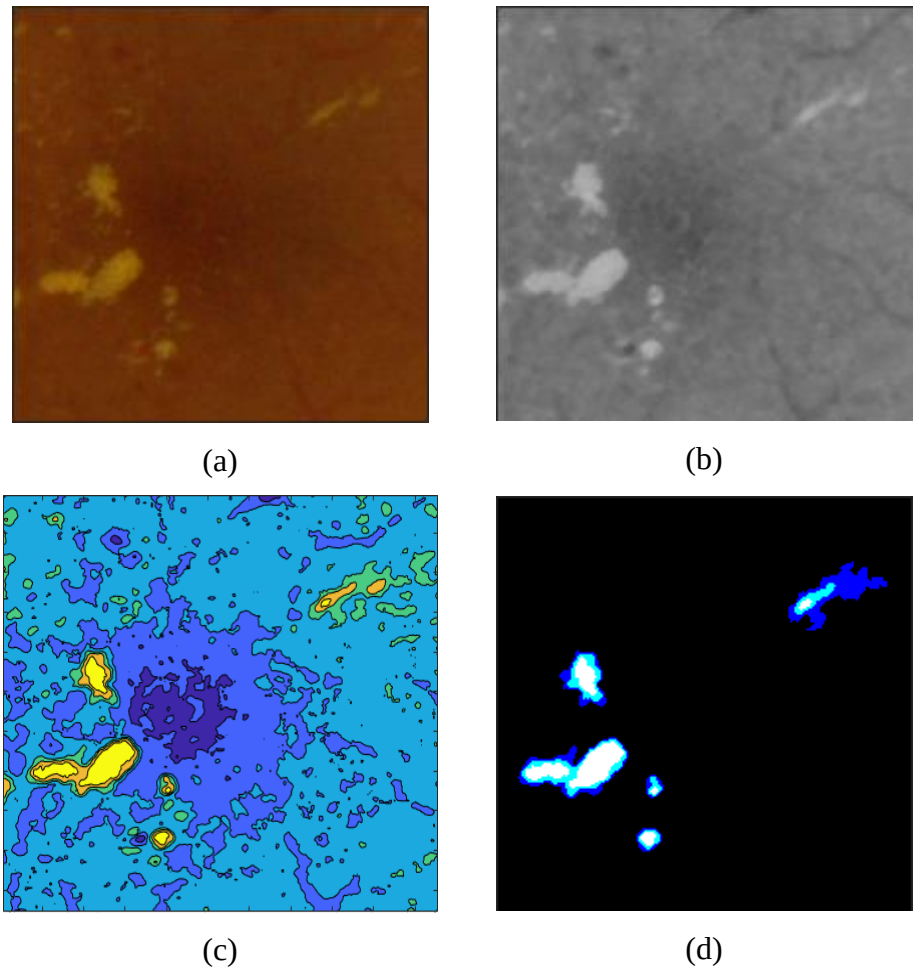

Figure 43 (a) ROI centered at the macula search region (1DD around). (b) GR channel representation of the image on (a). (c) Contour map of the image on (c) with five levels. (d) Contour regions that are contained into each other (ImgE).

- **Features extraction**

Features extraction stage aims to represent the natural characteristics trough experts make the diagnosis. As mentioned in the handbooks for fundus image diagnosis trainings [98], besides their high intensity values, hard exudates are distinguished from another bright lesions (soft exudates, drusen and cotton wool spots), due to their sharp edges and high contrast. As in the previous stage the bright regions with non-concentric

intensity variations were filtered, the following measurements are proposed to calculate the contrast and the edge sharpness:

- Maximum green intensity value of the pixels conforming the candidate region.
- Mean green intensity value of the pixels conforming the candidate region.
- The number of different gray levels found in the region in the green channel.
- Maximum border intensity value: calculated extending the candidate region and applying the range filter. The region is extended in order to include background information.

These four features are extracted for each candidate region per image, and are arranged in a vector named the feature vector. Table 10 summarizes the algorithm for exudates features extraction.

Algorithm 3: Exudate features extraction

input : Image containing potential exudates (ImgE)
output : A vector containing the set of features to classify the exudate regions (Feature_Vector)

Begin
for each candidate region of ImgE extract
    Maximum green intensity value of the region (mgI)
    Mean green intensity value of the pixels of the region (avgI)
    (nLv) as the number of different gray levels found in the region in the green channel
    Maximum border intensity value: calculated extending the candidate region and applying the range filter (mbI)
    Feature_Vector=[mgI; avgI; nLv; mbI]

8 **end**

9 **End**

Table 10. Algorithm to generate the features for the exudate's region candidates.

- **Classification**

Based on the four characteristics defined, a series of systematic tests are conducted, aiming to find the range values for the combination of characteristics with which the sensitivity and specificity are achieved, 80% and 95% respectively. The rules and ranges for each one of the four characteristics are shown in Table 11. If a high sensitivity were the target, could be obtained relaxing the range values of the characteristics, but at the cost of a resulting decrement on the specificity. High specificity means that the system probability to give a false diagnosis is low.

Algorithm 4: Exudate classification

input : A vector containing the set of features to classify the exudate regions (Feature_Vector)

output : Image containing exudates regions (ImgEx)

```
1   Begin
2   for each feature vector per image
3       if mgI > 60 && nLv > 20
4           Exudate=true;
5       end
6       if mgI>60 && nLv>10 && nLv<=20 && (mgI - avgI)>=6 &&
7  mbI>19
8           Exudate=true;
```

9	**end**
10	ImgEx=255 for the pixel member of the candidate exudate region
11	classified as exudate
12	**end**
	End

Table 11. Algorithm to classify the exudate's region candidates.

Results

5.1 Analysis of thresholding techniques for OD location in color fundus images

Using all 89 images from DiaretDBv1 database, the three thresholding methods were applied: Triangle, Mean Peak, and Maximum Entropy on a three set of images based on their contrast and quality: high contrast, low contrast, and poor quality; with 58, 16, and 15 images respectively. The test setup consists of the three set images, the three thresholding methods and common green channel and CLAHE on the green channel pre-processing, as input image to the method. The performance of each thresholding technique was evaluated with the percentage of intersected pixels with the Groundtruth. The results obtained are summarized in the Table 12**.**

Triangle		**Maximum Entropy**		**Mean Peak**		**Performance metric**
Green Channel	**Green Channel + CLAHE**	**Green Channel**	**Green Channel + CLAHE**	**Green Channel**	**Green Channel + CLAHE**	
63.48 % 58/58	70.78 % 58/58	48.82 % 58/58	60.06 % 58/58	25.10 % 45/58	68.04 % 58/58	**Mean value of intersection on high contrast images / # of located ODs**

47.89 % 15/16	63.28 % 16/16	37.53 % 13/16	53.37 % 16/16	19.02 % 8/16	50.94 % 15/16	**Mean value of intersection on low contrast images / # of located ODs**
56.23 % 15/15	66.87 % 15/15	32.76 % 15/15	61.10 % 15/15	22.76 % 11/15	56.30 % 15/15	**Mean value of intersection on low quality images/ # of located ODs**

Table 12. Results by group of images.

5.2 Optic Disc Location

Four publicly available datasets were used: DIARETDB1 [20], DIARETDB0 [21], e-ophtha-EX [22]and DRIVE [23]. The algorithm for the proposed method was implemented with MATLAB R2017a in a laptop with Windows 10, 8 GB of RAM, and Intel i7 processor at 2.3 GHz. An OD location accuracy of 99.7% is obtained for the 341 retinal images within the four publicly datasets. Comparing with work from [14],[15] which are recent methods found in the literature for the DIARETDB0, DIARETDB1 and DRIVE datasets, [14] obtained 100% accuracy for each one, and outperforms the results of [15] for DIARETDB0 and DIARETDB1. For e-ophtha-EX dataset, we obtained 98.78% accuracy, meaning that OD location failed only in one case. The reason why the method fails to detect OD on image DS000F4K.jpg is because the total OD disc region is not captured on the photograph, making that the pattern of the column wise pixel intensity variation profile could not be found. For a meaningful clinical diagnosis, it is necessary that the important landmarks such as optic disc, macula, fovea and vasculature can be clearly distinguishable in the fundus image, so in practice these

types of fundus images are discarded and replaced for another retinal photographic capture of the same eye.

The obtained results show that the proposed method is robust and achieves high detection rate in the four compared databases. Distinctly, the results of the proposed approach were achieved without any alterations to the sizes of the input images or tested with a fraction of the images of the data set. The results obtained are summarized in the Table 13**.**

Author	Dataset	Method type	#Images	OD success rate
Harangi et al. [43]	DIARETDB1	Combination of methods	89	(88/89) 98.88
	DIARETDB0		130	(128/130) 98.46
	DRIVE		40	100
Basit et al. [99]	DIARETDB1	Combination of methods	89	(88/89) 98.88
	DRIVE		40	100
Xiong et al. [100]	DIARETDB1	Combination of methods	89	(87/89) 97.75
	DIARETDB0		130	99.23
	DRIVE		40	100
Soares et al. [36]	DIARETDB1	Convergence of blood vessels	89	(88/89) 98.88
	DIARETDB0		130	(128/130) 98.46
	DRIVE		40	100
	e-ophtha-EX		82	(81/82) 98.78
Wu et al. [38]	DIARETDB1	Convergence of blood vessels	89	100
	DIARETDB0		130	100
	DRIVE		40	100

Rahebi et al. [32]	DIARETDB1 DRIVE	Property-based	89 40	(84/89) 94.38 100
Wang et al. [40]	DIARETDB1 DIARETDB0 DRIVE	Model-based	89 130 40	(87/89) 97.75 (127/130) 97.69 100
Bharkad [101]	DIARETDB1 DIARETDB0 DRIVE	Combination of methods	89 130 40	(88/89) 98.88 (126/130) 96.92 100
Rodrigues et al. [102]	DRIVE DIARETDB1	Combination of methods	20	(19/40) (19/20) 95
Panda et al. [103]	DIARETDB0 DRIVE e-ophtha-EX	Convergence of blood vessels	89 130 40 82	100 (126/130) 96.92 100 100
Proposed method	DIARETDB1 DIARETDB0 e-ophtha-EX DRIVE	**Combination of methods**	**89** **130** **82** **40**	**(89/89) 100** **(130/130) 100** **(81/82) 98.78** **(40/40) 100**

Table 13. Comparison of OD detection success rates (expressed in %) in DIARETDB1, DIARETDB0, E-OPHTA and DRIVE public datasets.

5.3 Detection of the fovea, macula and exudates for the pre-diagnosis of Diabetic Macular Edema (DME)

- *Macula Location*

As images: 04_test, 05_test, 23_training, 31_training, 34_training from DRIVE and image 20051020_55346_0100_PP from MESSIDOR, did not contain the macula region or the region is only partially seen, are excluded from the analysis. Many previous works do not include all images.

The results are evaluated using the mean, minimum and maximum percent of overlap with the macula Groundtruth. For HRF, DRIVE, Diaretdb1 and MESSIDOR publicity available datasets, the percent of [mean, minimum and maximum overlap] obtained are [87.95%, 40%, 98%], [87.8%, 45%, 97%], [82.17%, 18%, 100%], [85.85%, 12%, 100%], respectively. The results obtained are summarized in the Table 14**.**

Author	Dataset	#Images	Fovea success rate
Kao et al. [59]	DIARETDB1	89	92.1% (82/89)
	MESSIDOR	1200	97.8% (1174/1200)
Deka al. [60]	DIARETDB1	89	95.5% (85/89)
	DRIVE	36	100%
	MESSIDOR	800	97.75% (782/800)
	HRF	45	100%
Aquino et al. [55]	DIARETDB1	89	94.38% (84/89)
	MESSIDOR	1136	98.24% (1116/1136)

Gegundez et al. [104]	MESSIDOR	1200	96.92% (1163/1200)
Balasubramanian et al. [58]	DIARETDB1	89	97.75% (87/89)
	DRIVE	40	100%
	MESSIDOR	1200	99.33% (1180/1200)
	HRF	45	100%
Proposed method	DIARETDB1	**89**	**100%**
	DRIVE	**35**	**100%**
	MESSIDOR	**225**	**100%**
	HRF	**45**	**100%**

Table 14. Comparison of OD fovea success rates in DIARETDB1, DRIVE, MESSIDOR and HRF public datasets.

- *DME diagnosis*

Two publicly available datasets were used: DIARETDB1 and MESSIDOR. The algorithm for the proposed method was implemented with MATLAB R2019a in a laptop with Windows 10, 8 GB of RAM, and Intel i7 processor at 2.3 GHz. For MESSIDOR the sensitivity and specificity were calculated at level image, as the Groundtruth consists in an Excel file with medical findings which can be used for testing purposes. The images are graded into different categories depending on the position of lesions. The set of images with exudate presence is selected for the evaluation of DME. For Diaretdb1, has no direct DME diagnosis Groundtruth, but in this case, as the exudates of each image are marked, DME diagnosis can be done establishing the existence of exudate region in the 1 DD diameter area around the fovea as CSME.

For MESSIDOR dataset a specificity of 95.65% and a sensitivity of 82.43% were obtained for the 217 images with exudates and for Diaretdb1 dataset a specificity of 96.49% and a sensitivity of 85.71% for the 89 images were obtained. The obtained results show that the proposed method for DME is robust and achieves the recommended diagnosis values for specificity and sensitivity in the two databases. Distinctly, the results of the proposed approach were achieved without any alterations to the sizes of the input images. The results obtained are summarized in the Table 15**.**

Author	Dataset	#Images	Performance measure
Marin et al. [77]	MESSIDOR	1058	SN=90%, SP=69.4%
Acharya et al. [75]	MESSIDOR	300	Acc=94.16%
Medhi et al. [76]	MESSIDOR	694	SN=95.07%, SP=95.45%
	DIARETDB1	38	SN=97.14%, SP=100%
Akram et al. [56]	MESSIDOR	1200	SN=98.6%, SP=97.2%
Marin et al. [105]	MESSIDOR	1058	SN=90%, SP=77%
Proposed method	DIARETDB1	**89**	**SN=85.71%, SP=96.49%**
	MESSIDOR	**217**	**SN=82.43%, SP=95.65%**

Table 15. Comparison of macular edema performance measurements in DIARETDB1 and MESSIDOR public datasets.

Conclusions and Discussion

6.1 Discussion

- Optic disc location

The proposed optic disc method has four main stages: OD pixel region candidate generation, promising OD regions detection, promising candidate features extraction, and classification. Given that datasets have images with non-uniform illumination, regional intensity variations are found along the fundus image, this to overcome the well-known unreliable use of a global high intensity threshold to locate promising OD regions. That led us to use a window partitioning approach for the extraction of local OD candidate regions. Recapitulating, the proposed approach consists of a top-down approach, from a group of high intensity local regions with coarse level features to finer features on extended regions with minimum requirements on size and intensity distribution, which form the most promising OD regions. A model for the column wise pixel intensity variation is proposed, and the features are defined according to the expected OD pattern on the column wise pixel intensity variation model: presence of a Left Lobe (LL), a Right Lobe (RL) and Vasculature (V) between them, and distances from LL to V and V to RL. Classification is done accordingly to the presence of the LL-V-RL pattern. The proposed algorithm can be negatively affected if the retinal vasculature is not distinguishable, i.e. vessels belonging to the main arcades have low contrast or are quite difficult to observe. On the OD pixel region candidate generation stage, the inclusion of the OD true region as candidate depends on OD true region having a relevant local intensity with respect of another bright regions or artifacts that might be present on the windowed section of the image. Another source of error could be when the vertical vessels that emerge from the OD are either not present or exhibit a low contrast in comparison with other vertical vessels in other regions of the retina, this could lead to an incorrect OD classification. For the correct classification of OD candidate regions using the model for the column wise pixel intensity variations across the optic disc it

is necessary that the majority of the actual OD region will be present on the analyzed fundus image.

- Macula location

The algorithm initially searches for the fovea region, macula center, with prior information that it is the darkest intensity region. A threshold is locally defined using k-means clustering. For the challenging images including those with the presence of large hemorrhages and low contrast, an alternative approach is applied based on the fact that fovea center is estimated to be at a constant distance of approximately 2.5 OD diameter of OD center and that is a region devoid of retinal blood vessels.

We identified two main reasons for the failure in successfully detecting macula in this study: (1) failure in correctly determining the macula search region (2) failure in determining macula candidate. The first failure is associated with variations on the standard distance between the OD center and the macula center given by the expression 2.5 OD diameter pixels which may be inaccurate in some cases. The second failure is associated with the images where macula is not present or partially present, affecting the proposed features. However, this kind of images in clinical practice should be retaken, as they lack quality for diagnosis.

- DME pre-diagnosis

Exudates are segmented based on their high intensity along with their sharp edges and high contrast characteristics. From the observation of the patterns of exudates lesions, we determined that exudates intensity variation present a gradual shift in concentric form, going from high intensity values at its center to lower values as background is reached. Aiming to represent this pattern, a contour map of the image was calculated. Exudate candidates with this pattern are further processed. Four

characteristics were extracted for each candidate exudate region: maximum green intensity value of the pixels conforming the candidate region, mean green intensity value of the pixels conforming the candidate region, the number of different gray levels found in the region in the green channel and the maximum border intensity value that was calculated extending the candidate region and applying the range filter. Based on these four characteristics, a series of systematic tests were conducted, aiming to find the range values for the combination of characteristics with which the target sensitivity and specificity are achieved, 80% and 95% respectively.

6.2 Conclusions

In this work, several advancements in retinal image processing aimed toward improving the state-of-the-art in automated screening were developed: *image enhancement, retinal structures location, lesion detection and disease classification*.

A solution for the location of the optic disc and macula, exudate detection and Diabetic Macular edema pre-diagnosis using color images of eye fundus was proposed and validated using multiple public image databases with different resolutions and achieving competent results with respect of the state-of-the-art approaches, achieving the main goal of this work. The important aspects of the proposed solution include: low computational cost, image resolution independence and robustness. According to the achieved performance of the proposed method and its simplicity, has the potential of assessing the integration into a retinal disease pre-screening tool.

A new approach for the location of the optic disc in fundus images was developed. The approach proved to be simple and reliable; especially for challenging images, including images with poor illumination, pathological changes, with dark OD due to uneven illumination and low contrast, with partial OD section and images with bright

exudates whose size and intensity are similar to OD. The robustness of the proposed technique is guaranteed by evaluating the method in four publicly-available datasets: DIARETDB1, DIARETDB0, e-ophtha-EX and DRIVE, obtaining a disc detection success rate of 100%, 100%, 98.78% and 100% respectively. Distinctly, since anatomical features calculated are relative to image's original resolution, the results of the proposed approach were achieved without any transformations to the sizes of the input images, making our detection algorithm scalable in terms of image resolution. Unlike most approaches, since no training was required for the classification stage, no additional datasets are needed for this task and the test results are calculated using all images of the datasets, versus previous works that use typically 30% of the images to test.

For macula location, a novel methodology combining anatomical and visual feature-based criteria is proposed. As the methods that only employ either only the visual or the anatomical features could fail in presence of lesions occluding the macula, the proposed algorithm can overcome these problems of failure or incorrect detection using all the macula characteristics i.e. low intensity, lack of blood vessels and distance with respect to OD. The results were evaluated using the mean, minimum and maximum percent of overlap with the macula Groundtruth. For HRF, DRIVE, Diaretdb1 and MESSIDOR publicity available datasets, the percent of [mean, minimum and maximum overlap] obtained were [87.95%, 40%, 98%], [87.8%, 45%, 97%], [82.17%, 18%, 100%], [85.85%, 12%, 100%], respectively. In addition, the proposed approach is independent of image resolution, since the anatomical constraints and features extracted are relative to OD estimation. Considering the results obtained, the proposed method yielded high detection accuracy along with robustness in macula location. The proposed method could be used as a tool to be integrated into a complete prescreening system for early retinal disease detection.

For Diabetic Macular Edema (DME) diagnosis, we developed a methodology for grading the risk of DME based on exudate detection in fundus images. Our proposed approach consists on using the coordinates of macula previously acquired and the distance of exudates from macula, the input fundus is graded in two categories, Non CSME and CSME. For MESSIDOR dataset a specificity of 95.65% and a sensitivity of 82.43% were obtained for the 217 images with exudates and for Diaretdb1 dataset a specificity of 96.49% and a sensitivity of 85.71% for the 89 images were obtained. The obtained results show that the proposed method for DME is robust and achieves the recommended diagnosis values for specificity and sensitivity in the two databases. Distinctly, the results of the proposed approach were achieved without any alterations to the sizes of the input images. The results demonstrated that the proposed methodology can be used in an automated medical system for the pre-diagnosis of diabetic macular edema.

6.3 Contributions

The presented approach in this thesis could comprise a model for the development of a system that can be used as a pre-diagnostic tool for retinal diseases. The proposed approach is less computationally demanding than compared to the commonly used operations for the state-of-the-art methods. The development of an automatic pre-diagnosis system in the future could reduce the future gap between the number of diabetic patients and the number of ophthalmologists worldwide and become an economical preliminary ophthalmologic diagnostic medium that facilitates the way in which routine preventive examinations are done. In this way the ophthalmologist's workload related to diabetic patients could be alleviated and the economic and time costs can be reduced, making eye screening affordable and facilitating that patients take the exam at least twice a year as it is recommended.

Considering that OD could present similar characteristics with some signs of diabetic retinopathy, the proposed OD location approach can be applied to remove the OD region before the detection of these signs, avoiding the possibility of erroneously classifying OD sections as pathology lesions in automated diabetic retinopathy (DR) screening.

Also, the design of a profile model of OD intensity variations was contributed. This model represents the nature of the variation of the pixel's intensities of the OD region which makes it tolerant to color variability in fundus images. Also, this model can be easily scaled for any resolution. This was verified when testing this model with four databases with different resolutions. Resolution independence is of great importance specially for large scale screening programs, where the images to be analyzed come from different fundus cameras thus having variety of resolutions.

6.4 Future work

There are numerous image processing techniques with different approaches that could possibly solve the problems posed with better results, but they are mostly complex, with high processing time, dataset dependent, and image resolution dependent. Some proposals that could be implemented in the future are:

Develop a module that can estimate the image quality, so that a minimum quality could be established for the fundus color retinal image of the patient as appropriate for automatic diagnosis. This problem could also be solved through quality control in the process of acquisition of the fundus image.

The development of a database with their respective Groundtruth where the lesions and retinal structures are marked as accurately as possible. Facilitating the evaluation and comparison of the proposed methodologies. In this way, it can become a standard database with which different methods can be compared in a simple way.

Add other pre-diagnoses of retinal diseases to the system. With the proposed optic disc approach, an automated method for grading glaucoma could be developed locating accurately the optic disc cup and the optic disc rim, as glaucoma is diagnosed based on the ratio relation between them.

References

[1] S. Resnikoff, W. Felch, T. Gauthier, and B. Spivey, "The number of ophthalmologists in practice and training worldwide : a growing gap despite more than 200 000 practitioners," *Britih Journal of Ophthalmology*, pp. 1–5, 2012, doi: 10.1136/bjophthalmol-2011-301378.

[2] S. H. P. Andrew Stokes, "Deaths Attributable to Diabetes in the United States: Comparison of Data Sources and Estimation Approaches," *PLoS ONE*, 2017.

[3] IAPB, "Diabetic retinopathy: Challenges and opportunities," 2016. [Online]. Available: http://www.iapb.org/vision-2020/what-is-avoidable-blindness/diabetic-retinopathy. [Accessed: 08-Feb-2017].

[4] I. N. de S. P. de Mexico, "Diabetes, causa principal de muerte en México." [Online]. Available: https://www.insp.mx/presencia-insp/3877-presencia-insp.html. [Accessed: 08-Feb-2017].

[5] K. V. K. Narasimhan, V.C. Neha, "An efficient automated system for detection of diabetic retinopathy from fundus images using support vector machine and bayesian classifiers," in *International Conference on Computing, Electronics and Electrical Technologies [ICCEET]*, 2012, pp. 964–969.

[6] M. S. de Salud, "Diagnóstico y tratamiento de retinopatía diabética," 2015.

[7] W. H. Organization, "country profiles," 2016.

[8] W. H. J. Díaz, "Diabetes and Cause-Specific Mortality in Mexico City," *The new england journal of medicine*, 2016.

[9] B. D. Association, "Retinal photography screening for diabetic eye disease," 1994.

[10] B. Liesenfeld *et al.*, "A telemedical approach to the screening of diabetic retinopathy: Digital fundus photography," *Diabetes Care*, vol. 23, no. 3, pp.

345–348, 2000, doi: 10.2337/diacare.23.3.345.

[11] Spector RH, “The Pupils,” in *Clinical Methods: The History, Physical, and Laboratory Examinations*, 1990, p. Chapter 58.

[12] M. Foracchia, E. Grisan, and A. Ruggeri, “Luminosity and contrast normalization in retinal images,” *Medical Image Analysis*, vol. 9, no. 3, pp. 179–190, 2005, doi: 10.1016/j.media.2004.07.001.

[13] T. Kauppi, “Eye fundus image analysis for automatic detection of diabetic retinopathy,” 2010.

[14] A. Fadzil M. Hani and H. Adi Nugroho, “Retinal vasculature enhancement using independent component analysis,” *Journal of Biomedical Science and Engineering*, vol. 02, no. 07, pp. 543–549, 2009, doi: 10.4236/jbise.2009.27079.

[15] T. Roy, *Handbook of Retinal Screening in Diabetes: Diagnosis and Management*. .

[16] R. J. Winder, P. J. Morrow, I. N. Mcritchie, J. R. Bailie, and P. M. Hart, “Algorithms for digital image processing in diabetic retinopathy,” *Computerized Medical Imaging and Graphics*, vol. 33, pp. 608–622, 2009, doi: 10.1016/j.compmedimag.2009.06.003.

[17] A. Pardo and G. Sapiro, “Visualization of high dynamic range images,” *IEEE Transactions on Image Processing*, vol. 12, no. 6, pp. 639–647, 2003, doi: 10.1109/TIP.2003.812373.

[18] R. Wallis, “An approach to the space variant restoration and enhancement of images,” in *Current mathematical problems in imaging science*, 1976, pp. 329–340.

[19] W. Gonzalez, *Digital Image Processing*. .

[20] T. B. Markham R. Osareh A. Mirmehdi M., “Automated identification of diabetic retinal exudates in digital color images,” *Brithish Journal of*

Ophthalmology, vol. 87, pp. 1220–1230, 2003.

[21] A. M. Gooch B. Shirley P. Reinhard E., "Color transfer between images," *IEEE Computer Graphics and Applications*, vol. 21, pp. 34–41, 2001.

[22] S. B. Sakchai V. Nattapol W. Akara S. Bunyarit U., "Fine exudate detection using morphological approach," *International journal of applied biomedical engineering*, vol. 1, no. 1, pp. 45–50, 2010.

[23] A. M. N. Allam, A. A. H. Youssif, and A. Z. Ghalwash, "Automatic segmentation of optic disc in eye fundus images: A survey," *Electronic Letters on Computer Vision and Image Analysis*, vol. 14, no. 1, pp. 1–20, 2015, doi: 10.5565/rev/elcvia.680.

[24] M. Ortega, M. G. Penedo, J. Rouco, N. Barreira, and M. J. Carreira, "Retinal Verification Using a Feature Points-Based Biometric Pattern," *EURASIP Journal on Advances in Signal Processing*, vol. 2009, no. 1, pp. 1–13, 2009, doi: 10.1155/2009/235746.

[25] Y. Jiang, "Blood vessel tracking in retinal images," in *Proceedings of Image and Vision Computing*, 2007, vol. 1, pp. 126–131.

[26] I. W. R. A. Abdel-Ghafar, T. Morris, T. Ritchings, "Progress Towards Automated Detection and Characterisation of the Optic Disk in Glaucoma and Diabetic Retinopathy," *Medical Informatics and the Internet in Medicine*, vol. 32, no. 1, pp. 19–25, 2007.

[27] B. G. Meindert Niemeijer, Michael D. Abràmoff, "Fast Detection of the Optic Disc and Fovea in Color Fundus Photographs," *Medical Image Analysis*, vol. 13, no. 6, pp. 859–870, 2009, doi: 10.1016/j.pestbp.2011.02.012.Investigations.

[28] R. J. Qureshi, L. Kovacs, B. Harangi, B. Nagy, T. Peto, and A. Hajdu, "Combining algorithms for automatic detection of optic disc and macula in fundus images," *Computer Vision and Image Understanding*, vol. 116, no. 1, pp. 138–145, 2012, doi: 10.1016/j.cviu.2011.09.001.

[29] A. V. Deshmukh, T. G. Patil, S. S. Patankar, and J. V. Kulkarni, “Features based classification of hard exudates in retinal images,” *2015 International Conference on Advances in Computing, Communications and Informatics, ICACCI 2015*, pp. 1652–1655, 2015, doi: 10.1109/ICACCI.2015.7275850.

[30] C. A. G. Sergio Bonafonte Royo, *retinopatía diabética*. Elsevier España, isbn:9788481748512.

[31] R. Pourreza-Shahri, M. Tavakoli, and N. Kehtarnavaz, “Computationally efficient optic nerve head detection in retinal fundus images,” *Biomedical Signal Processing and Control*, vol. 11, no. 1, pp. 63–73, 2014, doi: 10.1016/j.bspc.2014.02.011.

[32] J. Rahebi and F. Hardalac, “A new approach to optic disc detection in human retinal images using the firefly algorithm,” *Medical & Biological Engineering & Computing*, vol. 54, no. 2, pp. 453–461, 2015, doi: 10.1007/s11517-015-1330-7.

[33] X.-S. Yang, “Firefly Algorithm,” in *Nature-Inspired Metaheuristics Algorithms*, 2nd ed., Frome: Luniver Press, 2010, pp. 81–89.

[34] M. S. Haleem, L. Han, J. van Hemert, and B. Li, “Automatic extraction of retinal features from colour retinal images for glaucoma diagnosis: A review,” *Computerized Medical Imaging and Graphics*, vol. 37, no. 7, pp. 581–596, 2013, doi: 10.1016/j.compmedimag.2013.09.005.

[35] M. Foracchia, E. Grisan, and A. Ruggeri, “Detection of optic disc in retinal images by means of a geometrical model of vessel structure,” *IEEE Transactions on Medical Imaging*, vol. 23, no. 10, pp. 1189–1195, 2004, doi: 10.1109/TMI.2004.829331.

[36] I. Soares, M. Castelo-Branco, and A. M. G. Pinheiro, “Optic Disc Localization in Retinal Images Based on Cumulative Sum Fields,” *IEEE Journal of Biomedical and Health Informatics*, vol. 20, no. 2, pp. 574–585, 2016, doi:

10.1109/JBHI.2015.2392712.

[37] D. Marin, M. E. Gegundez-Arias, A. Suero, and J. M. Bravo, “Obtaining optic disc center and pixel region by automatic thresholding methods on morphologically processed fundus images,” *Computer Methods and Programs in Biomedicine*, vol. 118, no. 2, pp. 173–185, 2015, doi: 10.1016/j.cmpb.2014.11.003.

[38] X. Wu, B. Dai, and W. Bu, “Optic Disc Localization Using Directional Models,” *IEEE Transactions on Image Processing*, vol. 25, no. 9, pp. 4433–4442, 2016, doi: 10.1109/TIP.2016.2590838.

[39] B. Dashtbozorg, A. M. Mendonca, and A. Campilho, “Optic disc segmentation using the sliding band filter.,” *Computers in biology and medicine*, vol. 56, pp. 1–12, 2015, doi: 10.1016/j.compbiomed.2014.10.009.

[40] C. Wang, D. Kaba, and Y. Li, “Level Set Segmentation of Optic Discs from Retinal Images,” *Journal of Medical and Bioengineering*, vol. 4, no. 3, pp. 213–220, 2015, doi: 10.12720/jomb.4.3.213-220.

[41] M. C. V. S. Mary, E. B. Rajsingh, J. K. K. Jacob, D. Anandhi, U. Amato, and S. E. Selvan, “An empirical study on optic disc segmentation using an active contour model,” *Biomedical Signal Processing and Control*, vol. 18, pp. 19–29, 2015, doi: 10.1016/j.bspc.2014.11.003.

[42] J. M. Molina-Casado, E. J. Carmona, and J. García-Feijoó, “Fast detection of the main anatomical structures in digital retinal images based on intra- and inter-structure relational knowledge,” *Computer Methods and Programs in Biomedicine*, vol. 149, pp. 55–68, 2017, doi: 10.1016/j.cmpb.2017.06.022.

[43] B. Harangi and A. Hajdu, “Detection of the optic disc in fundus images by combining probability models,” *Computers in Biology and Medicine*, vol. 65, pp. 10–24, 2015, doi: 10.1016/j.compbiomed.2015.07.002.

[44] F. Ren, W. Li, J. Yang, H. Geng, and D. Zhao, “Automatic optic disc localization

and segmentation in retinal images by a line operator and level sets," *Technology and Health Care*, vol. 24, pp. S767–S776, 2016, doi: 10.3233/THC-161206.

[45] A. Basit and M. M. Fraz, "Optic disc detection and boundary extraction in retinal images.," *Applied optics*, vol. 54, no. 11, pp. 3440–7, 2015, doi: 10.1364/AO.54.003440.

[46] L. Xiong and H. Li, "An approach to locate optic disc in retinal images with pathological changes," *Computerized Medical Imaging and Graphics*, vol. 47, pp. 40–50, 2016, doi: 10.1016/j.compmedimag.2015.10.003.

[47] M. Haloi, S. Dandapat, and R. Sinha, "An Unsupervised Method for Detection and Validation of The Optic Disc and The Fovea," *Computer Vision and Pattern Recognition*, pp. 1–8, 2016.

[48] D. Díaz-Pernil, I. Fondón, F. Peña-Cantillana, and M. A. Gutiérrez-Naranjo, "Fully automatized parallel segmentation of the optic disc in retinal fundus images," *Pattern Recognition Letters*, vol. 0, pp. 1–9, 2016, doi: 10.1016/j.patrec.2016.04.025.

[49] Z. Fan *et al.*, "Optic Disk Detection in Fundus Image Based on Structured Learning," *IEEE Journal of Biomedical and Health Informatics*, vol. 22, no. 1, pp. 224–234, 2018, doi: 10.1109/JBHI.2017.2723678.

[50] O. Faust, R. Acharya U., E. Y. K. Ng, K. H. Ng, and J. S. Suri, "Algorithms for the automated detection of diabetic retinopathy using digital fundus images: A review," *Journal of Medical Systems*, vol. 36, no. 1, pp. 145–157, 2012, doi: 10.1007/s10916-010-9454-7.

[51] L. P. Aiello *et al.*, "Diabetic retinopathy technical review," *Diabetes Care*, vol. 21, pp. 143–156, 1998.

[52] J. W. Yau *et al.*, "Global prevalence and major risk factors of diabetic retinopathy," *Diabetes Care*, vol. 3, no. 35, pp. 556–564, 2012.

[53] N. Bhagat, R. A. Grigorian, A. Tutela, and M. A. Zarbin, “Diabetic macular edema: pathogenesis and treatment,” *Surv. Ophthalmol.*, vol. 54, no. 1, pp. 1–32, 2009.

[54] M. R. K. Mookiah *et al.*, “Application of different imaging modalities for diagnosis of Diabetic Macular Edema: A review,” *Computers in Biology and Medicine*, vol. 66, pp. 295–315, 2015, doi: 10.1016/j.compbiomed.2015.09.012.

[55] A. Aquino, “Establishing the macular grading grid by means of fovea centre detection using anatomical-based and visual-based features,” *Computers in Biology and Medicine*, vol. 55, pp. 61–73, 2014, doi: 10.1016/j.compbiomed.2014.10.007.

[56] M. U. Akram, A. Tariq, S. A. Khan, and M. Y. Javed, “Automated detection of exudates and macula for grading of diabetic macular edema,” *Computer Methods and Programs in Biomedicine*, vol. 114, no. 2, pp. 141–152, 2014, doi: 10.1016/j.cmpb.2014.01.010.

[57] M. U. Akram and S. A. Khan, “Multilayered thresholding-based blood vessel segmentation for screening of diabetic retinopathy,” *Engineering with Computers*, vol. 29, no. 2, pp. 165–173, 2013, doi: 10.1007/s00366-011-0253-7.

[58] R. GeethaRamani and L. Balasubramanian, “Macula segmentation and fovea localization employing image processing and heuristic based clustering for automated retinal screening,” *Computer Methods and Programs in Biomedicine*, vol. 160, pp. 153–163, 2018, doi: 10.1016/j.cmpb.2018.03.020.

[59] E. F. Kao, P. C. Lin, M. C. Chou, T. S. Jaw, and G. C. Liu, “Automated detection of fovea in fundus images based on vessel-free zone and adaptive Gaussian template,” *Computer Methods and Programs in Biomedicine*, vol. 117, no. 2, pp. 92–103, 2014, doi: 10.1016/j.cmpb.2014.08.003.

[60] D. Deka, J. P. Medhi, and S. R. Nirmala, “Detection of macula and fovea for

disease analysis in color fundus images," *2015 IEEE 2nd International Conference on Recent Trends in Information Systems, ReTIS 2015 - Proceedings*, pp. 231–236, 2015, doi: 10.1109/ReTIS.2015.7232883.

[61] A. Aquino, M. E. Gegúndez-Arias, and D. Marín, "Detecting the Optic Disc Boundary in Digital Fundus Feature Extraction Techniques," *Ieee Transactions on Medical Imaging*, vol. 29, no. 11, pp. 1860–1869, 2010.

[62] D. Marín, A. Aquino, M. E. Gegúndez-Arias, and J. M. Bravo, "A new supervised method for blood vessel segmentation in retinal images by using gray-level and moment invariants-based features," *IEEE Transactions on Medical Imaging*, vol. 30, no. 1, pp. 146–158, 2011, doi: 10.1109/TMI.2010.2064333.

[63] N. Y. Garaibeh, M. a. Al-Smadi, and M. Al-Jarrah, "Automatic Exudate Detection Using Eye Fundus Image Analysis Due to Diabetic Retinopathy," *Computer and Information Science*, vol. 7, no. 2, pp. 48–55, 2014, doi: 10.5539/cis.v7n2p48.

[64] E. Imani and H. R. Pourreza, "A novel method for retinal exudate segmentation using signal separation algorithm," *Computer Methods and Programs in Biomedicine*, vol. 133, pp. 195–205, 2016, doi: 10.1016/j.cmpb.2016.05.016.

[65] B. Harangi and A. Hajdu, "Automatic exudate detection by fusing multiple active contours and regionwise classification," *Computers in Biology and Medicine*, vol. 54, pp. 156–171, 2014, doi: 10.1016/j.compbiomed.2014.09.001.

[66] M. Esmaeili, H. Rabbani, A. M. Dehnavi, and A. Dehghani, "Automatic detection of exudates and optic disk in retinal images using curvelet transform," *IET Image Processing*, vol. 6, no. 7, pp. 1005–1013, 2012, doi: 10.1049/iet-ipr.2011.0333.

[67] U. M. Akram and S. A. Khan, "Automated detection of dark and bright lesions in retinal images for early detection of diabetic retinopathy," *Journal of Medical*

Systems, vol. 36, no. 5, pp. 3151–3162, 2012, doi: 10.1007/s10916-011-9802-2.

[68] C. Pereira, L. Gonçalves, and M. Ferreira, "Exudate segmentation in fundus images using an ant colony optimization approach," *Information Sciences*, vol. 296, no. October, pp. 14–24, 2015, doi: 10.1016/j.ins.2014.10.059.

[69] A. Elbalaoui, M. Boutaounte, H. Faouzi, M. Fakir, and A. Merbouha, "Segmentation and detection of diabetic retinopathy exudates," *International Conference on Multimedia Computing and Systems -Proceedings*, vol. 91, no. 16, pp. 171–178, 2014, doi: 10.1109/ICMCS.2014.6911368.

[70] R. Bhargavi V and R. K. Senapati, "Bright Lesion Detection in Color Fundus Images Based on Texture Features," *Bulletin of Electrical Engineering and Informatics*, vol. 5, no. 1, pp. 92–100, 2016, doi: 10.11591/eei.v5i1.553.

[71] S. Lahmiri and M. Boukadoum, "Automated detection of circinate exudates in retina digital images using empirical mode decomposition and the entropy and uniformity of the intrinsic mode functions," *Biomedizinische Technik*, vol. 59, no. 4, pp. 357–366, 2014, doi: 10.1515/bmt-2013-0082.

[72] S. Ali *et al.*, "Statistical atlas based exudate segmentation," *Computerized Medical Imaging and Graphics*, vol. 37, no. 5–6, pp. 358–368, 2013, doi: 10.1016/j.compmedimag.2013.06.006.

[73] M. U. Akram, A. Tariq, M. A. Anjum, and M. Y. Javed, "Automated detection of exudates in colored retinal images for diagnosis of diabetic retinopathy," *Applied Optics*, vol. 51, no. 20, pp. 4858–4866, 2012, doi: 10.1364/AO.51.004858.

[74] Q. Liu *et al.*, "A location-to-segmentation strategy for automatic exudate segmentation in colour retinal fundus images," *Computerized Medical Imaging and Graphics*, 2016, doi: 10.1016/j.compmedimag.2016.09.001.

[75] U. R. Acharya *et al.*, "Automated diabetic macular edema (DME) grading system using DWT, DCT Features and maculopathy index," *Computers in*

Biology and Medicine, vol. 84, no. February, pp. 59–68, 2017, doi: 10.1016/j.compbiomed.2017.03.016.

[76] J. P. Medhi and S. Dandapat, "An effective fovea detection and automatic assessment of diabetic maculopathy in color fundus images," *Computers in Biology and Medicine*, vol. 74, pp. 30–44, 2016, doi: 10.1016/j.compbiomed.2016.04.007.

[77] D. Marin *et al.*, "An exudate detection method for diagnosis risk of diabetic macular edema in retinal images using feature-based and supervised classification," *Medical and Biological Engineering and Computing*, vol. 56, no. 8, pp. 1379–1390, 2018, doi: 10.1007/s11517-017-1771-2.

[78] C. Sinthanayothin, J. F. Boyce, H. L. Cook, and T. H. Williamson, "Automated localisation of the optic disc, fovea, and retinal blood vessels from digital colour fundus images," *British Journal of Ophthalmology*, vol. 83, no. 8, pp. 902–910, 1999, doi: 10.1136/bjo.83.8.902.

[79] M. Usman Akram, A. Khan, K. Iqbal, and W. H. Butt, "Retinal images: Optic disk localization and detection," *Lecture Notes in Computer Science (including subseries Lecture Notes in Artificial Intelligence and Lecture Notes in Bioinformatics)*, vol. 6112 LNCS, no. PART 2, pp. 40–49, 2010, doi: 10.1007/978-3-642-13775-4_5.

[80] K. Noronha and K. Nayak, "Fundus image analysis for the detection of diabetic eye diseases-a review," in *International Conference on Biomedical Engineering (ICoBE)*, 2012, pp. 242–246.

[81] H. Yu *et al.*, "Fast Localization and Segmentation of Optic Disk in Retinal Images Using Directional Matched Filtering and Level Sets," *IEEE Transactions on information technology in biomedicine*, vol. 16, no. 4, pp. 644–657, 2012.

[82] O. C. Huiqi Li, "Automatic location of optic disk in retinal images," in

International Conference on Image Processing, 2001, pp. 837–840.

[83] G. S. A. G. Vimala and S. K. Mohideen, "Automatic Detection of Optic Disk and Exudate from Retinal Images Using Clustering Algorithm," in *International Conference on Intelligent Systems and Control (ISCO 2013)*, 2013, pp. 280–284.

[84] A. I. Bandos, H. E. Rockette, T. Song, and D. Gur, "Area under the Free-Response ROC Curve (FROC) and a Related Summary Index," *biometrics*, vol. 65, pp. 247–256, 2009, doi: 10.1111/j.1541-0420.2008.01049.x.

[85] Araceli Fernandez Revuelta, "Técnica de exploración del fondo de ojo." [Online]. Available: www.amf-semfyc.com/web/article_ver.php?id=1016.

[86] G. D. Joshi, J. Sivaswamy, and S. R. Krishnadas, "Optic disk and cup segmentation from monocular color retinal images for glaucoma assessment," *IEEE Transactions on Medical Imaging*, vol. 30, no. 6, pp. 1192–1205, 2011, doi: 10.1109/TMI.2011.2106509.

[87] L. J. Uribe-Valencia and J. F. Martínez-Carballido, "Thesholding Methods Review for the Location of the Optic Disc in Retinal Fundus Color Images," in *13th International Conference on Electrical Engineering,Computing Science and Automatic Control*, 2016, pp. 1–6.

[88] E. Rogers and G. W. Zack, "Automatic measurement of sister chromatid exchange frequency," *Histochemical Cytochemistry*, pp. 11–14, 1977.

[89] J. M. Prewitt and M. L. Mendelsohn, "The analysis of cell images," *Annals of the New York Academy of Sciences*, vol. 128, no. 3, pp. 1035–1053, 1966.

[90] A. K. C. W. J.N. Kapur, P.K. Sahoo, "A New Method for Gray-Level Picture Thresholding Using the Entropy of the Histogram," *Computer vision, graphics, and image processing*, vol. 29, pp. 273–285, 1985.

[91] Mehmet Sezgin and Bulent Sankur, "Survey over image thresholding techniques

and quantitative performance evaluation," *Journal of Electronic Imaging*, vol. 13, no. 1, pp. 146–168, 2004, doi: 10.1117/1.1631316.

[92] L. J. Uribe-Valencia and J. F. Martínez-Carballido, "Automated Optic Disc region location from fundus images: Using local multi-level thresholding, best channel selection, and an Intensity Profile Model," *Biomedical Signal Processing and Control*, vol. 51, pp. 148–161, 2019, doi: 10.1016/j.bspc.2019.02.006.

[93] A. Osareh, M. Mirmehdi, B. Thomas, and R. Markham, "Comparison of colour spaces for optic disc localisation in retinal images," *Proceedings - International Conference on Pattern Recognition*, vol. 16, no. 1, pp. 743–746, 2002, doi: 10.1109/icpr.2002.1044865.

[94] D. Arthur and S. Vassilvitskii, "K-means++: The advantages of careful seeding," *Proceedings of the Annual ACM-SIAM Symposium on Discrete Algorithms*, vol. 07-09-Janu, pp. 1027–1035, 2007.

[95] A. F. Frangi, W. J. Niessen, K. L. Vincken, and M. A. Viergever, "Multiscale vessel enhancement filtering," *Lecture Notes in Computer Science (including subseries Lecture Notes in Artificial Intelligence and Lecture Notes in Bioinformatics)*, vol. 1496, pp. 130–137, 1998, doi: 10.1007/bfb0056195.

[96] V. Kyrki and D. Kragic, *Computer and robot vision*, vol. 1. Addison-Wesley Publishing Company, isbn:978-0201108774.

[97] J. P. Boyd, "Contour plots." [Online]. Available: http://www-personal.umich.edu/~jpboyd/eng403_chap4_contourplts.pdf. [Accessed: 20-Dec-2019].

[98] P. H. Scanlon, A. Sallam, and P. van Wijngaarden, *A Practical Manual of Diabetic Retinopathy Management*. Wiley-Blackwell, isbn:978-1-119-05895-3.

[99] a Basit, "Optic disc detection and boundary extraction in retinal images," *Applied Optics*, vol. 54, no. 11, pp. 3440–3447, 2015, doi:

10.1364/AO.54.003440.

[100] L. Xiong and H. Li, “An approach to locate optic disc in retinal images with pathological changes,” *Computerized Medical Imaging and Graphics*, vol. 47, pp. 40–50, 2016, doi: 10.1016/j.compmedimag.2015.10.003.

[101] S. Bharkad, “Automatic segmentation of optic disk in retinal images,” *Biomedical Signal Processing and Control*, vol. 31, pp. 483–498, 2017, doi: 10.1016/j.bspc.2016.09.009.

[102] L. C. Rodrigues and M. Marengoni, “Segmentation of optic disc and blood vessels in retinal images using wavelets, mathematical morphology and Hessian-based multi-scale filtering,” *Biomedical Signal Processing and Control*, vol. 36, pp. 39–49, 2017, doi: 10.1016/j.bspc.2017.03.014.

[103] R. Panda, P. N.B., and G. Panda, “Robust and accurate optic disk localization using vessel symmetry line measure in fundus images,” *Biocybernetics and Biomedical Engineering*, vol. 37, no. 3, pp. 466–476, 2017, doi: 10.1016/j.bbe.2017.05.008.

[104] M. E. Gegundez-Arias, D. Marin, J. M. Bravo, and A. Suero, “Locating the fovea center position in digital fundus images using thresholding and feature extraction techniques,” *Computerized Medical Imaging and Graphics*, vol. 37, no. 5–6, pp. 386–393, 2013, doi: 10.1016/j.compmedimag.2013.06.002.

[105] D. Marin, M. E. Gegundez-Arias, C. Ortega, J. Garrido, B. Ponte, and F. Alvarez, “Automated Detection of Diabetic Macular Edema Risk in Fundus Images,” in *Bioinformatics and Biomedical Engineering: 4th International Conference*, 2016, vol. 9656, pp. 380–390, doi: 10.1007/978-3-319-31744-1.

Appendix A

Download at: https://doi.org/10.1109/ICEEE.2016.7751228

2016 13th International Conference on Electrical Engineering, Computing Science and Automatic Control (CCE), Mexico, City, Mexico

Thesholding Methods Review for the Location of the Optic Disc in Retinal Fundus Color Images

Laura J. Uribe-Valencia, Jorge F. Martinez-Carballido
Electronics Department
National Institute of Astrophysics, Optics, and Electronics
Tonantzintla, Puebla/México
{lauraj.uribe, jmc}@inaoep.mx

***Abstract*— This work compares Triangle, Maximum Entropy and Mean Peak thresholding methods to locate the optic disc in color fundus images. Localizing the optic disc is a significant task in an automated retinal image analysis process as it is used on most vessel segmentation, disease diagnostic, and retinal recognition algorithms. The DIARETDBv1 dataset includes 89 retinal images are used to evaluate the 3 thresholding methods. To analyze the effect of image conditions on the performance of the thresholding methods, three set of images are created based on their contrast and quality: high contrast, low contrast, and poor quality; with 58, 16, and 15 images respectively. As green channel in the fundus image provides best contrast, it is used to extract the Optic disc. We analyze the effect of applying a previous preprocessing technique, each thresholding method is applied to 2 versions of the image: the original green channel and the original green channel with CLAHE. In terms of OD location, CLAHE preprocessing shows a great improvement for all thresholding methods. The average Method performance is evaluated with the percentage of intersected pixels with the groundtruth. From all results Triangle thresholding method performs consistently better than Maximum Entropy and Mean Peak, achieving 70.78% mean overlap with groundtruth in the best case and locating OD in 89/89 images.**

Keywords— Optic disc, CLAHE, Triangle thresholding method, Max entropy thresholding, Mean Peak thresholding.

I. Introduction

Retina is the innermost layer of the eye which can be visualized using adequate equipment such as a fundus camera. Fundus images are used for diagnosis by trained clinicians to check for any abnormalities or changes in the retina. A healthy retinal image contains anatomical structures like the macula, the optic disc (OD), blood vessels, fovea and optic cup. The OD is the exit point of retinal nerve fibers from the eye, and the entrance and exit point for retinal blood vessels. It is a brighter region than the rest of the ocular fundus and its shape is usually round. Although the OD main features and characteristics are relatively easy to describe, individual differences, diseases and other factors will influence characteristics of the optic disc, making its automatic localization a difficult task. Image quality can also affect the appearance of the OD. A retinal image may be unevenly illuminated or poorly focused, resulting in a less distinct and blurred OD. Therefore, optic disc location methodology involves extensive research interest [1] .

The location of OD is important in retinal image analysis because it is a key reference for recognition algorithms [2], blood vessels segmentation [3], and diagnosing some diseases such as diabetes and for registering changes within the optic disc region due to diseases such as glaucoma and the development of new blood vessels [4]. The OD is also a landmark for other retinal features, such as the distance between the OD and the fovea [5], which is often used for estimating the location of the macula [6] and is also used as a reference length for measuring distances in retinal images. In addition, it is important to detect and isolate OD region because, most of the algorithms designed to segment/detect abnormalities such as hard exudates in DR will detect lots of false positives in OD region as the color tone of the OD is similar to the hard exudates. Accurate identification of OD can be used to reduce the false positive rate while detecting the lesions [7]. Fig. 1 shows a color retinal fundus image of a healthy eye with its fundamental features.

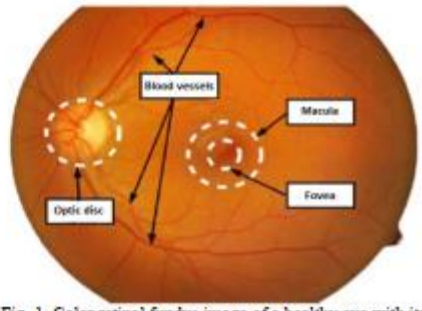

Fig. 1. Color retinal fundus image of a healthy eye with its fundamental features.

Applying illumination equalization such as histogram equalization, histogram specification, and other normalization

978-1-5090-3511-3/16/$31.00 ©2016 IEEE

Appendix B

Download at: https://doi.org/10.1016/j.bspc.2019.02.006

Biomedical Signal Processing and Control 51 (2019) 148–161

Contents lists available at ScienceDirect

Biomedical Signal Processing and Control

journal homepage: www.elsevier.com/locate/bspc

Automated Optic Disc region location from fundus images: Using local multi-level thresholding, best channel selection, and an Intensity Profile Model

Laura J. Uribe-Valencia*, Jorge F. Martínez-Carballido

Instituto Nacional de Astrofísica, Óptica y Electrónica, Tonantzintla, Puebla, Mexico

ARTICLE INFO

Article history:
Received 15 February 2018
Received in revised form
15 December 2018
Accepted 9 February 2019

Keywords:
Optic disc
Color fundus image
Medical image analysis
Diabetic retinopathy

ABSTRACT

Background and objective: Location of optic disc, which corresponds to the visible part of the optic nerve in the eye, is of high importance for bright lesion detection of Diabetic Retinopathy by extracting it and avoiding false positives. Glaucoma detection processes details on the optic disc zone. Location of the macula uses optic disc location as a reference. Thus, the location of optic disc is relevant for several diagnosis procedures on retinal images. Several methods for OD detection in fundus images can be found in the literature; however, the issue is still open to reach better results in terms of accuracy, robustness and complexity. This work provides a simple and image resolution independent method for Optic Disc location for methods that use the optic disc zone elimination or extraction to perform some diagnosis.
Methods: This work proposes a simple and reliable method for OD region location in fundus images using four known publicity available datasets: DRIVE, DIARETDB1, DIARETDB0 and e-ophtha-EX. We are introducing an OD region location method based on OD's characteristic high intensity and a novel method for feature's extraction that aims to represent the essential elements that define an optic disc by proposing a model for the pixel intensity variations across the optic disc (column wise). The approach has four main stages: OD pixel region candidate generation, promising OD regions detection, promising candidate features extraction, and classification. All images from the four datasets were used for testing, since no training was used for classification.
Results: An OD location accuracy of 99.7% is obtained for the 341 retinal images within the four publicly datasets.
Conclusions: The obtained results show that the proposed method is robust and achieves the maximum detection rate in all four compared databases, which demonstrates its effectiveness and suitability to be integrated into a complete prescreening system for early diagnosis of retinal diseases. Use of promising OD region location reduces processing area in about 40%.

1. Introduction

Morphological detection of retinal structures such as the optic disc (OD), blood vessels, macula and fovea are a common step in most systems for automatic detection and screening of different retinal pathologies. Fundus images are used for diagnosis by trained clinicians to check for any abnormalities or changes in the retina. To alleviate physician work, images can be processed by an automated system that provides probable lesion areas, that the ophthalmologists will diagnose [1]. In particular, the detection of the OD, which corresponds to the visible part of the optic nerve in the eye, is an important task in retinal image analysis because it is a key reference for recognition algorithms [2], blood vessels segmentation [3,4], and diagnosing some diseases such as diabetic retinopathy (DR) [5,6] and for registering changes within the optic disc region due to diseases such as glaucoma [7–9] and the development of new blood vessels [10]. The OD is also a landmark for other retinal features, such as the distance between the OD and the fovea [11,12], which is often used for estimating the location of the macula [13] and is also used as a reference length for measuring distances in retinal images [14]. In addition, it is important to detect and isolate OD region because, most of the algorithms designed to segment/detect abnormalities such as hard exudates in DR will detect lots of false positives in OD region since the optic disc could present similar color, shape and size characteristics which can lead to potentially

* Corresponding author at: Instituto Nacional de Astrofísica, Óptica y Electrónica, Luis Enrique Erro # 1, Santa María Tonantzintla, Puebla, Pue. 72840 Mexico.
E-mail addresses: lauraj.uribe@inaoep.mx (L.J. Uribe-Valencia), jmc@inaoep.mx (J.F. Martínez-Carballido).

https://doi.org/10.1016/j.bspc.2019.02.006
1746-8094/